

Institut für Theoretische Physik
Fakultät Mathematik und Naturwissenschaften
Technische Universität Dresden

Dynamics of endosomal trafficking

Dissertation

zur Erlangung des akademischen Grades

Doctor rerum naturalium

(Dr. rer. nat.)

vorgelegt von

Jonathan Edward Dawson

geboren am 04. Juli 1985 in Kadapa, Indien



Max-Planck-Institut für Physik komplexer Systeme

Dresden, 2011

Gutachter

Prof. Dr. Frank Jülicher

Dr. Clifford P. Brangwynne

Tag der Einreichung bei der Fakultät

06. März 2012

Tag der Verteidigung

15. Juni 2012

Inasmuch ... as biological phenomena are very closely related to physical phenomena, we shall ... whenever possible, look for physical interpretations, in line with the desire to unify all natural sciences.

- Nicolas Rashevsky, 1938.

Abstract

Endosomes are dynamic vesicular structures which transport cargo molecules internalized into the cell via endocytosis. Endosomal trafficking of cargo involves a large number of individual endosomes that regularly interact with each other via fusion and fission and thus form a dynamic network wherein endocytosed cargo is sorted and transported to various other intracellular compartments. In this study we present a general theoretical framework that takes into account individual endosomes and several key microscopic interaction processes among them. By combining theory with quantitative experiments, we seek to address the fundamental question of how the behaviour of the endosomal network emerges from the interactions among many individual endosomes of different sizes and cargo contents. Our theory is based on distributions of endosomes of various sizes and cargo amount. We compare our theory to experimental time course distributions of LDL, a degradative cargo, in a population of early endosomes. Early endosomes display a broad distribution of cargo with a characteristic power law, which we show is a consequence of stochastic fusion events of cargo carrying early endosomes. A simple model can quantitatively describe time-dependent statistics of LDL distributions in individual early endosomes. From fits of the theory to experimental data we can determine key parameters of endosomal trafficking such as the endosome fusion rate and the fluxes of cargo into and out of the network. Our theory predicts several experimentally confirmed scaling behaviours, which arise as a result of endosome fusion. Our theory provides a link between the dynamics at individual endosome level and average properties of the endosomal network. We show from our theory that some features of the endosomal distributions, which arise from interactions among individual endosomes, are sensitive to alterations in chosen parameters. This provides a direct means to study perturbation experiments wherein the cargo distribution can vary in response to changes of the endocytic system. Our analysis provides a powerful tool for the study of genetic and chemical perturbations that may alter specific systems properties and for extracting various kinetic rates involved in endosomal trafficking from only still images at different points.

Acknowledgements

I would like to thank a number of people whose guidance, support and friendship have not only made this work possible, but also enjoyable. At the very outset I would like to thank my advisor, Prof. Dr. Frank Jülicher for providing me with the opportunity to work in his group, for his encouragement and constant support. Though not always the easiest person to track down, Prof. Jülicher taught me the techniques that will hopefully guide me through a life of good science. I would like to thank Dr. Lionel Foret for his guidance all throughout my research work. Several conversations I had with him about this project, over telephone as well during his visits to Dresden, have been very useful. Furthermore, I thank Prof. Dr. Marino Zerial and Dr. Yannis Kalaidzidis for the thought provoking discussions during numerous meetings we had in the last three years. Thanks to Roberto Vilaseñor and Claudio Collinet for performing the biological experiments that made this thesis possible. I would also like to thank all the members of our Biophysics group, who not only helped me out with the innumerable little questions that have occurred in the course of this project, but who also made my life enjoyable at our institute. I would also like to thank Dr. Cliff Brangwynne for reviewing this thesis. Thanks to Chiu Fan Lee and Sekhar Burada for critical reading of several chapters of this manuscript. Last but not the least, I thank God for blessing me with a wonderful family, my parents and brother, without whose support all this would have not been possible.

Dedicated to my parents.

Contents

1	Introduction	1
1.1	Dynamic cell: Intracellular organization and trafficking	2
1.1.1	Endocytic pathway - bring 'em in and get 'em there	4
1.2	Endosomes: key players of endocytic pathway	4
1.2.1	Morphology and structure of endosome	5
1.2.2	Endosomal population - distinct compartments	6
1.2.3	Dynamic endosome: endosome motility	8
1.2.4	Early endosomes - a cargo sorting machinery	8
1.2.5	Theoretical compartmental analysis - average behaviour	10
1.3	Physics of traffic phenomena in Biology	13
1.3.1	Theoretical approaches for studying traffic phenomena	13
1.3.2	Smoluchowski kinetic theory for aggregation	15
1.4	Overview of this work	17
2	Dynamics of endosomal trafficking: experiments and observations	19
2.1	Cargo trafficking by endosomes - experiments to theory	20
2.1.1	Endosome marker - Identifying an endosome	20
2.1.2	Cargo uptake experiments	20
2.1.3	Image analysis - Statistics of endosomal population	23
2.1.4	Number density distribution: individual endosome statistics	24
2.1.5	Integral quantities: endosome population statistics	25
2.1.6	LDL in early endosomes - Colocalization	26
2.2	Conclusion	28
3	Physical description of endosomal dynamics	29
3.1	Dynamics of early endosomes	29
3.1.1	Exchange processes	31
3.1.2	Endosomal number and components balance	37
3.2	Two component description: Rab5 plus Cargo	38
3.2.1	Transport equation for the cargo load of an endosome	40
3.3	Dynamics of cargo trafficking in Rab5 endosomes	43

3.4	Conclusion	46
4	Entry-Fusion-Exit model to describe cargo trafficking by early endosomes	47
4.1	Entry and Fusion : A minimal scenario	49
4.1.1	Exact solution for the cargo distribution $n(s, t)$	50
4.1.2	General properties of the cargo distribution $n(s, t)$ for large s	50
4.1.3	General properties of the cargo distribution $n(s, t)$ for small s	55
4.2	Entry-Fusion-Exit : Conversion model	56
4.2.1	Steady state distribution $n(s)$ in the conversion model	57
4.2.2	Total amount of cargo and total number of endosomes: Different timescales for saturation	58
4.2.3	Effect of cargo dependent fusion and conversion rates	60
4.3	Entry-Fusion-Exit: Budding model	61
4.3.1	Constant out-flux: Phase transition scenario	62
4.3.2	Constant budding rate	64
4.3.3	Total amount of cargo and total number of endosomes	66
4.4	Conversion and Budding at constant rate: Similarities between the models	67
4.5	Conclusion	68
5	Comparison between theory and experiment	71
5.1	Continuous cargo uptake experiment	72
5.1.1	Processes shaping the steady state cargo distribution	74
5.2	Entry-Fusion-Exit model to describe LDL trafficking	75
5.2.1	Effect of varying cargo concentration	78
5.2.2	Entry-Fusion-Exit: Conversion model versus budding model	82
5.2.3	Existence of homotypic fission	83
5.3	Dynamics of Rab5	85
5.4	Conclusion	87
6	Summary and outlook	89
A	Numerical analysis of continuum description	95
B	Fit of EFE model to experimental data : procedure	97
C	Contribution of Influx via CCV fusion	99

Chapter 1

Introduction

Traffic and transport processes are ubiquitous in nature. Examples abound, vehicular traffic on a national highway, nutrient and lipid transport by blood flow to molecular motor driven vesicular traffic inside a eukaryotic cell [120, 116, 117, 121, 107]. Nature exhibits traffic phenomena at length and time scales that differ by orders of magnitude [121]. Even with the diversity in the nature of systems that exhibit such phenomena, there exists some generalities. Such processes usually involve a large number of active motile elements that transport material between two distinct locations in space. Another feature of traffic phenomena is that the traffic flow mostly takes place on tracks or trails [107, 116]. For example, in vehicular traffic the motile elements like automobiles run on road or lanes [120], whereas intracellular traffic which consists of vesicles and other intracellular organelles is mainly driven by motor proteins on tracks of microtubules [116]. At the cellular level, cell internalizes certain molecules from its environment, a process known as endocytosis. These molecules, termed cargo, have to be sorted and transported to different intracellular locations for further synthesis [76]. Several hundreds of intracellular organelles, which are mainly carriers of cargo molecules, collectively accomplish this task. Cells ability to efficiently handle such huge traffic of cargo and organelles eventually determines how accurately it senses and responds to its environment [4, 10, 11]. Intracellular trafficking involves a large number of organelles, therefore, complex collective behaviour emerges as a result of interaction between them. The complexity of the intracellular trafficking pathways in terms of number and type of organelles, dynamics of protein sorting and transport, poses however the challenge of developing theoretical and experimental tools necessary to elucidate the structure and function of the organelle network. This thesis is a step in that direction. To identify the general principles governing the dynamics of intracellular trafficking of a specific class of organelles known as endosomes and try to answer the question of how the behaviour of endosomal network emerges from the microscopic interactions.

1.1 Dynamic cell: Intracellular organization and trafficking

The cell, the basic unit of life, is a highly dynamic system that operates far out of equilibrium [79, 78]. It means that it consumes energy to maintain its internal organization. But rarely does a living cell operate in a static environment. It operates in a highly dynamic and fluctuating environment [81]. Trillions of individual cells which make up a multicellular organism regularly communicate with each other during the growth and development of the organism. The ability of a cell to sense the changes in its environment and respond accordingly is vital for its survival. The complexity in the internal organization of eukaryotic cells, also known as mammalian cells, evolved, it seems, to enable the cell to respond to various different kinds of signals from its environment simultaneously. This has enabled the multicellular organisms to carry out diverse activities. Schematic representation of a eukaryotic cell with its internal organization is shown in Fig.1.1. Cell senses and responds to the signals from its environment by taking up and secreting many different molecules [13, 1, 3, 9, 20, 10]. Intracellular trafficking involves mainly sorting and transport of the internalized molecules and underlies several important cellular functions [71]. The intracellular trafficking can be understood from two different standpoints: cargo trafficking and membrane trafficking.

Cargo trafficking: Cargo molecules that cell internalize or synthesize intracellularly are to be transported to different destinations inside the cell [13, 1, 3, 9, 20]. Some proteins and protein complexes simply diffuse through the cell cytoplasm and reach their destination, whereas others are transported by the intracellular organelles [75, 76, 86, 109]. Organelles, which are membrane-bound structures play a very important role in sorting and transporting different types of cargo. For example, certain types of cargo have to be carried out of the cell to the extracellular medium whereas there are other types of cargo which are degraded inside the cell. Several hundreds of organelles collectively accomplish the task of cargo trafficking that involves both cargo sorting and cargo transport. Proper trafficking of cargo enables the cell to correctly sense and respond to its environment [84, 85, 10].

Membrane trafficking: Cells reservoir of membrane comprises of the plasma membrane, that separates cells interior from its environment, and the membrane that makes up all the intracellular organelles [75, 5]. Cargo molecules that cannot simply diffuse through the plasma membrane are endocytosed into the cell via endocytic vesicles. The endocytic vesicles are enclosed by membrane directly derived from the plasma membrane of the cell. Most of the endocytic events thus rob the

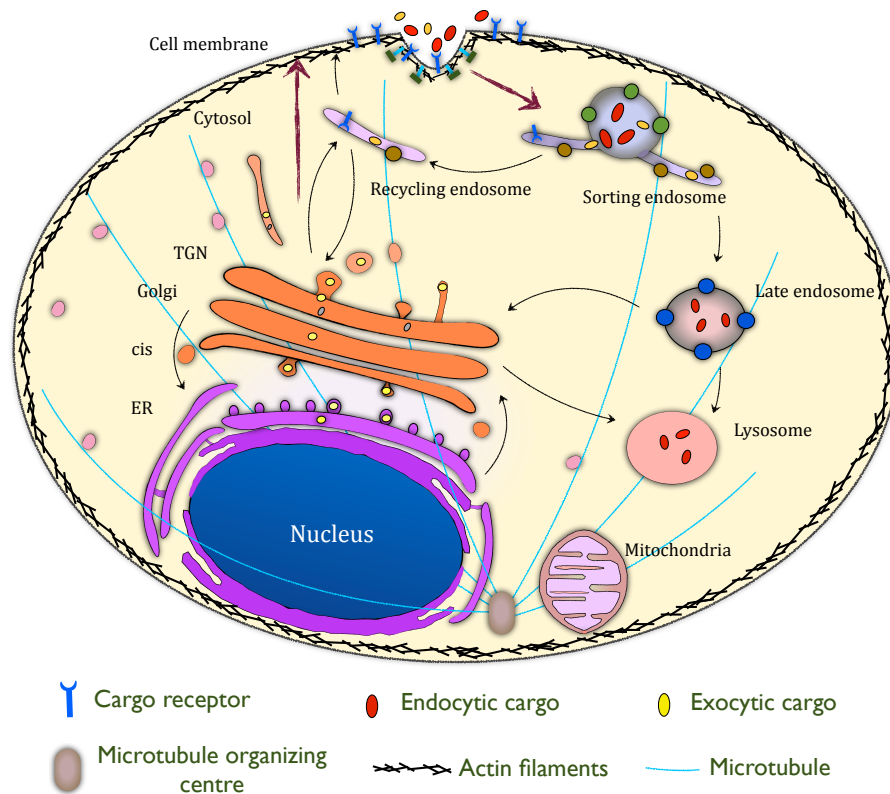


Figure 1.1: **Endocytosis and Intracellular transport - organelles and trafficking pathways**

A schematic diagram of the principle organelles and pathways involved in endocytosis and intracellular transport. Certain types of cargo molecules bind to specific regions known as receptors on the outer membrane of the cell. Subsequently the cargo molecules as well as their receptors are internalized into the cell. Following internalization the cargo molecules enter the endocytic pathway and are sorted and transported to various destinations inside the cell. Thus, the endocytic pathway originates at the cell membrane and is directed cell inward. The organelles that play a major role along this pathway are: *Clathrin coated vesicles*, *Sorting/Early endosomes*, *Recycling endosomes*, *Late endosomes* and *Lysosomes*. On the other hand exocytic pathways originates intracellularly and is directed cell outward to extra cellular environment. The organelles that play a major role along this pathway are: *Endoplasmic reticulum (ER)*, *Golgi-apparatus*, *intermediate vesicles* and *Recycling endosomes*.

cell of a bit of its surface plasma membrane [39, 75, 76]. If the cell would continue to uptake extracellular material, it would eventually shrink itself to death. How does cell maintain its size and volume? Membrane trafficking addresses this problem [75, 39]. When intracellular organelles fuse with the plasma membrane, cell gains membrane area thus balancing the membrane loss during endocytosis. Membrane trafficking, which involves several hundreds of intracellular organelles,

is essential to maintain proper cell physiology.

1.1.1 Endocytic pathway - bring 'em in and get 'em there

Intracellular trafficking, whether it be of cargo or membrane, is organized into distinct pathways [75, 76]. Most of the intracellular organelles have been characterized as operating along one of these pathways [75, 76]. Two major trafficking pathways are the *endocytic* and the *exocytic* pathways. As discussed in the previous section, intracellular trafficking constitutes not only the transport of cargo molecules but also cellular membrane which make up the outer layer of organelles. Endocytic trafficking originates at the plasma membrane, with the internalization of cargo molecules into the cell, and is directed cell inward. There are numerous different ways by which extra cellular material cargo can be internalized into the cell. Not only different mechanisms are employed by cargo molecules to gain entry into the cell, but even several different types of cargo enter the cell all the time via endocytosis. For example there are some cargo types that have to be degraded in the cell and others have to be recycled back to the cell membrane [75, 11, 1]. The cell has to properly and efficiently handle all the different kinds of proteins it internalizes, a requirement it has to meet for its own survival and eventually that of the organism as a whole. This raises the question, how does a cell control and organize the huge traffic of cargo molecules intracellularly? How does a cell make sure that the huge variety of cargo molecules that it internalizes is properly sorted and delivered to their right destinations? A series of intracellular organelles, termed endosomes, with distinct morphological and biochemical characteristics, are responsible for this vital task [5, 11]. The dynamics of endocytosis and, subsequent cargo sorting and transport along the endocytic pathway have been subject of intense study in the past, both experimentally and theoretically [74, 76].

1.2 Endosomes: key players of endocytic pathway

Irrespective of the entry mechanism employed to gain entry into the cell, most of the cargo and associated receptors (in the case of receptor-mediated endocytosis) following endocytosis are delivered to endosomes [76, 77, 4]. Endosomes are highly dynamic vesicular structures involved in intracellular trafficking along the endocytic pathway [11, 5, 97]. Endosomes form a dynamic network of thousands of vesicles that interact with each other via fusion and fission and thereby accomplish the vital task of sorting the cargo molecules and transporting them to their

appropriate intracellular destinations Fig.1.2 [9, 97].

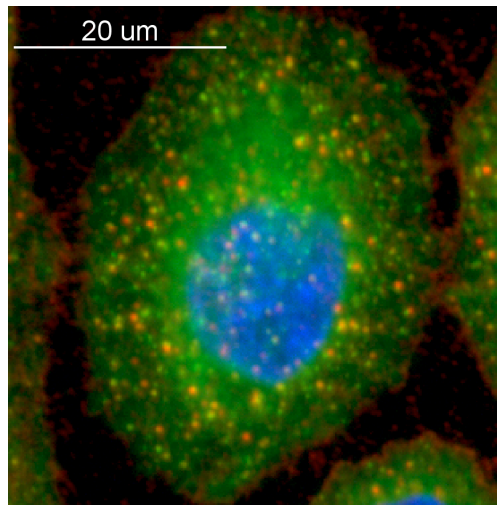


Figure 1.2: **Early endosomes: intracellular organelles transport cargo**

A confocal microscopy image of a HeLa cell expressing Rab5 (green), LDL cargo (red) and nuclei (blue), after 60 minutes of cargo uptake. Early endosomes are characterized by Rab5 protein. The red spots in the image represent the red fluorescence associated with the cargo LDL. Rab5, represented by green fluorescence, in inactive state fills the cytoplasmic volume of the cell and in active state is bound to the membrane of early endosomes. All those red spots which are also positive to green represent Rab5-positive endosomes carrying cargo.

Dynamics of endosomes is tightly regulated and governed by two factors. First is the endosomal membrane proteins, which play a crucial role in interaction between endosomes like fusion and fission. Second, the motor proteins that move the endosomes along microtubule tracks are responsible for the endosomal motility, an aspect crucial for traffic and transport processes. Any endeavor towards gaining an insight and physical understanding of cargo trafficking through the endocytic pathway must begin with the endosomes. In the immediate following we will study endosomes, their structure and motility from a more biological standpoint.

1.2.1 Morphology and structure of endosome

Endosomes are vesicular structures bounded by a lipid bilayer that separates their inner environment from the exterior [1, 19, 97]. The cargo molecules and associated receptors delivered to endosomes following endocytosis reside inside the endosome [97]. The interior of an endosome is slightly acidic compared to the surrounding cytosolic environment. The acidic interior plays a role in sorting and organizing the cargo molecules in different domains inside the endosome [97, 99]. The outer membrane of an endosome harbors several different membrane proteins, Fig.1.3

[97, 5]. The function of endosomes in sorting and trafficking is governed by the dynamic assembly on the membrane of a multi-protein machinery organized by small GTPases of the Rab family [5, 97, 19, 23, 98]. Rab proteins specify the function of distinct intracellular compartments [5, 6, 7, 8, 98]. These proteins operate between the GTP-bound active state and GDP-bound inactive state [8]. The switch between the GDP/GTP cycle determines the membrane association of Rab proteins. Rab proteins function as regulators of several activities carried out by an endosome, from fusion between endosomes to their motility on the microtubule tracks. [88, 5, 91].

1.2.2 Endosomal population - distinct compartments

Fusion between endosomes is governed by specific membrane bound Rab proteins, Fig1.3. Based on the localization of these specific Rab proteins on the membrane of endosomes, the whole endosomal population is divided into three distinct compartments of interacting endosomes, Fig.1.3 [20, 74, 97, 5]. The identity of an endosomal compartment is maintained by Rab proteins by maintaining the specificity of fusion between endosomes, referred to as homotypic fusion.

Early endosomes: Early endosomes are characterized by Rab5 and their respective effectors. Following internalization the cargo is delivered first primarily to a population of Rab5-positive early endosomes. Rab5 plays a very important role in homotypic fusion of early endosomes[90, 94]. Early endosomal compartment is the major sorting station along the endocytic pathway. Here the endocytosed cargo is sorted either for recycling back to cell membrane or degradation in lysosomes. The recycling cargo is delivered to the recycling endosomes which carry the cargo out of the cell whereas the cargo to be degraded is delivered to the late endosomes [29]. Early endosomes are slightly acidic (pH \sim 6.0) [100].

Electron microscopy images reveal that the early endosomes are vesiculo-tubular structures with a vesicular body of \sim 0.5 μ m in diameter and tubules of \sim 50 nm in diameter [101, 19].

Recycling endosomes: The recycling cargo, for example cargo receptors, is delivered to recycling endosomes [7, 97]. Recycling endosomes are characterized by Rab4, Rab11 and their effectors [5, 29]. Recycling endosomes are slightly less acidic (pH \sim 6.5) compared to early endosomes and have a tubular morphology [17]. Recycling endosomes carry the cargo to the cell periphery where they fuse with the plasma membrane and deliver the cargo molecules to the extracellular milieu.

Late endosomes: Late endosomes are characterized by Rab7 and its respective effectors [20]. The cargo to be degraded in the cell is delivered by the early endosomes to the late endosomes [5]. Late endosomes carry the cargo to lysosomes,

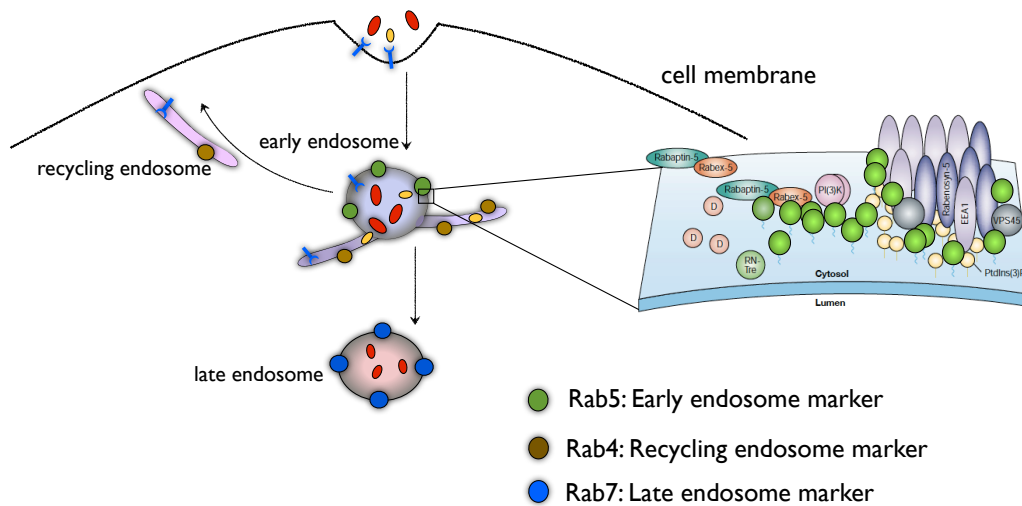


Figure 1.3: **Endosomes: structure and organization along endocytic pathway**

Cargo internalized into the cell is delivered primarily to a population of Rab5-positive early endosomes, which are vesiculo-tubular structures. Here the cargo molecules are sorted out and transported to various intracellular destinations or recycled back to cell membrane. The membrane of an endosome is a mosaic of different membrane proteins. A schematic cross-section shows the various membrane proteins and their effectors of early endosomes. Rab protein, a small GTPase, (shown in the membrane cross-section in color light green) is the key identifiers of an endosome. Early endosomes are characterized by Rab5 and its effector, Late endosomes by Rab7 and Recycling endosomes by Rab4/11 and their effectors. The endocytosed cargo molecules are delivered to Rab5-positive early endosomes, where they are sorted out to either Rab4/11-positive recycling endosomes to be transported back to cell membrane or to Rab7-positive late endosomes for degradation in lysosomes. Population of early endosomes is therefore an important hub for the incoming cargo.

Schematic of endosome membrane cross-section obtained from Ref.[5].

where the cargo is eventually degraded. Late endosomes are mainly spherical and have a highly acidic lumen (pH \sim 5.0-6.0) [18].

Apart from the main distinct populations of endosomes which form different compartments (as discussed above), there are several other intracellular structures that operate along the endocytic pathway whose localization to any one of these compartments is not clearly defined. Such vesicular structures, like endocytic carrier vesicles shuttle between different compartments and act as carriers of cargo between these mutually non-interacting compartments [28].

1.2.3 Dynamic endosome: endosome motility

Endosomes are highly dynamic motile structures. Their transport is orchestrated by microtubules, a network of polarized filamentous polymers. Motility of endosomes is powered by a small set of distinct motors on the microtubule tracks. Kinesin motor moves the organelle towards the plus end (towards cell periphery) and dynein towards the minus end (cell nucleus) of the microtubule [87, 86, 107]. Early endosomes have been shown to move centripetally to the juxtannuclear position following endocytosis of cargo at the cell periphery. Their complex motion is regulated by the attached motors, interaction with other endosomes and organelles and with the associated microtubule network. Even though quite a lot has been contributed to the physical understanding of such active transport processes it is still in a developing phase [103, 104, 105, 106, 107, 108]. Motors not only play an important role in keeping the endosomes mobile but disruption of dynein motor on endosomes have shown to disrupt early endosome localization and lead to defects in cargo sorting [89]. A recent study, aimed at quantifying the dynamics at single endosome level, showed the mean square displacement (t^β) of several individual endosomes whose trajectories were traced for nearly 2 minutes [103]. At very short time scales ($t < 2$ seconds) endosomes motion was observed to be nearly ballistic ($\beta \sim 1.8$). However, at long times ($t > 10$ seconds) the vesicles exhibit a diffusive scaling ($\beta \sim 1$) [103]. Interactions between cargo carrying endosomes via fusion and fission, coupled with their bi-directional motility regulated by motors leads to an asymmetric distribution of cargo in the cell [103].

1.2.4 Early endosomes - a cargo sorting machinery

We have seen in previous sections that endosomes of a given compartment form a dynamic network of membranes undergoing fusion and fission. One such compartment is that of early endosomes, characterized by membrane proteins, namely Rab5 and their effectors [5, 20, 19]. Cargo molecules internalized into the cell are captured in the endocytic vesicles which are subsequently delivered to early

endosomes. How the endocytic vesicles deliver the cargo to early endosomes remains unclear. The endocytic vesicles can either fuse with the Rab5-positive early endosomes in what is called as heterotypic fusion or they could undergo transformation wherein the vesicular membrane gains Rab5 proteins and thus becoming Rab5-positive structures or simply early endosomes.

Rab5-positive early endosomes are the major sorting station for the endocytosed cargo [97]. Here the cargo is sorted to be eventually delivered to various destinations within the cell. For example, cargo receptors which are taken into the cell during receptor mediated endocytosis have to be delivered back to the cell for further uptake of cargo molecules. Certain types of cargo like signaling molecules have to be degraded inside the cell, otherwise the signal would indefinitely grow. Thus, cargo receptors and other such recycling cargo have to be sorted for recycling back to the cell membrane whereas degradative cargo to be degraded inside the cell [90, 97, 1]. Early endosomal population thus plays a pivotal role along the endocytic pathway, that of cargo sorting, Fig.1.3. How do endosomes exactly accomplish this rather subtle job of segregating the different types of cargo that enter them is not very well understood.

In a study it was shown that the acidic luminal pH of early endosomes ($\text{pH} \sim 6.0$) causes the ligands to dissociate from their receptors and sort them to transport to various intracellular destinations [100, 1, 2]. Regular fusions between early endosomes coupled with the early endosome morphology could play a role in the cargo sorting. Lipid segregation has been observed in tubulated endosomes [102]. The role of curvature of vesicles in lipid sorting has been studied both theoretically and experimentally [110]. Membrane curvature might drive certain lipids into sorting tubules. Fusion process between vesicles is an ubiquitous mechanism for generating tubules because of excess of membrane area and thermodynamical instability it generates. Early endosomal population consist of Rab5-positive endosomes of various different size and cargo content. Interestingly, in an extensive study carried out recently, it was observed that early endosomes show a distinct spatio-temporal organization (see next section) [20]. Large Rab5-positive endosomes were observed to be located in the peri-nuclear region whereas smaller endosomes at the cell periphery, closer to the plasma membrane [21]. Cargo was also observed to be concentrated in the peri-nuclear region at late times following the cargo uptake by endocytosis [103]. Endosomes of different size and cargo content might arise due to endosomal fusion [21]. How the early endosomal compartment communicates and exchanges cargo with other endosomal compartments is not clearly understood. For example, the mechanism of transfer of cargo from early to late endosomes is hotly debated. This transfer of cargo can occur either by conversion of a cargo carrying Rab5-positive endosome into a Rab7-positive late endosome [20, 26]. Such a conversion process has been observed in experiments

where a cargo carrying Rab5-positive endosome gradually became depleted of all the Rab5 on its membrane and was replaced by Rab7 [20, 26, 24, 27]. However, another mode of cargo transfer from early to late endosomes exists wherein budding of carrier vesicles from early endosomes and their subsequent fusion with late endosomes was observed [28, 24]. It is unclear as to what extent different types of cargo or different cell types use one mechanism, the other or both.

Self-Organization of early endosomes

The dynamics of endocytosis and, subsequent cargo sorting and transport along the endocytic pathway have been a subject of intense study in the past, both experimentally and theoretically [74]. By tracking individual endosomes as well as endosomal populations [20] it was shown that the endocytic cargo (Low Density Lipoprotein) progressively flows from small endosomes at the periphery of the cell to large endosomes at the center, which eventually convert into late endosomes leading to cargo degradation [20]. Such a spatial-temporal progression was summarized in *funnel* model, wherein numerous small endosomes at the cell periphery fuse with each other regularly to form fewer but bigger vesicles that move towards the cell centre. In a recent genomic survey by RNA interference [21], a Bayesian network analysis revealed general rules underlying the organization of the endocytic system and provided unbiased experimental support to the *funnel* model of the endosomal network. The study showed that depletion of various genes caused cargo to be distributed in endosomes that are arrested at different stages along the spatio-temporal progression. A highlight of this study is that the stochastic fusion events between endosomes leads to a stable organization where cargo is sorted out and transported from plasma membrane to its final destination. Since such behaviours can emerge from many interacting endosomal units even in the absence of external controller, this is termed self-organization process [125, 124].

1.2.5 Theoretical compartmental analysis - average behaviour

Although the structure and spatial distribution of the endosomal network is important to understand cargo sorting and flux, theoretical approaches have typically focused on the time-dependence and kinetic rules associated with the arrival of internalized ligands into whole endosomal compartments (eg. early and late) without resolving the role of individual endosomes [33, 36, 39, 34, 37]. Such approaches therefore focused on the average behaviour of the endosomal system while ignoring the details of the spatio-temporal organization of the entire endosomal network.

In the compartmental approach only average quantities can be identified. Early, late or recycling endosomes collectively form three different compartments of mutually interacting endosomes. Cargo can enter and leave these endosomal compart-

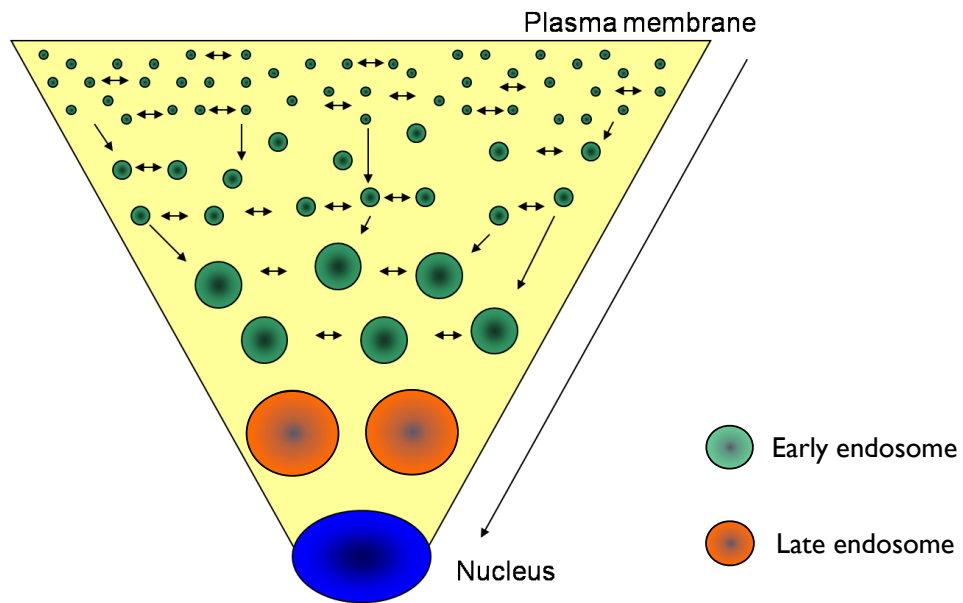


Figure 1.4: **Organization of early endosomes and cargo progression along the endocytic pathway**

Funnel model for the cargo progression along the endocytic pathway suggests that small endosomes appear at the cell periphery. These small endosomes undergo regular homotypic fusion while moving centripetally and thus generating fewer bigger endosomes at perinuclear region (figure taken from doctoral dissertation of Claudio Collinet).

ments. What one can measure then is the flux of cargo across a given compartment, Fig1.5. If the cells are allowed to internalize cargo continuously for a certain duration of time, the cargo gradually enters the compartments. The amount of cargo in a particular endosomal compartment increases with time. In the presence of an exit for cargo from the compartment the increase in the amount of cargo eventually reaches a steady state Fig1.5. If we denote by Φ the total amount of cargo in the endosomal compartment, then the rate of change of Φ is given by,

$$\frac{d\Phi}{dt} = J_{in} - J_{out} \quad (1.1)$$

where, $J_{in/out}$ represent the in/out-flux of cargo through the endosomal compartment. The characteristic time for reaching the steady state is governed by the

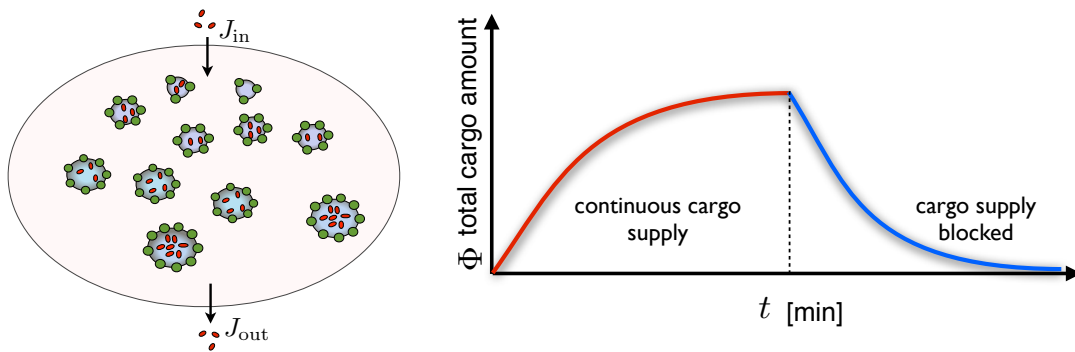


Figure 1.5: **Average behaviour of an endosomal compartment**

Cargo enters and leaves the endosomal compartment (early, late or recycling) all the time. The cargo flux can be measured by the total amount of cargo Φ in the compartment at any given time. Without resolving the cargo amount in individual endosomes of the compartment one can write down the equation for global fluxes of cargo through the endosomal compartment. The amount of cargo in the compartment (devoid of cargo initially) increases following endocytosis in the case of continuous cargo uptake. The cargo exit mechanism, that might relate to cargo exchange with other compartments, will eventually balance the cargo influx (red curve). The total amount of cargo Φ in a compartment will thus reach a steady state within a characteristic time. When cargo supply to the cell is blocked the cargo will gradually drain out of the compartment within a characteristic time (blue curve).

strength of influx and outflux of cargo. Similarly after some time of cargo uptake if the cargo supply to the cell is blocked then, the cargo will drain out of the endosomal compartment within a characteristic time governed by the exit mechanism, Fig1.5.

It was earlier studies using the compartmental approach that provided the additional information about the distinct endosomal compartments. Different time scales were observed for cargo exit from the early, late and recycling endosomal

compartment suggesting that these different compartments can also be distinguished, apart from the Rab proteins, by the time it takes for the endocytosed material to reach them [36]. Cargo enters and therefore exits the Rab5-positive early endosomal compartments much earlier than the Rab7-positive late endosomal compartment [32].

1.3 Physics of traffic phenomena in Biology

Traffic processes involve large number of interacting motile elements. Such processes exhibit interesting collective behaviour, like self-organization. Intracellularly large number of organelles whose motility is powered by molecular motors on tracks of microtubules and actin filaments constitute the traffic. Intracellular trafficking involves the sorting of cargo and transporting them to various intracellular destinations. Our focus in this study is on a special class of organelles, termed endosomes, which are key players of cargo sorting and transport along the endocytic pathway. There are several different aspects to traffic phenomena, so that there is not one definite approach that would provide us with complete and comprehensive understanding of such processes. A variety of approaches have been used to gain physical understanding of the traffic like phenomena, few examples being cellular automaton model and particle hopping model [115, 116, 114]. Since the pioneering work of Prigogine and Herman on kinetic theory of vehicular traffic, cars in a traffic have been considered as a system of interacting particles [117, 118]. Several interesting features like traffic jam, phantom traffic jam have been explained by these models. When the number of motile elements in the traffic is quite large, modeling the traffic flow using hydrodynamical approach in terms of one dimensional compressible gas is quite useful, features like shock waves have been predicted by such an approach [117, 119]. In this section we will present or rather review some aspects of traffic processes and corresponding theoretical approaches which are quite generic, so that we don't miss the woods for the trees. We will be very brief in most of the theoretical approaches, but spend some time towards the end at studying the aggregation process as a model for traffic like processes.

1.3.1 Theoretical approaches for studying traffic phenomena

All the theoretical approaches that have been employed so far towards gaining physical understanding of the trafficking processes can be broadly divided into two categories, namely *individual particle based* approach and *population based* approach. The individual particle based approach encapsulates all those models

that deal with the traffic system on a microscopic level. On the contrary, the population based approach is a mean-field approach whose description breaks down at very low density of the trafficking particles. Traffic processes are collective in nature, interaction among the traffic entities can lead to spatio-temporal organization and are thus an example of self-organization. Another feature of traffic processes is that they are usually characterized as operating far from equilibrium. The motile entities that constitute the traffic are active in nature, i.e they exchange energy and/or information with their environment. Let us briefly review the two approaches mentioned above.

1.3.1.1 Individual particle based approach

In this approach the particles are identified individually as residing in some state at time t . Accounting for the forces and the interactions between particles one can evaluate the time evolution of the system at $t + \delta t$. Intracellular organelles are active motile entities [107]. To start with, one can write down the Newton's equation of motion for individual active particles or elements of the traffic [120].

$$m_i \ddot{x}_i(t) = F_{ext}(x_i(t), t) - \gamma_i v_i(t) + \xi_i(t) + \sum_{i \neq j} F_{ij}(t) \quad . \quad (1.2)$$

The first term in Eq.(1.2), $F_{ext}(x_i(t), t)$ represents the external force acting on the particle. The second term $\gamma_i v_i(t)$ represents the friction force acting on the particle, the friction coefficient given by γ_i . In general, friction coefficient can also be a function of velocity $\gamma_i(v(t))$, which could originate from the collective motion of molecular motors on microtubule filaments. The third term $\xi_i(t)$ represents the force generated by the thermal noise from the environment. Intracellularly the cytoplasm is filled with viscous material and a dense network of microtubules that generate a force on the organelle similar to the thermal noise, either colored or white noise, acting on a brownian particle in fluid. The last term $F_{ij}(t)$ is the interaction force between two particles labelled by the indices i and j respectively. The interaction force could depend on the absolute location $x_i(t)$ and $x_j(t)$ of the interacting particles or their relative separation or even on their velocities $v_i = \dot{x}_i(t)$. From this microscopic description of the particles dynamics one can derive macroscopic quantities like particle density, momentum density etc.

1.3.1.2 Population based approaches

This is a coarse grained method. One of the approaches might be to look at the density or cluster of the particles $n(\mathbf{x}, t)$ at a location \mathbf{x} . If particle conservation holds then one can write down a continuity equation:

$$\frac{\partial n}{\partial t} = -\nabla \cdot \mathbf{J} \quad (1.3)$$

where \mathbf{J} is the current density for the particle density n .

However, a distinguishing feature of traffic like collective phenomena is the formation of clusters. Clusters of individual particles form because of some sort of prevailing interactions between them. Size of clusters change over time as a result of different fluxes that bring in to or remove particle from a cluster. Intracellularly, aggregation phenomena is exhibited by both membrane bound structures like organelles as well as non-membranous structures like p-granules and nucleoli [20, 48, 49]. Traditional approach towards understanding such cluster forming process is writing down the corresponding master equation [120, 123]. Let us say that at any given time t the probability of finding a system of identical particles of cluster size \mathbf{n} is $P(\mathbf{n}, t)$. Here $\mathbf{n} = \{n_1, n_2, \dots, n_L\}$ denotes the set of parameters that describes the state of a cluster at a given time t . The master equation for such systems assuming the process to be Markov in nature is given by,

$$\frac{dP(\mathbf{n}, t)}{dt} = \sum_{\mathbf{n}' \neq \mathbf{n}} T(\mathbf{n}|\mathbf{n}'; t) P(\mathbf{n}', t) - \sum_{\mathbf{n}' \neq \mathbf{n}} T(\mathbf{n}'|\mathbf{n}; t) P(\mathbf{n}, t) \quad (1.4)$$

where, $T(\mathbf{n}|\mathbf{n}'; t)$ denotes the transition rates from state \mathbf{n}' to state \mathbf{n} .

1.3.2 Smoluchowski kinetic theory for aggregation

Classical kinetic theory of aggregation is a good model for studying traffic process in terms of the dynamics of cluster size of particles that constitute the traffic. Aggregation systems consists initially of unitary particles that interact with each other and form aggregates of higher order, see Fig.1.6 [41, 64, 123, 47, 51]. In a traffic, clusters of particles may represent aggregates. Aggregation process is usually described by the particle size distribution function $\varphi(\mathbf{n}_k, t)$, such that $dN = \varphi(\mathbf{n}_k, t) d\mathbf{n}_k$ denotes the number of particles in space at a given time t made up of elementary units in the range \mathbf{n}_k and \mathbf{n}_{k+dk} . Here $\mathbf{n}_k = \{n_k^1, n_k^2, \dots, n_k^L\}$ denotes the set of parameters that characterize a cluster k . For example, endosomes can be characterized by their luminal volume (quantified by the amount of fluorescence tagged cargo inside the organelle) or the surface area (quantified by the amount of one of the membrane proteins). Both of these (and others) can be plausible candidates for parameters given by \mathbf{n}_k that characterize an endosome. The elementary unit of a traffic would be a single particle, and therefore cluster is defined as composed of several k such elementary particles stuck together and behaving as one unit.

The master equation that describes the dynamics of the size distribution func-

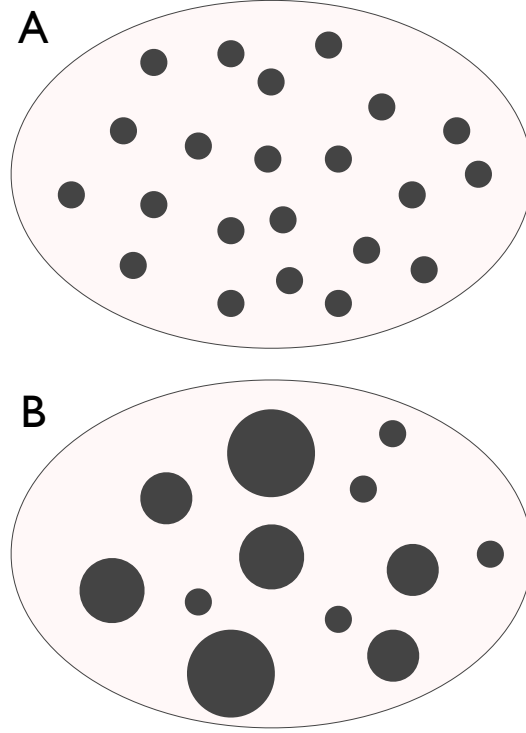


Figure 1.6: **Illustration of fusion dynamics of aggregating system of drops**

Aggregation system consists of similar particles of unitary size, lowest possible size in the system, at $t = 0$ as shown in (A). The size of a particle could be characterized by its volume, effective surface area (in case of non-spherical particles), specifically those features of a particle which are conserved during the fusion process. The particles undergo fusion resulting in a distribution of particles of various sizes, (B). The distribution evolves in time due to the fusion dynamics.

tion $\varphi_k(t)$ is given by,

$$\frac{d\varphi(\mathbf{n}_k, t)}{dt} = \frac{1}{2} \sum_{\substack{i+j=k \\ i=1}}^{i=k-1} \beta_{ij}(t) \varphi(\mathbf{n}_i, t) \varphi(\mathbf{n}_j, t) - \varphi(\mathbf{n}_k, t) \sum_{k=1}^{\infty} \beta_{ik}(t) \varphi(\mathbf{n}_i, t) \quad (1.5)$$

where, $\beta_{ij} = \beta(\mathbf{n}_i, \mathbf{n}_j; t)$ denotes the coagulation frequency function which could depend on various parameters associated with the aggregating particles as well as the system. The solution of Eq.(1.5) depends on the functional form of the coagulation frequency function β_{ij} . In 1917, Smoluchowski derived the expression for the coagulation frequency for Brownian coagulation and laminar shear. For the case of a system consisting of brownian particles,

$$\beta_{ij} = 4\pi(D_i + D_j)(r_i + r_j) \quad (1.6)$$

where D is the diffusion coefficient of the particles and r the corresponding radius. Using the Stokes-Einstein relation for the diffusion coefficient given by

$D = k_B T / (6\pi\mu r)$ in Eq.(1.5) one gets the coagulation frequency function for a inert spherical brownian particle,

$$\beta_{ij} = \frac{2k_B T}{3\mu} (r_i + r_j) (1/r_i + 1/r_j) \quad . \quad (1.7)$$

It important to point out here that the time dependance in the coagulation frequency function β_{ij} has been dropped because we assume that particles are in an infinite dilution, which is also necessary for the Stokes-Einstein relation. Solving Eq.(1.5) analytically for $\varphi(\mathbf{n}_k, t)$ using the general coagulation frequency function as given by Eq.(1.7) is impossible, so simplification based on assumptions are made to gain some basic understanding of the system under particular conditions.

1.4 Overview of this work

In the immediate next chapter we will present experiments wherein cargo distributions are quantified in a population of Rab5-positive endosomes using fluorescence microscopy. We discuss briefly experimental methods, steps involved in image analysis and finally some results of data analysis.

In the Third chapter we present a general theoretical framework that describes the collective dynamics of an endosomal population in a cell. Endosomal population here referring to endosomes belonging to any one particular compartment, i.e either early (Rab5 positive), late (Rab7 positive) or recycling (Rab4/11 positive) endosomes. In this chapter we limit our attention to only a population of early Rab5-positive endosomes. In our theoretical framework we take into account several microscopic processes at the level of individual endosomes.

In the Fourth chapter we present a simplified model of the general theoretical framework to describe cargo trafficking in Rab5-positive endosomes. We refer to this model as Entry-Fusion-Exit (EFE) model. In this model only three endocytic process are taken into account, namely the appearance of new cargo carrying Rab5-positive endosomes following endocytosis, homotypic fusion between the existing cargo carrying endosomes and conversion of cargo carrying Rab5-positive endosomes into other vesicular structures like Rab7-positive endosomes. With the cargo exit mechanism, we study the two hotly debated processes i.e endosome conversion and vesicle budding and discuss the presence of these processes in the trafficking of LDL by early Rab5-positive endosomes.

In the Fifth chapter we compare the results of Entry-Fusion-Exit model with the experiments wherein cargo in a population Rab5-positive endosomes was quantified in continuous cargo uptake experiments. We fit the theory to experimentally obtained cargo distributions at different times following endocytosis and extract

magnitude of key kinetic parameters. The experiments confirm scaling features predicted by theory.

Finally we conclude with Chapter six, with a discussion of what has been achieved through the approach presented in this thesis towards the understanding of endosomal trafficking and also an outlook of what can be done in the future.

Chapter 2

Dynamics of endosomal trafficking: experiments and observations

To develop an understanding of the endosomal trafficking of endocytosed cargo we will focus our attention on one specific population of endosomes, known as sorting or early endosomes. Basic concepts related to endosomes, their structure, morphology and function, are presented in the Introduction. An endosome is characterized either by endosomal membrane proteins or the endocytosed cargo that resides inside the endosome [19, 5, 11]. Sorting or early endosomes are characterized by a class of membrane protein Rab5, a GTPase protein that regulates the early endosomal fusion (see Introduction). In this chapter we will briefly present some experiments where cargo is quantified in a population of Rab5-positive endosomes. In these experiments, referred to as continuous uptake experiments, cells that are initially devoid of fluorescent cargo are supplied with fluorescently labelled cargo from a particular time onwards. Cells gradually internalize the fluorescent cargo molecules which subsequently enter and fill the Rab5-positive endosomal compartment. We will show that the cargo in individual Rab5-positive endosomes can be quantified in these experiments, and present distributions of different cargo types in a population of Rab5-positive endosomes at different times following the cargo uptake. The research work presented in this thesis is the result of a close collaborative effort with the experimental lab of Marino Zerial at the Max Planck institute of Molecular Cell Biology and Genetics (MPI-CBG), also located in Dresden. All the experiments presented here were performed by Roberto Villasenr and Claudio Collinet. The images obtained from automated fluorescence microscopy were analyzed for vesicle identification and colocalization of various endosomal markers with the help of *Motiontracking*, an image analysis software based on the algorithm developed by Yannis Kalaidzidis, who is also based at MPI-CBG [40].

This Chapter is by no means an exhaustive information about the experimental methods. The aim here is to just give an idea of some of the major steps involved in the experiments and image analysis. Experiments discussed here and the image analysis involve far more complexity than described here, as great care has to be taken in performing such experiments for the validity of results to make careful comparisons with theory.

2.1 Cargo trafficking by endosomes - experiments to theory

Endosome visualization is made possible by the developments in the Green Fluorescent Protein (GFP) Technology. By tagging proteins associated with an endosome with specific fluorescent proteins, we can identify and track endosomes and quantify their characteristics. In vitro time course experiments, wherein endosomal marker proteins express GFP, provide a great means to study and understand the dynamics of endosomes. Since endosomes are carriers of majority of the endocytosed cargo, therefore using fluorescently labelled cargo in experiments wherein cargo is internalized into the cells and subsequently delivered to a population of endosomes is great way to not only understand the dynamics of endosomes but also the dynamics of cargo trafficking by endosomes.

2.1.1 Endosome marker - Identifying an endosome

Endosome identification is the first step towards obtaining any kind of statistical data from endosomal population. Endosomes can be identified when one of the endosome associated protein expresses fluorescence, which is possibly only by tagging such proteins with fluorescent proteins. Now, the endosome associated proteins can be either membrane proteins that reside on the outer membrane of an endosome or the internalized cargo molecules that resides in the interior or lumen of the endosome . Here we will focus only on the early endosomes, which are characterized by a particular class of membrane proteins, Rab5 (for details see Introduction). To limit our observance in experiments to only Rab5-positive endosomes we will use cells that express GFP-Rab5. We will follow fluorescent cargo in only those endosomes that are fluorescent in Rab5.

2.1.2 Cargo uptake experiments

To study the cargo trafficking by Rab5-positive early endosomes we performed cargo uptake experiments. The cargo used in these experiments was Low Density Lipoprotein (LDL), a class of proteins that enables transport of cholesterol in

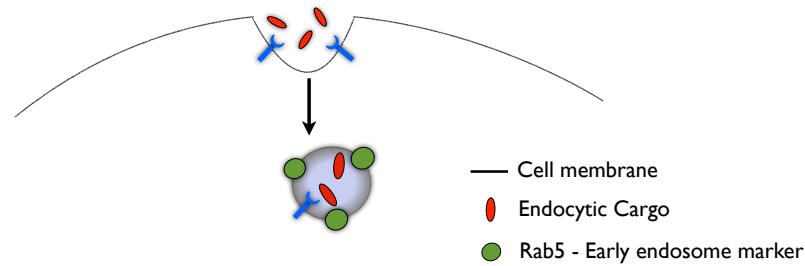


Figure 2.1: **Labelling an endosome - endosome marker**

Schematic representation of endocytosis of cargo molecules (red). Following endocytosis, the cargo is delivered to Rab5-positive early endosomes. Rab5 (green) is a membrane protein that resides on the outer membrane of the endosome and regulates among other things the fusion of Rab5-positive endosomes with each other. The endocytosed cargo resides in the lumen or inner volume of the endosome.

the water-based blood stream. Following endocytosis, LDL is delivered to Rab5-positive early endosomes where they are sorted to be predominantly delivered to Rab7-positive late endosomes for degradation in lysosomes. In these experiments two fluorescent markers were used to identify endosomes, namely Rab5, the early endosome membrane marker expressing green fluorescence and LDL (Low Density Lipoprotein), an endocytic cargo that resides inside the early endosomes, tagged with red fluorescent protein.

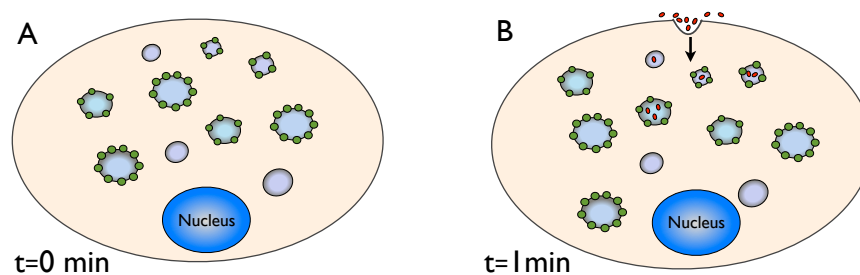


Figure 2.2: **Continuous cargo uptake experiment**

(A) Schematic representation of cell with a population of Rab5-positive early endosomes and other non Rab5-positive vesicular structures. Initially at $t = 0$ minutes, there is no fluorescently labelled cargo present inside the cell.

(B) The cells are incubated in a pool of fluorescently labelled cargo LDL. The cargo enters the cell via receptor-mediated endocytosis and is subsequently delivered to Rab5-positive early endosomes and other intracellular organelles. With time, the population of Rab5-positive endosomes is gradually filled with LDL.

Initially at $t = 0$ min there is no cargo inside the cell, Fig.2.2(A). Starting from a fixed time $t = 1$ min, the cells are incubated in a medium containing cargo molecules, LDL tagged to red fluorescence proteins. Cells are allowed to internalize cargo for different durations of time, after which they are fixed for

image acquisition. Gradually the endosomal compartment gets filled with LDL as more and more Rab5-positive endosomes attain cargo and thus become both Rab5 and LDL-positive endosomes, Fig.2.2(B). A general scheme of the continuous cargo uptake experiments with the various steps (broadly speaking) involved is described schematically in Fig.2.3.

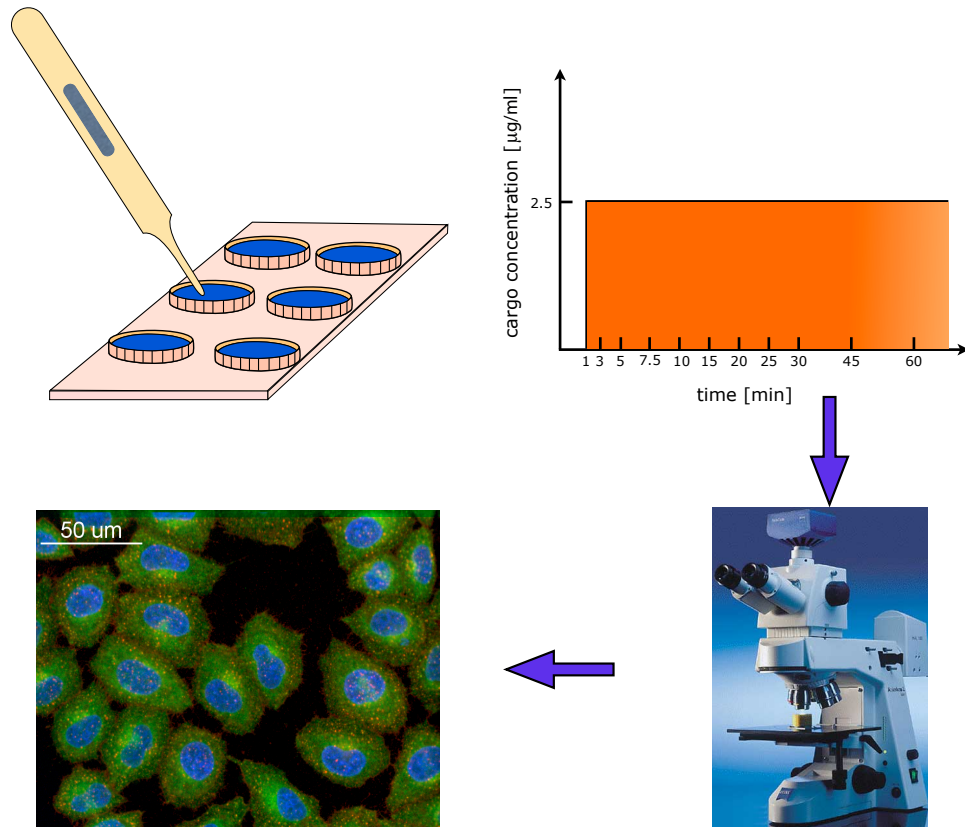


Figure 2.3: Continuous cargo uptake experiments - method

(A) HeLa cells expressing GFP-tagged Rab5c were grown in full medium in 96-well plates for 24 hrs.

(B) At different time points a dilution of fixed concentration of LDL was added sequentially to the cells. The cells were incubated in the dilution of LDL for a varying period of time, from 1 min up till 60 min.

(C) After the time course, all cells were fixed simultaneously stained with anti-apoB for LDL and DAPI for labeling the cell nuclei. The cells were then imaged using an automated confocal microscope.

(D) One hundred images per time point were collected. An image contains in average 20 cells.

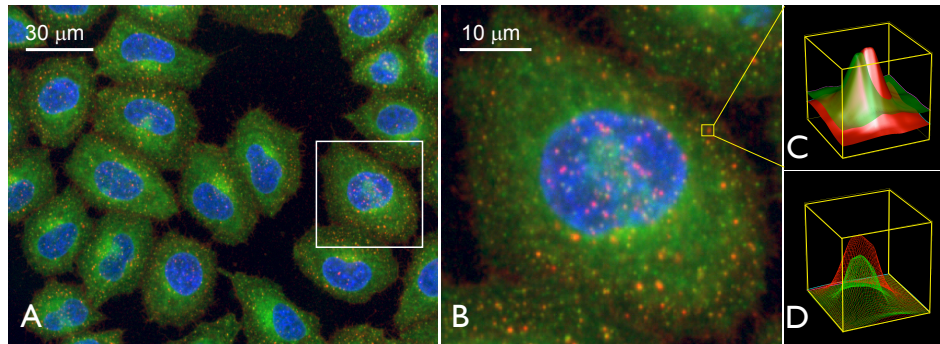


Figure 2.4: **Automated fluorescence microscopy and image processing**

(A) Representative image of HeLa GFP-Rab5c BAC cells after 60 minutes internalization of LDL. GFP-Rab5c (green) is expressed under control of the endogenous Rab5 promoter; human LDL (red) is labeled by an antibody against apo-B; nuclei (blue) are labeled by DAPI.

(B) Higher magnification of a single cell. High-resolution images allow for the identification of individual endosomes. Statistical analysis was carried out for endosomes containing both GFP-Rab5c (green) and LDL (red).

(C-D) Vesicle fitting of an individual endosome by Motion-Tracking image analysis software [20]. The GFP-Rab5c (green) and LDL (red) raw fluorescence intensity profile (C) are used to fit a model function (D) given by Eq.(2.1) from which vesicle parameters (x - y coordinates, integral intensity, area) are quantified.

2.1.3 Image analysis - Statistics of endosomal population

After acquiring images of the cells with various endosomal markers using the confocal/laser scanning microscope (LSM), the next major step, towards obtaining some kind of statistical information from the experiments, is that of Image analysis. An example of an image acquired after the microscopy is shown in Fig.2.4(A). Each cell consists of fluorescent spots of different endosomal markers, which in these experiments are Rab5 and LDL (cargo). Rab5, the early endosome membrane protein is expressing green fluorescence and the endocytosed cargo LDL is tagged to red fluorescent protein, thus it appears in red color in the image, Fig.2.4(B). Image analysis consists of identifying the fluorescent spots that appear in the image and quantifying the various characteristics associated with it, like number of fluorescent spots of a given type or color, position (x - y coordinates) of the fluorescent spots, total spot area, total fluorescence intensity of the spot etc. The image analysis is carried out using the algorithm developed by Yannis Kalaidzidis at the MPI-CBG. The algorithm identifies all the fluorescent spots both green (Rab5) and red (LDL) independently. The fluorescence intensity, FI is measured

in arbitrary units.

$$I(x_i, y_i) = A_i \left\{ 1 + \left(\left[\frac{(x - x_i) \cos(\alpha_i) - (y - y_i) \sin(\alpha_i)}{w_i} \right]^2 + \left[\frac{(x - x_i) \sin(\alpha_i) - (y - y_i) \cos(\alpha_i)}{h_i} \right]^2 \right)^2 \right\}^{-1} + B(x_i, y_i) \quad (2.1)$$

where, $I(x_i, y_i)$ is the fluorescence intensity at the coordinate x_i, y_i and A_i is the fluorescence intensity at the centre. w_i, h_i is the width by perpendicular dimensions, α is the angle between main axis and the image axis, $B(x_i, y_i)$ is the background residue in the vicinity of the particle. The result of the fit of the model function to the fluorescence intensity profile for one such profile of Rab5 (green) and LDL (red) is shown in Fig.2.4 (C-D).

2.1.4 Number density distribution: individual endosome statistics

The whole intensity interval $[I_{min}, I_{max}]$ is logarithmically binned into N_b number of bins, such that a given bin of intensity is placed at

$$I_k = I_{min} e^{\gamma k} \quad , \quad (2.2)$$

where $\gamma = (\ln(I_{max}/I_{min}))/N_b$ and the bin-width between two bins on the intensity axis is $\Delta I = I_{k+1} - I_k$. The algorithm detects the endosomes with Rab5 and LDL fluorescent spots and quantifies their characteristics (position, area, elongation, fluorescence intensity, etc.) and counts the number of spots

$$N_{rab5/LDL}(I) \quad , \quad (2.3)$$

in all the images with integral fluorescence intensity of either Rab5 or LDL in the range $[I, I_k + \Delta I]$. We thus obtain a histogram of the number of endosomes (Rab5 or LDL) *versus* the integral fluorescence intensity I . From the histogram we obtain the number density of endosomes per cell with a certain amount of fluorescence intensity I of either Rab5 or LDL as follows,

$$n(I) = \frac{N(I)}{N_{cell} V \Delta I} \quad (2.4)$$

where, N_{cell} is the number of cell in a given sample or image and V the associated cell cytoplasmic volume of each cell. For each time point we obtain about 70

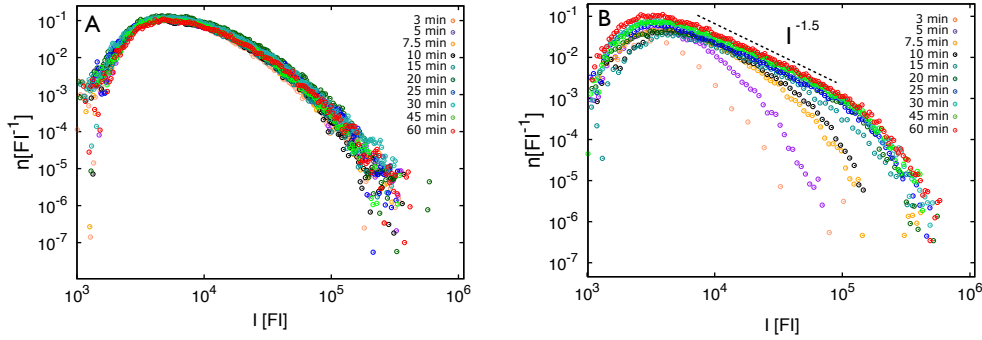


Figure 2.5: Distribution of endosomal fluorescence intensity of Rab5 and LDL. $n(I)$ is the number density of endosomes carrying an amount I of a particular endosomal marker. Integral fluorescence intensity, FI is measured in arbitrary units. **(A)** Distribution of total Rab5 fluorescence intensity of vesicles in the whole cell at different times. Vesicles carrying membrane protein Rab5 are characterized as Rab5-positive early endosomes. **(B)** Distribution of total LDL fluorescence intensity of vesicles in the whole cell, which would include not only endosomal compartments but also other intracellular compartments in the cell where LDL might be present, at different times after addition of LDL.

images. Each image consists about 20-30 cells. We collect the statistics for each time point averaged over all the images. Fig.2.5(A-B) presents the number density distribution of Rab5 and LDL integral fluorescence intensities in the whole cell at different times during the course of LDL uptake. As can be observed, the Rab5 distribution, Fig.2.5(A) is always at steady state, since Rab5 is not an endocytic cargo but a membrane protein of early endosomes and it's amount inside the cell is always fixed. However, LDL is an endocytic cargo and therefore LDL distribution inside the cell evolves during the period of it's uptake, Fig.2.5(B). Interestingly, LDL distribution $n(I)$ at late times, around 60 minutes, shows a prominent power law decay with a decay exponent ~ -1.5 , Fig.2.5(B).

2.1.5 Integral quantities: endosome population statistics

Fig.2.5(A & B) tells how Rab5 and LDL cargo are distributed in individual endosomes and other vesicular structures inside the cell. From the distribution $n(I, t)$ shown in Fig.2.5(A & B), we can also obtain two other quantities,

$$N(t) = \sum_{I=I_{min}}^{I_{max}} \Delta I n(I, t) \quad (2.5)$$

$$\Phi(t) = \sum_{I=I_{min}}^{I_{max}} \Delta I I n(I, t) \quad (2.6)$$

where, N is the total number of LDL or Rab5 vesicles (identified during the image analysis) and Φ is the total amount of LDL or Rab5 in all these vesicles. These two quantities, N and Φ respectively, reflect the average or global properties of endosomal network. Following endocytosis the amount of LDL inside the cell increases from 1 minute onwards up till 60 minutes, Fig.2.6(A). The data shows almost a linear growth until 30 minutes followed by a slow saturation. In contrast to the total amount of LDL, the number of LDL carrying vesicles, N reaches a saturation as early as 20 minutes from the start of LDL uptake, Fig.2.6(B).

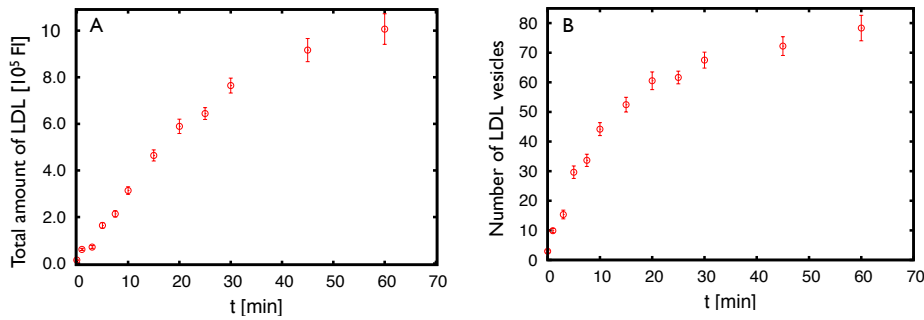


Figure 2.6: **Integral properties of endosomal population**

(A) Total amount of LDL Φ , defined as Eq.2.6, in the whole cell during the course of cargo (LDL) uptake.

(B) Total number of LDL vesicles N , defined as Eq.2.6 during the course of cargo uptake.

2.1.6 LDL in early endosomes - Colocalization

Up until now we had considered the statistics of LDL cargo in the whole cell. In this section we will look at number density distribution of LDL during the time course confined to only Rab5-positive early endosomes. To obtain the statistics of LDL in only Rab5-positive endosomes we identify those endosomes that colocalize both the Rab5 and LDL.

As discussed earlier, the image analysis algorithm detects the fluorescent spots of Rab5 and LDL, Fig.2.7(A-B). For endosomes to be double-positive to LDL and Rab5, the area of the Rab5 fluorescent spot has to overlap by more than 40 % of the area of LDL, Fig.2.7(C). After testing the endosomes for double-positive to both Rab5 and LDL as described in the previous section we can obtain the number density distribution of LDL only in Rab5-positive endosomes. Fig.2.8(A) shows the LDL distribution in Rab-positive endosomes. The total amount of LDL Φ in the Rab5-positive endosomal population is presented in Fig.2.8(B). Since only endosomes which are Rab5-positive interact with each other, the Rab5-positive

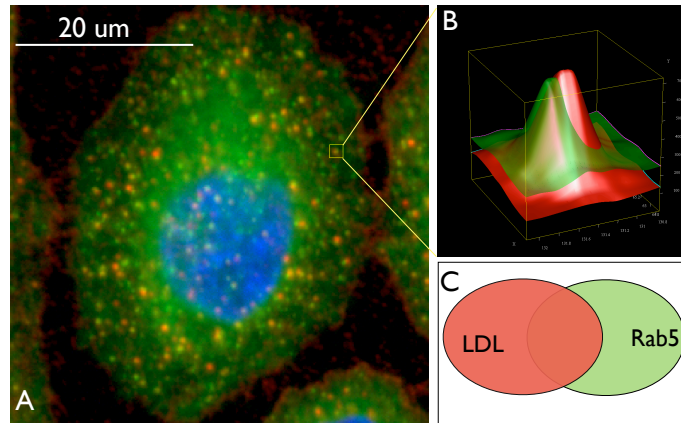


Figure 2.7: **Colocalization of endosomal markers**

(A-B) The image analysis algorithm detects the fluorescent spots of Rab5 and LDL in the cell. The intensity profile is fitted to a model function given by Eq.2.1 as shown in (B).
 (C) A Rab5-positive endosome is colocalized to LDL only if more than 40 % of the area of Rab5 fluorescent spot is covered by LDL.

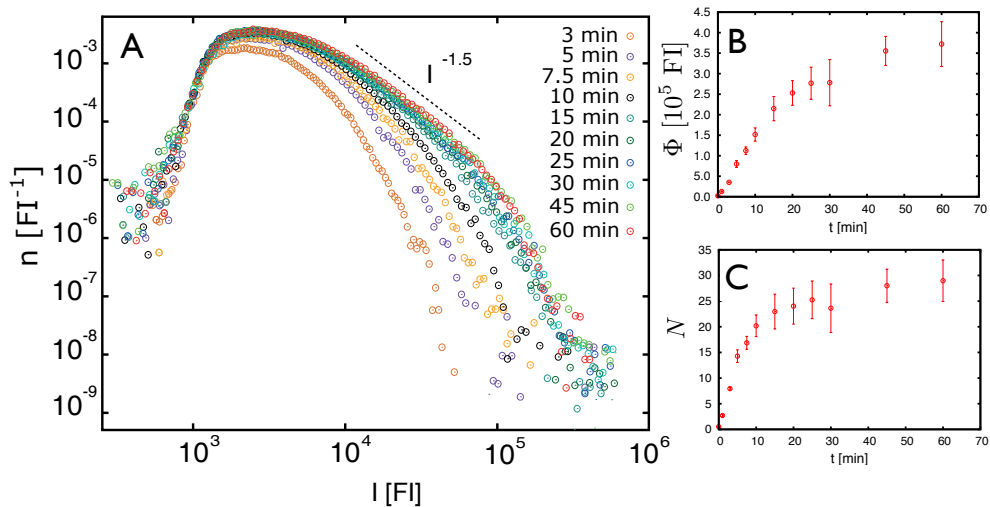


Figure 2.8: **Time course of distribution of LDL in Rab5-positive endosomal population.**

$n(I)$ is the number density of endosomes carrying an amount I of LDL.

(A) Time evolution of number density distribution of LDL only in Rab5-positive endosomes.

(B) Time evolution of total amount of LDL Φ , defined as Eq.2.6, in Rab5-positive endosomal population.

(C) Time evolution of total number N of LDL carrying Rab5-positive endosomes, defined Eq.2.6.

endosomal population forms a closed system with the influx of cargo via endocytosis and outflux of cargo to other populations of mutually interacting endosomes, like late and recycling endosomes.

2.2 Conclusion

In this chapter we discussed briefly the continuous cargo uptake experiment. We specifically looked at experiments in which Low Density Lipoprotein (LDL) was used as cargo. LDL is predominantly sorted in early endosomal compartment to be delivered to late endosomes and eventually degraded in lysosomes. We discussed the steps involved in image and data analysis and looked at the experimental data for total LDL and Rab5, both being markers of an endosome. For obtaining the statistics of LDL in Rab5-positive endosomes we discussed the method of colocalization of Rab5 and LDL. A Rab5-positive endosome was colocalized to LDL if the area of fluorescence spots of the two markers overlapped more than 40 %. Even though the total amount of LDL in the cell, irrespective of any specific intra-cellular compartment, was growing even up till 60 minutes, the LDL amount in only Rab5-positive early endosomal compartment seemed to converge to a steady state much earlier. This suggests that the early endosomal compartment can be thought of as a closed compartment where fluxes of cargo constantly bring in and remove the cargo from the compartment, which eventually would lead the system to relax to a steady state. The steady state distribution of LDL in Rab5-positive endosomal population has a characteristic shape. The distribution exhibits power law decay in the intermediate LDL intensity ranges and decays much faster beyond some intensity value. What processes shape the LDL distribution at steady state and describe its time evolution? Can we learn something about the endosomal trafficking from these distributions? This will be the goal of the next chapters. To build a self consistent theoretical framework to describe dynamics of trafficking of endosomal markers and to understand how they relate to the underlying dynamics of endosomes.

Chapter 3

Physical description of endosomal dynamics

In this chapter we present a theory, a mathematical framework that describes the collective dynamics of an endosomal population in a cell. By an endosomal population we mean endosomes belonging to any one particular compartment, i.e either early (Rab5 positive), late (Rab7 positive) or recycling (Rab4/11 positive) endosomes. As a novelty compared to existing approaches, in addition to influx and outflux of cargo, in our theoretical description we study the endosomal dynamics by taking into account several microscopic processes at the level of individual endosomes. In this chapter we will limit our attention to only a population of Rab5-positive early endosomes. However, the theory is very general and can be applied to any other endosomal compartment (i.e early, late or recycling) with a population interacting endosomes. We will start off by first developing the theory wherein a Rab5-positive endosome is characterized by only the amount of membrane bound protein, Rab5. We refer to this as one component description (Section 3.1). To study trafficking of endocytosed cargo by a population of Rab5-positive endosomes, we then extend our framework to two component description. In this description the state of an endosome is characterized by not only the amount of the membrane protein, Rab5, but also by the amount of endocytosed cargo it carries (see Section 3.2). We will then show that the two component description can be effectively reduced to that of one component, i.e cargo in only Rab5-positive endosomes (see Section 3.3).

3.1 Dynamics of early endosomes

In our description presented here, we consider the endosomal membrane protein Rab5 as the endosomal marker. The state of the population of early endosomes at

a time t is characterized by $n(c, t)$, which defines the number density of endosomes per cell with c number of Rab5 molecules. More precisely, $n(c)\Delta c$ is the number of endosomes per cell for which the amount of Rab5, c is in the interval between c and $c + \Delta c$. The variable c is a continuous entity and is directly proportional to the total fluorescence intensity of the fluorescently tagged Rab5 molecule. The dimension of $n = 1/([V][s])$, where $[V]$ is the cytoplasmic volume of the cell.

§ **Notation:** Within the length and the breadth of this thesis we will often refer to an early endosome with c number of Rab5 molecules as a c -endosome. We will call such an endosome as being in the state c .

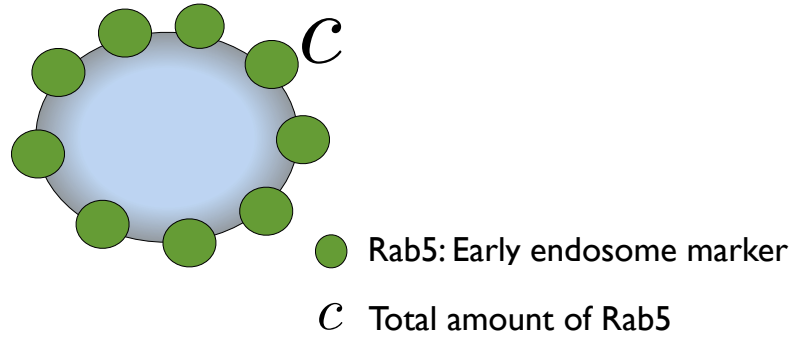


Figure 3.1: **Characterization of the state of an endosome.**

The state of an endosome at a given instant of time t is characterized by the number of Rab5 molecules c it carries.

The total number of Rab5-positive endosomes is denoted by N_c

$$N_c = \int_0^{\infty} n(c)dc \quad (3.1)$$

and the total amount of endosome components is denoted by Φ_c

$$\Phi_c = \int_0^{\infty} c n(c)dc \quad . \quad (3.2)$$

The change over time of $n(c)$ reflects the collective dynamics of early endosomes. Our description is based on the idea that the distribution of Rab5 in early endosomal population is shaped by endosome fusion and fission in addition to the in-flux and out-flux of Rab5. The evolution of the distribution over time is described by a general kinetic equation for the Rab5 distribution $n(c)$ which accounts for all the key processes governing the endosomal interaction (see Fig.3.2). The parameters that enter this kinetic equation are the rates at which each one of these

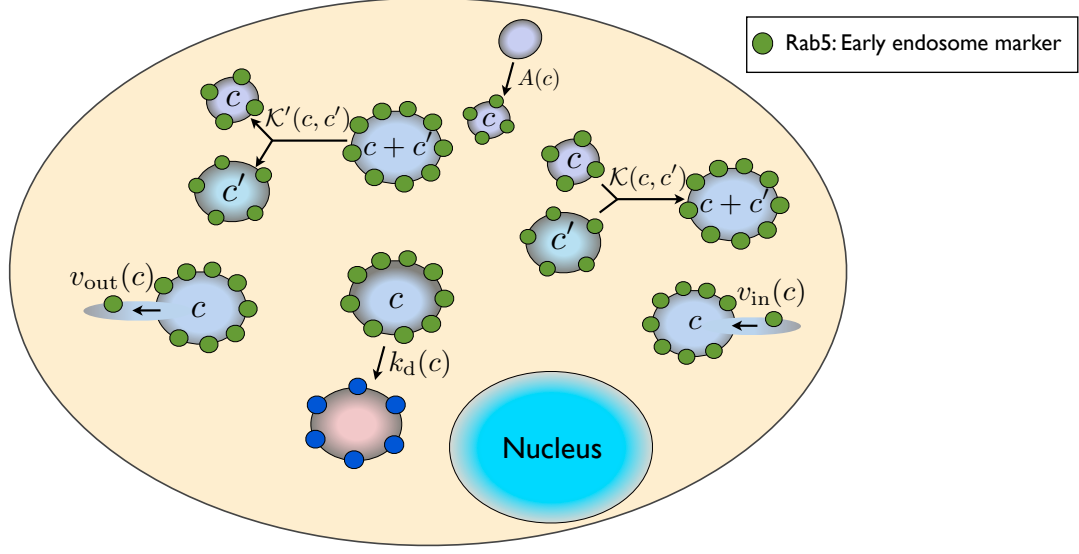


Figure 3.2: **Dynamics of Rab5 endosomes**

Figure shows various process involved in endosomal trafficking. Rab5-positive endosomes collectively form a population of interacting endosomes. The state of the endosomal network is described by the number $n(c, t)dc$ of endosomes per cell, carrying the amount of Rab5 in the interval between c and $c + dc$ at time t . $n(c, t)$ changes due to various endosomal interaction processes given in Eq.(3.3). The various processes are discussed in detail in the Section 3.1.1.

processes occurs.

$$\begin{aligned}
 \frac{\partial n(c, t)}{\partial t} &= \frac{1}{2} \int_0^c K(c', c - c') n(c', t) n(c - c', t) dc' - \int_0^\infty K(c, c') n(c, t) n(c', t) dc' \\
 &+ \int_0^\infty K'(c, c') n(c + c', t) dc' - \frac{1}{2} \int_0^c K'(c', c - c') n(c, t) dc' \\
 &+ A(c) - k_d(c) n(c, t) - \frac{\partial}{\partial c} (v_{in}(c) n(c, t)) + \frac{\partial}{\partial c} (v_{out}(c) n(c, t))
 \end{aligned} \tag{3.3}$$

This equation is a generalization of the Smoluchowski coagulation equation [41]. Similar equations have been studied theoretically in a variety of problems such as colloidal aggregation, polymerization, self-assembling and droplet coalescence [64, 42, 43, 45, 47, 44, 49].

3.1.1 Exchange processes

The general kinetic equation, given by Eq.(3.3), takes into account various microscopic processes that might be involved in the endosomal trafficking. Each para-

metric function that appears in the general kinetic equation represents a physical process. The functions are as follows:

$$K(c, c'), K'(c, c'), A(c), k_d(c), v_{\text{in}}(c), v_{\text{out}}(c) \quad .$$

These parametric functions can assume varied form of dependency on the variable c , that represents the total amount Rab5 that an endosome carries. In this section we will discuss as to what each term that enters Eq.(3.3) might biologically correspond to in the context of endosomal trafficking.

(1) Endosome fusion and fission

Endosomes are highly dynamic structures that regularly undergo fusion or fission with each other. During fusion and fission events, the total number of endosomal components, in the present case being Rab5, is conserved.

(A) Fusion: In our mean-field description Eq.(3.3), the increment of the mean density of endosomes with c number of Rab5 molecules, $n(c)$, per time unit, due to fusions corresponds to

$$-n(c, t) \int_0^\infty dc' \mathcal{K}(c, c')n(c', t) + \frac{1}{2} \int_0^c dc' \mathcal{K}(c', c - c')n(c', t)n(c - c', t) \quad (3.4)$$

Two endosomes, each carrying c and c' amount of Rab5 respectively, fuse at the rate $\mathcal{K}(c, c')$ to form a new endosome which carries $c + c'$ components (Fig.3.2). A big assumption that has been made here is that the rate $\mathcal{K}(c, c')$ is independent of time which follows from assuming that endosomes of different sizes c are well mixed inside the cell. It has been observed that early endosomes have a high capacity for homotypic fusion [19]. Fusion of an endosome belonging to one class

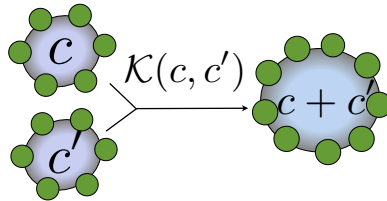


Figure 3.3: **Schematic representation of endosome-endosome fusion**

with an endosome of another class or the fusion of an endosome with any other intracellular structure is referred to as "*absorption of components or material*"

(see **(3)**). In the description the endosome-endosome interaction leading to their fusion into one cluster is an instantaneous process without failure. The quantity,

$$\int_0^\infty ds' \mathcal{K}(c, c') n(c', t) \quad , \quad (3.5)$$

is the rate at which average fraction of endosomes in the state c undergo a fusion. The fusion rate kernel is symmetric and non-negative: $\mathcal{K}(c, c') = \mathcal{K}(c', c) > 0$. The first term of Eq.(3.4) denotes the loss in the density of c -endosomes per unit time due to fusion of an c -endosome with any other endosome. The second term denotes the gain in the density of c -endosomes produced by the fusion of a c' -endosome and a $c - c'$ -endosome per time unit. Much of the literature on this subject of coagulation processes has been devoted to studying the analytical solution of the coagulation equation for various fusion kernels. A good review where various functional forms of the fusion kernels are dealt with a good mathematical treatment can be found in [51, 64].

(B) Fission: The increment of the mean density of c -endosomes, $n(c)$, per time unit, due to fission events corresponds to

$$-\frac{1}{2}n(c, t) \int_0^c dc' \mathcal{K}'(c', c - c') + \int_0^\infty dc' \mathcal{K}'(c, c') n(c + c', t) \quad . \quad (3.6)$$

The quantity,

$$\mathcal{K}'(c, c') \quad , \quad (3.7)$$

is the rate at which an endosome carrying $c + c'$ amount of Rab5 undergoes fission

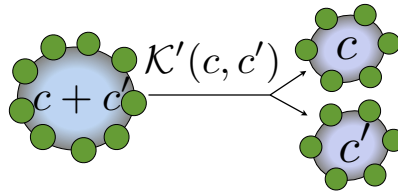


Figure 3.4: **Schematic representation of endosome fission**

and thereby redistributes the Rab5 into two newly formed endosomes (Fig.3.2). The Rab5 molecules may be distributed symmetrically, asymmetrically or in some other arbitrary fashion into the the two newly emerging endosomes. Such processes can be represented by choosing an appropriate fission kernel. If the fission of a Rab5-positive endosome creates an endosomal structure that is not positive to Rab5 then it is referred to as "*release of materials*" (See **(3)**). The first term

of Eq.(3.6) accounts for the loss in the density of c -endosomes when they divide. The second term represents the gain in the density of c -endosome resulting from the fission of $(c + c')$ -endosomes.

§ **Fusion and Fission conserve endosomal components:** If we define the i^{th} moment of the number density of s -endosomes, $n(c, t)$, as:

$$\int_0^\infty c^i n(c, t) dc = M_i \quad (3.8)$$

The time evolution of $M_i(t)$ because of fusion and fission processes, regardless of the specific functional form of their kernels $\mathcal{K}(c, c')$ and $\mathcal{K}'(c, c')$, can be written down as:

$$\frac{dM_i}{dt} = \frac{1}{2} \int_0^\infty dc' \int_0^\infty dc [\mathcal{K}(c, c') n(c, t) n(c', t) - \mathcal{K}'(c, c') n(c+c', t)] [(c+c')^i - c^i - c'^i]. \quad (3.9)$$

For the first moment, $i = 1$,

$$\frac{dM_1}{dt} = 0 \quad . \quad (3.10)$$

The first moment M_1 is the same as Φ ,

$$M_1(t) = \Phi(t) = \int_0^\infty c n(c, t) dc \quad (3.11)$$

which denotes the total amount of components in the endosomal network at time t . Therefore, Eq. (3.10) implies that fusion and fission process conserve the endosomal components in the network at any time t .

(2) Endosome appearance and conversion

The endosomal membrane comprises of several membrane-bound proteins (for detailed discussion see Chapter 2). These proteins are not randomly distributed on the membrane but organized in domains. Even though the endosomal compartments are clearly characterized by specific membrane proteins, it has been observed and thus argued that the boundaries between some compartments are blurred at molecular level, in part because some of the key membrane proteins are often found in more than one compartment. A possibility could be that an endosome remodels its membrane protein composition and change its type from one compartment or class to another. Infact it has been reported that such a remodeling of the membrane protein composition does occur [20]. In the study

the authors performed in-vivo tracking of a Rab5-positive early endosome and observed that the fluorescence intensity of Rab5 on the early endosome gradually decreased until there was no Rab5 on the membrane of that endosome. The loss of Rab5 from the endosome membrane was concomitantly followed by increase in the Rab7 fluorescence. Rab7 is a membrane protein that characterizes the late endosomes. This suggests that a Rab5-positive endosome can undergo remodelling of the membrane proteins and

(A) Endosome appearance: New Rab5-positive endosomes can appear via different ways, which can be broadly summarized as follows:

(1) Following endocytosis the cargo carrying endocytic vesicles gain Rab5 and thus convert into Rab5-positive endosomes. Therefore, new Rab5-positive endosomes carrying cargo appear immediately following endocytosis. One could think that such vesicles might be the smallest in size, as they have not undergone any fusion at that instance.

(2) Some Rab5-positive early endosomes with low amount of Rab5 may go undetected by fluorescence microscopy or during image analysis, because their total fluorescence intensity falls below the threshold limit for identification by fluorescence microscopy. Several such undetected endosomes may fuse with each other regularly and instantaneously appear, only because their total fluorescence intensity crosses the minimum threshold for detection.

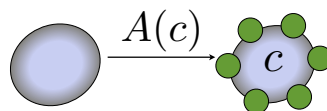


Figure 3.5: **Schematic representation of endosome appearance**

All these processes would result in the appearance of new Rab5-positive endosomes. We denote by

$$A(c) \quad , \quad (3.12)$$

the gain in the density of c -endosomes per unit time due to the appearance of new Rab5-positive endosomes. As can be seen, both of the aforementioned possibilities for endosome appearance result in appearance of relatively small sized of endosomes. Thus one can think of modelling $A(c)$ by a function confined to only small

c and rapidly vanishes for large c . We write,

$$A(c) = A_0 \zeta(c) \quad (3.13)$$

where A_0 is the flux of cargo that enters the early endosomal network due to newly appearing endosomes. $A(c)$ should be bounded and thus should satisfy the following normalization condition,

$$\int_0^\infty ds A(c) = A_0 \quad , \quad (3.14)$$

$$\int_0^\infty dc c^n A(c) = A_0 s_0^n \quad . \quad (3.15)$$

(B) Endosome conversion or disappearance: The ability of an endosome to remodel its membrane protein composition could not only lead to appearance of new endosomes in an endosomal population, but it could also lead to their disappearance from that population. We refer to such processes as *endosome*

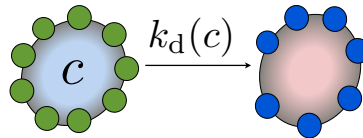


Figure 3.6: **Schematic representation of endosome conversion**

conversion or *disappearance*. One example is the early to late endosome conversion. In the early to late endosome conversion, an early endosome which is Rab5-positive loses its membrane-bound Rab5 molecules instantaneously, and subsequently gains Rab7 molecules, and thus appear as late endosome. This has been reportedly observed in experiments [20, 26]. We denote by,

$$k_d(c) \quad (3.16)$$

the loss in the density of c -endosomes per unit time.

The net increase of the density of s -endosomes per unit time due to appearances and conversions of endosomes, can be written as the balance of the appearance rate, $A(s)$, and the conversion rate, $k_d(s)$,

$$A(c) - k_d(c). \quad (3.17)$$

(C) Absorption and release of components by endosomes

An endosome can change or alter its number of Rab5 molecules not only by undergoing fusion and fission with other endosomes but also by absorbing or releasing Rab5 from or to external sources respectively. Rab5 is present in the cell cytoplasm in the inactive state but can bind to an endosome and be active. The exchange of material by absorption or release can occur by two processes:

(1) Rab5 is a membrane bound protein and resides on the outer surface of the membrane of an endosome. Rab5 is also present in the cell cytosol in the inactive form and therefore undergoes regular exchange with Rab5 on the endosome membrane.

(2) Another possibility might arise wherein endosomal structures carrying very low amount of Rab5, therefore undetected, fuse with already detected endosomes.



Figure 3.7: Schematic representation of (a) absorption and (b) release of Rab5 molecules by an endosome.

Average number of Rab5 molecules absorbed or released by a c -endosome, per unit time is denoted by, $v_{\text{in}}(c)$ and $v_{\text{out}}(c)$, respectively. The total flux of Rab5 towards the population of endosomes in the state c is then given by,

$$j(c, t) = n(c, t)(v_{\text{in}}(c) - v_{\text{out}}(c)). \quad (3.18)$$

In other words, $j(c, t)$ is the mean density of endosomes that grow from the state c to $c + dc$ per unit time.

3.1.2 Endosomal number and components balance

The endosomal network is a dynamic system in which new Rab5-positive endosomes appear and disappear regularly and there is a flux of Rab5 molecules into and out of the endosomes. One can write down the balance relations for total number of Rab5-positive endosomes, already defined as in Eq.(3.1), and the total amount of Rab5, Eq.(3.2) in the whole early endosomal network respectively.

The equation for the total endosome number balance is given by,

$$\begin{aligned} \frac{dN_c}{dt} = & \frac{1}{2} \int_0^\infty \int_0^\infty dc dc' \mathcal{K}'(c, c') n(c + c', t) + \int_0^\infty dc A_+(c) \\ & - \frac{1}{2} \int_0^\infty \int_0^\infty dc dc' \mathcal{K}(c, c') n(c, t) n(c', t) - \int_0^\infty dc k_-(c) n(c, t) \end{aligned} \quad (3.19)$$

The relation for the total amount of endosomal components balance is given by,

$$\begin{aligned} \frac{d\Phi_c}{dt} = & \int_0^\infty dc n(c, t) v_{\text{in}}(c) + \int_0^\infty dc A_+(c) c \\ & - \int_0^\infty dc n(c, t) v_{\text{out}}(c) - \int_0^\infty dc k_-(c) n(c, t) c \quad . \end{aligned} \quad (3.20)$$

One can see from Eq.(3.19) and Eq.(3.20), that the fusion and fission events respectively contribute to the loss and gain of the overall endosome number but do not affect the total amount of endosomal components in the network. Whereas, absorption and release of components respectively increases and decreases the total amount of component in the network but does not change the number of endosomes. The appearance and conversion of endosomes respectively, affects both the number of endosomes and the amount of components.

3.2 Two component description: Rab5 plus Cargo

In the previous section we had introduced theoretical description for dynamics of Rab5-positive endosomes, in the absence of any cargo. We will now extend our description to include dynamics of cargo in the endosomes as well. Most of the cargo endocytosed into the cell at first ends up in Rab5-positive early endosomes. From here it is sorted to other intracellular compartments. Now, in order to study the trafficking of cargo in a population of Rab5-positive early endosomes we need to account for both, the amount of Rab5 on an endosome as well as the amount of cargo carried by it. In our theoretical description up till now, we had characterized the state of an endosome by only its amount of Rab5 c . We introduce another quantity

$$s \quad (3.21)$$

that denotes the amount of cargo or number of cargo molecules an endosome carries. Therefore,

$$n(c, s; t) \quad (3.22)$$

the number density of endosomes per cell carrying c number of Rab5 molecules and s number of cargo molecules at a time t . More precisely, $n(c, s; t) \Delta c \Delta s$ is the

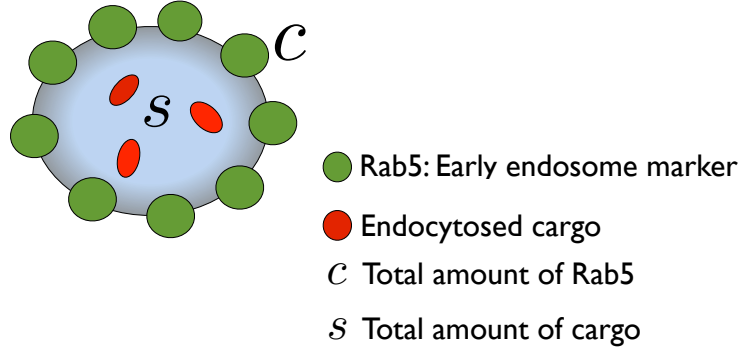


Figure 3.8: **Characterization of the state of an endosome in two component description.**

The state of an endosome at a given instant of time t is characterized by the number of Rab5 molecules c and cargo molecules s it carries.

number of endosomes per cell for which the amount of Rab5, c is in the interval between c and $c + \Delta c$ and the amount of cargo s is in the interval s and $s + \Delta s$. In the same spirit as in the previous section, we will now extend Eq.(3.3) to include cargo as the endosomal marker too.

$$\begin{aligned}
 \frac{\partial n(c, s; t)}{\partial t} = & \frac{1}{2} \int_0^s ds' \int_0^c \mathcal{K}(c', s'; c - c', s - s') n(c', s'; t) n(c - c', s - s'; t) dc' \\
 & - \int_0^\infty ds' \int_0^\infty \mathcal{K}(c, s; c', s') n(c, s; t) n(c', s'; t) dc' \\
 & + \int_0^\infty ds' \int_0^\infty \mathcal{K}'(c, s; c', s') n(c + c', s + s'; t) dc' \\
 & - \frac{1}{2} \int_0^s ds' \int_0^c \mathcal{K}'(c', s'; c - c', s - s') n(c, s; t) dc' \\
 & + A(c, s) - k_d(c, s) n(c, s; t) - \frac{\partial}{\partial s} (j_s(c, s; t)) - \frac{\partial}{\partial c} (j_c(c, s; t)) \quad (3.23)
 \end{aligned}$$

where,

$$j_s(c, s; t) = j_c(c, s) = v(c, s) n(c, s; t) = (v_{\text{in}}(c, s) - v_{\text{out}}(c, s)) n(c, s; t) \quad (3.24)$$

We introduce a quantity $q_s(c, t)$ defined as,

$$q_s(c, t) = \int_0^\infty s n(c, s; t) ds \quad (3.25)$$

which denotes the total amount of cargo s carried by an ensemble of endosomes with c amount of Rab5. We will call this the cargo load of an endosome. The total

number of cargo molecules in the early endosomal network at any time t is given by,

$$\Phi(t) = \int_0^\infty q_s(c; t) dc \quad (3.26)$$

3.2.1 Transport equation for the cargo load of an endosome

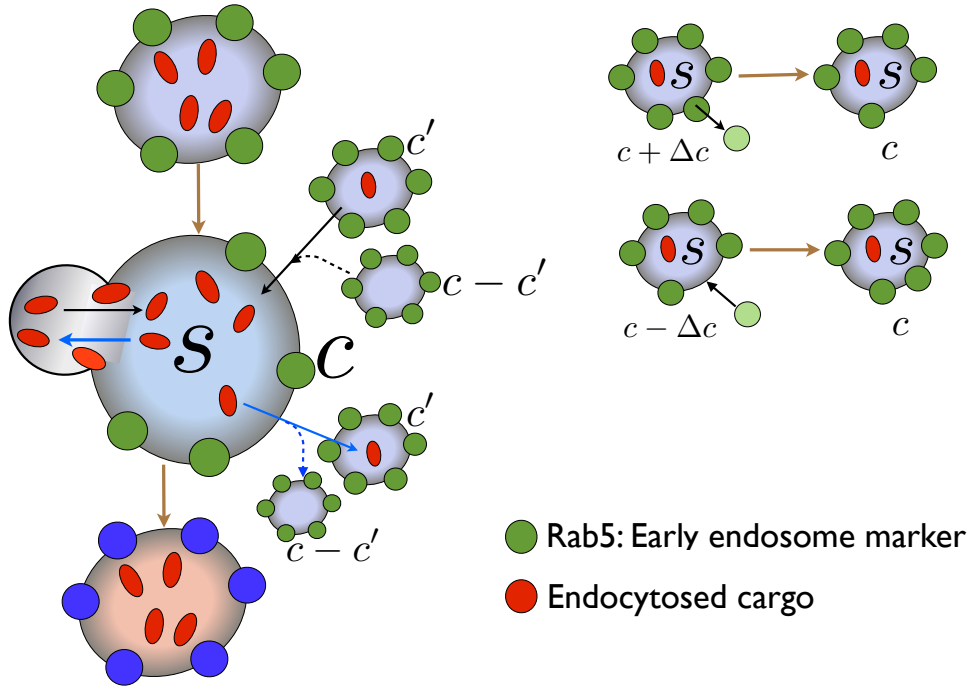


Figure 3.9: **Two component description of endosomal trafficking**

Schematic representation of the trafficking of an endosome that is in state s, c .

The figure shows the possible mechanisms via which an endosome in state c , i.e c number of Rab5 molecules, can change its cargo content s .

In the previous section we introduced a quantity $q_s(c, t)$ defined as Eq.(3.25). Time evolution of this quantity, which can be obtained by integrating Eq.(3.23) according to the definition given by Eq.(3.25), tells us how cargo flows in an ensemble of endosomes with a specific number of Rab5 molecules c . Some types of cargo, for example cargo receptors, do not disturb the usual dynamics of endosomes, which they would exhibit in the absence of cargo. Such class of cargo are referred to as *passive cargo*. In the language of our theoretical description this would imply all

the kinetic rates that enter our theory given by Eq.(3.23) are independent of the amount of cargo s carried by the endosomes and only depend on the amount of Rab5 c they carry. But there are other types of cargo, like the signaling molecules or growth factors, whose presence in the endosomal population effects or alters their usual dynamics. Within the framework of this thesis we only consider the case of *passive* cargo. In the case of *passive* cargo the following functions can be expressed as,

$$\begin{aligned}
\mathcal{K}(c, s; c', s') &= \mathcal{K}(c, c') \\
\mathcal{K}'(c, s; c', s') &= \mathcal{K}'(c, c')\delta(s - \varphi(c, c')(s + s')) \\
k_d(s, c) &= k_d(s) \\
j_s(s, c) &= v^s n(s, c; t) = v(s) n(s, c; t) \\
j_c(s, c) &= v^c n(s, c; t) = v(c) n(s, c; t)
\end{aligned} \tag{3.27}$$

As can be seen in the above expressions the fission is expressed as,

$$\mathcal{K}'(c, s; c', s') = \mathcal{K}'(c, c')\delta(s - \varphi(c, c')(s + s')) \quad . \tag{3.28}$$

It denotes that the c -endosome resulting from the fission of a $c + c'$ endosome contains proportional number of s component molecules. Here $\varphi(c, c')$ denotes the fraction of $c + c'$ component that c -endosome contains.

With assumptions stated above the time evolution of $q_s(c, t)$ reads as,

$$\begin{aligned}
\frac{\partial q_s(c; t)}{\partial t} &= \frac{1}{2} \int_0^\infty \mathcal{K}(c', c - c')n(c - c', t)\theta(c - c')q_{s'}(c', t)dc' \\
&\quad - q_s(c, t) \int_0^\infty \mathcal{K}(c, c')n(c', t)dc' \\
&\quad + \int_0^\infty ds' \mathcal{K}'(c, c' - c)\varphi(c, c' - c)\Theta(c' - c)q_{s'}(c', t)dc' \\
&\quad - \frac{1}{2}q_s(c, t) \int_0^c \mathcal{K}'(c', c - c')\Theta(c - c')dc' \\
&\quad + \int_0^\infty s A(c, s)ds - k_d(c)q_s(c, t) + \int_0^\infty j_s(c, s; t)dc - \frac{\partial}{\partial c}(v^c q_s(c, t))
\end{aligned} \tag{3.29}$$

We can re-write the above equation in the following way:

$$\frac{\partial q_s(c; t)}{\partial t} = \int_0^\infty dc' \left[W(c', c)q_{s'}(c', t) - W'(c, c')q_s(c, t) \right] - \frac{\partial J(c, t)}{\partial c} + S_{\text{in}}(c, t) - S_{\text{out}}(c, t) \tag{3.30}$$

where,

$$W(c, c') = \mathcal{K}(c, c')n(c', t) - \frac{1}{2}\mathcal{K}'(c - c', c') \quad (3.31)$$

$$W'(c', c) = \frac{1}{2}\mathcal{K}(c - c', c')n(c - c', t)\Theta(c - c') + \mathcal{K}'(c, c' - c)\varphi(c, c' - c)\Theta(c' - c) \quad (3.32)$$

$$J(c) = (v_{\text{in}}(c) - v_{\text{out}}(c))q_s(c, t) \quad (3.33)$$

$$S_{\text{in}}(c, t) = \int_0^\infty j_{\text{in}}^s(c, s; t)ds + \int_0^\infty s A(c, s)ds \quad (3.34)$$

$$S_{\text{out}}(c, t) = k_d(c)q_s(c, t) + \int_0^\infty j_{\text{out}}^s(c, s; t)ds \quad (3.35)$$

(A) Cargo trafficking rate

The cargo trafficking rate denotes the rate at which the cargo is transported between endosomes of different states, where the state is characterized by the amount of Rab5, c , an endosome carries.

$$W(c, c') \quad (3.36)$$

denotes the probability per unit time for cargo s in an endosome with c number of Rab5 molecules to be transferred in an endosome with c' number of Rab5 molecules. Both fusion and fission processes, as given by Eq.(3.33-3.34) can lead to such a transfer.

(B) Endosome entry and exit

The cargo trafficking accounts for the transfer of cargo between endosomes of different states, however new endosomes carrying both Rab5 c and cargo s may appear following endocytosis. Transport of cargo down the endocytic pathway may also lead to disappearance of existing endosomes with both Rab5 and cargo. Endosomes with Rab5, c , can increase their cargo content by the process wherein the flux is towards only cargo s . In a similar way but opposite in nature, an endosome in state c can lose little cargo if a non-endosomal structure carrying little cargo pinches off from a cargo carrying Rab5-positive endosome. For example, during tubulation. Such processes are accounted by the entry Eq.(3.36) and exit Eq.(3.37) terms in the transport equation. The net contribution to new endosomes with Rab5 and cargo due to these two processes is:

$$S_{\text{in}}(c, t) - S_{\text{out}}(c, t) \quad (3.37)$$

(C) Flux of Rab5

If the flux to an a cargo carrying Rab5 endosome is towards to the Rab5, c , then this could change the state of the endosome from c to $c + \Delta c$. Similarly an outflux of Rab5 molecules from an endosome changes the state of the endosome from c to $c - \Delta c$. Such events are denoted by the term (c) of Eq.(3.37). The net gain or loss of endosomes in state c due to the flux of Rab5 molecules to the c -endosome is given by:

$$(v_{\text{in}}(c) - v_{\text{out}}(c))q_s(c) \quad (3.38)$$

3.3 Dynamics of cargo trafficking in Rab5 endosomes

In order to follow the cargo in Rab5-positive endosomes, in the previous section, we had presented the description wherein an endosome was characterized by both the amount of Rab5 denoted by c as well amount of cargo, denoted by s . Now, we can also follow the dynamics of only cargo in the whole Rab5-positive endosomal population. We can arrive at this quantity $n(s, t)$, which denotes the number density of Rab5-positive endosomes with cargo amount s , as follows,

$$\int_0^\infty dc n(c, s; t) = n(s, t) \quad . \quad (3.39)$$

To simplify things a little, in the previous section we had considered a *passive* cargo. In other words, the cargo does not perturb the dynamics of endosomes. This consideration is reflected in our theory by the suppressing the dependency of the kinetic parameters, like the fusion and fission kernels, on the amount of cargo s and retaining only dependency on Rab5 c . We will now write down the equation describing the dynamics of trafficking of such a *passive* cargo in the Rab5-positive endosomal population. We arrive at this equation starting from the general two-component description. Before moving further we will define a quantity which would be used in the next steps of simplification.

$$P(s|c) = n(c, s; t)/n(s, t) \quad (3.40)$$

where, $P(s|c)$ denotes the conditional probability that an endosome carrying s amount of cargo also contains c number of Rab5 molecules. With the above definitions we can write down the kinetic equation for the quantity $n(s, t)$ by integrating

Eq.(3.23) over dc .

$$\begin{aligned}
\frac{\partial n(s, t)}{\partial t} &= \frac{1}{2} \int_0^s \mathcal{K}(s', s - s') n(s') n(s - s') ds' - \int_0^\infty \mathcal{K}(s, s') n(s) n(s') ds' \\
&+ \int_0^\infty \mathcal{K}'(s, s') n(s + s') ds' - \frac{1}{2} \int_0^s \mathcal{K}'(s', s - s') n(s) ds' \\
&+ A(s) - k_d(s) n(s) - \frac{\partial}{\partial s} (j^s)
\end{aligned} \tag{3.41}$$

where,

$$\begin{aligned}
\mathcal{K}(s, s') &= \int_0^\infty dc \int_0^\infty dc' \mathcal{K}(c, c') P(s'|c') P(s|c) \\
\mathcal{K}(s - s', s') &= \int_0^\infty dc \int_0^\infty dc' \mathcal{K}(c - c', c') P(s - s'|c - c') P(s'|c') \Theta(c - c') \\
\mathcal{K}'(s, s') &= \int_0^\infty dc \int_0^\infty dc' \mathcal{K}'(c, c') P(s + s'|c + c') \\
\mathcal{K}'(s - s', s') &= \int_0^\infty dc \int_0^\infty dc' \mathcal{K}'(c - c', c') P(s|c) \Theta(c - c') \\
j^s &= v_{\text{in}}(s) - v_{\text{out}}(s) = v_{\text{in}}(s, c) P(s|c) - v_{\text{out}}(s, c) P(s|c) \quad .
\end{aligned} \tag{3.42}$$

A summary of the kinetic equation that describes the dynamics of cargo trafficking in a population of Rab5-positive endosomes, and the biological relevance of the various parameters that enter the equation is given in Fig. 3.10.

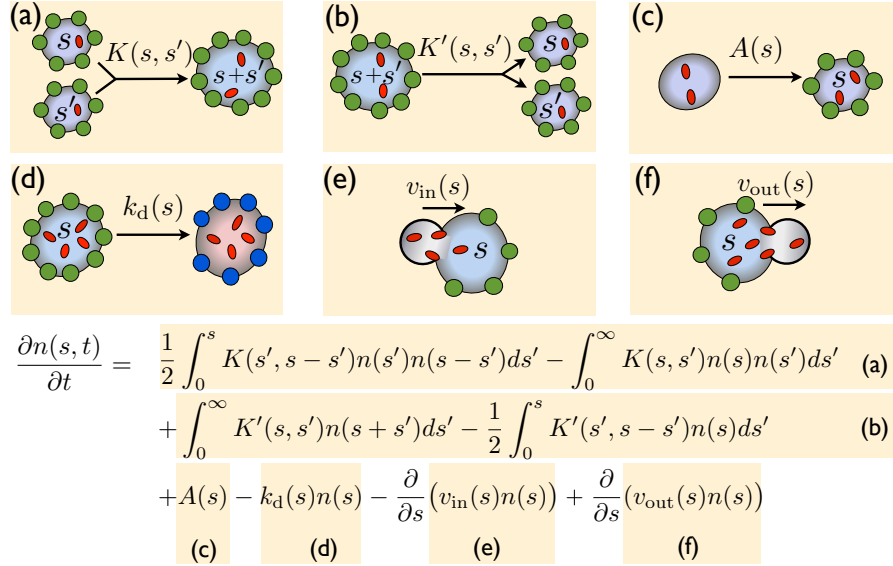


Figure 3.10: **Theoretical description of endosome network dynamics**

The schemes (a-f) represent the different processes that govern the distribution of cargo in the early endosomes as given by Eq.(3.41). The state of the endosomal network is described by the number $n(s, t)ds$ of endosomal objects per cell, carrying the cargo amount in the interval between s and $s + ds$ at time t . The cargo distribution $n(s, t)$ obeys a general dynamic equation that accounts for the processes (a - f). (a) Homotypic fusion of two endosomes carrying the cargo amounts s and s' leads to the replacement of the two endosomes by a new one carrying the cargo amount $s + s'$. Such fusion occurs at the rate $K(s, s')$. (b) Two endosomes carrying the cargo amounts s and s' can be produced by the fission of endosomes carrying the cargo amount $s + s'$. Such fission occurs at the rate $K'(s, s')$. (c) New endosomes carrying the amount s of cargo appear at the rate $A(s)$. (d) Endosomes disappear from the system by undergoing conversion at the rate k_d . Finally, endosomes can take up additional cargo by fusing with endocytic vesicles (e) and can lose cargo by budding off vesicular structures (f). The currents $v_{\text{in}}(s)$ and $v_{\text{out}}(s)$ are the average cargo amount per unit time respectively gained and lost by an endosome carrying the cargo amount s . Cargo enters the network via the processes (b) and (e). The total cargo influx is $J = \int_0^\infty (sA(s) + v_{\text{in}}(s)n(s))ds$.

3.4 Conclusion

In this chapter we have presented a general theoretical framework to describe the endosomal dynamics and cargo trafficking. We started off by presenting the theoretical framework that describes the time evolution of number of density of endosomes with certain amount of Rab5. At this level an endosome at any given instant of time is characterized by the amount of Rab5 bound to its membrane. We then extended our description to incorporate the trafficking of endocytosed cargo. To do this, we characterize the state of an endosome by not only the amount Rab5 but also the amount of cargo it carries. This is referred to as two component description. From the two component description, we derived the dynamic equation for time evolution of the cargo distribution specifically in the Rab5-endosomal population. We simplified our description by considering a *passive* cargo, which reduces the dependency of the various kernels entering the equation to only one component, i.e Rab5.

Our continuum description takes into account several microscopic processes that might be involved in trafficking of various types of cargo that enter the cell via endocytosis. These processes that describe endosomal trafficking, enter our theoretical description in the form of parametric functions. It is almost impossible to study the general theoretical framework that we have presented here as whole, analytically as well as numerically. In order to gain any further understanding of the endosomal system from the theoretical framework presented in this chapter, we will first investigate some simple scenarios. These scenarios will consists of only few processes. This will be the goal of the next chapter. However, the central focus of this thesis is to apply the theoretical description developed here to the experiments and try to understand the behavior of various experimentally measurable quantities using only few parameters from our theoretical description and with simple expressions to describe them (see Chapter 5).

Chapter 4

Entry-Fusion-Exit model to describe cargo trafficking by early endosomes

In the previous chapter, Chapter 3, we derived the dynamic equation for the quantity $n(s, t)$, which characterizes the cargo distribution in Rab5-positive early endosomal population. The quantity $n(s, t)$ is defined such that at any time t , $n(s)\Delta s$ is the number of Rab5 positive-endosomes per cell which contain cargo amount in between s and $s + \Delta s$. The cargo distribution $n(s)$ evolves in time as a result of several endosomal trafficking processes as given in Eq.(3.41). In Eq.(3.41), the time dependence of $n(s)$ on the right hand side of the equation is suppressed for ease of notation. Following internalization the cargo is first delivered to a population Rab5-positive early endosomes which regularly interact with each other via fusion and fission. Cargo carrying early endosomes thus forms a system of interacting endosomes, where cargo flows into the system as new cargo carrying early endosomes appear following endocytosis. We want to understand the properties of such a system. How does the cargo distribute itself in the early endosomal system? Do endosomal interactions play a role in shaping the distribution? In this chapter we will investigate a simple model which we refer to as "Entry-Fusion-Exit" model, abbreviated a EFE model. Our motivation in studying this model is to build up an understanding of the endosomal dynamics by studying the cargo distributions in a population of Rab5-positive endosomes from theoretical stand point. We want to know what are the basic ingredients from theory that shape the cargo distributions that can be obtained from experiments, a comparison which we will do in the next chapter. In the chapter we will study the properties of the EFE model using both analytical and numerical tools.

In the EFE model, cargo can enter the endosomal network only by generation or appearance of new early Rab5-positive cargo carrying endosomes. Such new

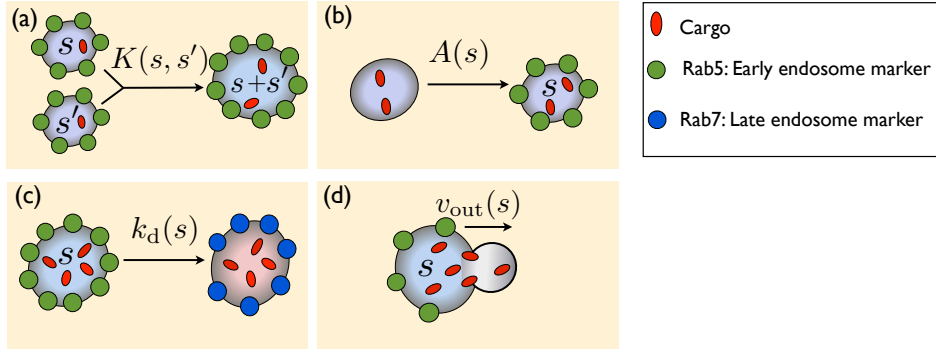


Figure 4.1: **Entry-Fusion-Exit model**

The schemes (A-D) represent the different processes in EFE model, that govern the cargo distribution in early endosomes $n(s)$.

(A) Homotypic fusion of two endosomes carrying the cargo amounts s and s' leads to the replacement of the two endosomes by a new one carrying the LDL amount $s + s'$. Such fusion occurs at the rate $\mathcal{K}(s, s')$.

(B) As cargo flows new endosomes carrying the amount s of cargo appear at the rate $A(s)$.

(C) Early endosomes disappear from the system by undergoing conversion to late endosomes at the rate $k_d(s)$.

(D) Finally, endosomes can lose cargo by budding off vesicular structures. The current $v_{out}(s)$ are the average cargo amount per unit of time respectively lost by an endosome carrying the cargo amount s .

endosomes appear at the rate $A(s)$ (Fig. 4.1(B)). On the other hand, we will explore two mechanisms by which the cargo can leave the early endosomal network. The cargo can leave the early endosomal network either by conversion of a cargo carrying Rab5-positive endosome into some other endosomal structure, like Rab5 to Rab7 conversion (Fig. 4.1(C)), or via heterotypic fission of small cargo carrying vesicles (Fig. 4.1(D)). For our study here we will focus on the trafficking of a degradative cargo, that is delivered to Rab7 endosomes from Rab5 endosomes. The transfer of cargo from Rab5 to Rab7 endosomes can occur either by full conversion, as described above, or via heterotypic fission. Another motivation of this chapter is study the two aforementioned scenarios of cargo exit theoretically and understand how much they are different from each other or for that similar. To what extent different types of cargo or different cell types use one mechanism, the other or both remains unclear. In addition to the above two processes, the cargo carrying early endosomes can subsequently, after their appearance, undergo homotypic fusion at the rate $\mathcal{K}(s, s')$, (Fig. 4.1(A)). As already mentioned earlier, by homotypic fusion we mean that only those two endosomes that are positive to Rab5 can fuse with each other. Fusion of a Rab5-positive early endosome with any other vesicular structure which is not Rab5-positive is termed as heterotypic fusion.

4.1 Entry and Fusion : A minimal scenario

In order to understand the complete EFE model we will first start with an even simpler scenario. The ingredients of such a simple scenario are :

(1) A source of new cargo carrying Rab5-positive endosomes at the rate $A(s)$. We will assume that the source function is narrowly confined on the cargo fluorescence intensity scale. For the sake of simplicity we choose to describe the source by the function $A(s) = (J/s_0^2)e^{-s/s_0}$.

(2) A constant fusion rate K .

All throughout the chapter we will summarize in a table the choice of parameter function that enter the kinetic equation given by Eq.(3.41). Choice of parameter function in entry and fusion scenario is summarized as follows:

$\mathcal{K}(s, s')$	K (constant)
$\mathcal{K}'(s, s')$	0
$A(s)$	$(J/s_0^2)e^{-s/s_0}$
$k_d(s)$	0
$v_{in}(s)$	0
$v_{out}(s)$	0

Table 4.1: Choice of parameters used in the Entry-Fusion model

The dynamic equation for $n(s)$ in this extremely simplified scenario with the choice of parameter functions as given in the table can be written as:

$$\frac{\partial n(s, t)}{\partial t} = \frac{K}{2} \int_0^s n(s')n(s-s')ds' - K \int_0^\infty n(s)n(s')ds' + \frac{J}{s_0^2}e^{-s/s_0} \quad (4.1)$$

The equation governing the total amount of cargo Φ is given by,

$$\frac{d\Phi}{dt} = \int_0^\infty s \left(\frac{\partial n(s, t)}{\partial t} \right) ds = J \quad (4.2)$$

The solution of Eq.(4.2) is given by

$$\Phi(t) = Jt \quad (4.3)$$

The total amount of cargo Φ , Eq.(4.3) is ever increasing which is expected, as we have not included any process that would account for the exit of cargo from the early endosomal network which would balance the influx due to $A(s)$. In this simple scenario the cargo accumulates infinitely in the network over time Eq.(4.3), which is bit unphysical. The cell must have a mechanism whereby it regulates the amount of cargo in the early endosomal network thus preventing such an infinite accumulation. Later in this chapter we will study introduce a mechanism that accounts for the cargo exit from early endosomes.

4.1.1 Exact solution for the cargo distribution $n(s, t)$

Eq. (4.1) can be solved using Laplace transforms [61]. Introducing the function $h(z, t) = \int_0^\infty n(s, t)(e^{-zs} - 1)ds$, Eq. (4.1) can be transformed to

$$\frac{\partial h}{\partial t} = \frac{K}{2}h^2 - \frac{Jz}{(1 + zs_0)} \quad (4.4)$$

The solution of Eq.(4.4) is,

$$h(z, t) = -\frac{\bar{k}(z)}{K} \tanh\left(\frac{t}{2}\bar{k}(z)\right) \quad (4.5)$$

where we have introduced

$$\bar{k}(z) = \left(\frac{2JKz}{1 + zs_0}\right)^{1/2} \quad (4.6)$$

Taking the inverse Laplace transform of $h(z, t)$ gives us the distribution $n(s, t)$ [50].

The shape of the cargo distribution $n(s)$ at different time points obtained by the numerical solution of the dynamic equation using the parameters given in Eq.(4.1) is shown in Figure 4.2(A). At early times the cargo distribution $n(s)$ is narrow and peaked around s_0 as it is dictated by the source function. Its amplitude rapidly saturates after a characteristic time $\tau = ((JK/(2s_0))^{-1/2}$ which depends on the rate of homotypic endosome fusion K and on the influx J , see Section 4.1.3. Subsequently, endosome fusion leads to broadening of the distribution which covers an increasingly large range of cargo amount s in which the distribution follows a power-law decay $n(s) \simeq s^{-3/2}$. The distribution profile at each time is characterized by a power-law followed by an exponential tail beyond some typical cargo amount s^* . While the cargo distribution $n(s)$ is broadening over time, the power law emerges by gradually shifting the exponential tail and thus the s^* towards increasing values of s . In the following sections we discuss separately the properties of the distribution during the time evolution phase and at steady state.

4.1.2 General properties of the cargo distribution $n(s, t)$ for large s

We will study in-depth the Entry and Fusion scenario introduced in the previous section. The scenario, owing to its simplicity can be solved analytically under various limits. After we have developed a thorough understanding of this over simplistic scenario using analytical as well as numerical tools, we will then study models that will include processes that account for the loss of cargo from the early endosomal network.

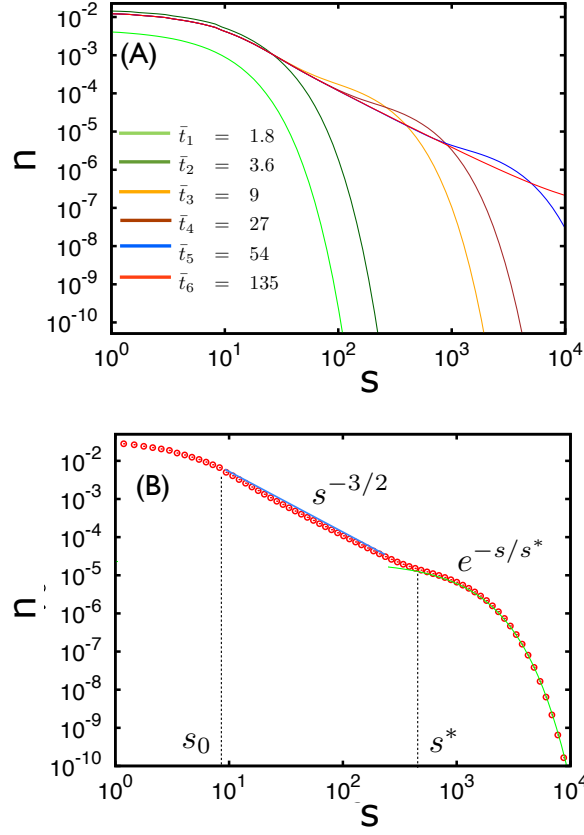


Figure 4.2: **Entry-Fusion model**

(A) Numerical solution of the kinetic equation for $n(s, t)$, Eq.(4.1) in the Entry-Fusion model at different dimensionless times $\tilde{t}_1 \rightarrow \tilde{t}_6$ (see Appendix B) after allowing the internalization of the labelled cargo into the endosomal network. At the initial time $\tilde{t} = 0$, the system does not contain cargo $n(s, \tilde{t} = 0) = 0$. (Here we set $J/K = 1.8 \cdot 10^6$, $s_0 = 10$)

(B) At any given time during the time evolution the distribution $n(s, t)$ displays a strict power law in the range $s_0 \ll s \ll s^*(t)$ and an exponential decay for $s \gg s^*(t)$.

4.1.2.1 Time evolution of $n(s, t)$

The time dependence of $n(s, t)$ can be obtained from the Eq.(4.5). In the limit $zs_0 \ll 1$ Eq.(4.5) simplifies to,

$$h(z, t) = -\left(\frac{2Jz}{K}\right)^{1/2} \tanh\left(\sqrt{3s^*(t)z}\right) \quad (\text{for } s \gg s_0) \quad (4.7)$$

where we have introduced $s^*(t) = JKt^2/6$. This equation implies that, in the range $s \gg s_0$, the distribution $n(s, t)$ depends on time only via the scaling factor $s^*(t)$. In the limit $zs^*(t) \gg 1$ and $zs_0 \ll 1$, Eq.(4.7) reduces to $h(z, t) \simeq -(2Jz/K)^{1/2}$.

By taking the inverse Laplace transform of this expression [50], we obtain,

$$n(s, t) \simeq \left(\frac{J}{2\pi K} \right)^{1/2} s^{-3/2} \quad (\text{for } s^*(t) \gg s \gg s_0) \quad (4.8)$$

On the other hand, for the limit $zs^*(t) \ll 1$ and $zs_0 \ll 1$, we can rewrite Eq.(4.7) in terms of $\sinh(z)$ and $\cosh(z)$ functions, and expand both the numerator and denominator by retaining terms only up to the leading order in s^*z ,

$$h(z, t) \sim - \left(\frac{12J}{3Ks^*(t)} \right)^{1/2} \left(\frac{z}{2/(3s^*(t)) + z} \right) \quad (4.9)$$

Finally, taking inverse Laplace transform of Eq.(4.9) we arrive at,

$$n(s, t) \sim \left(\frac{6J}{Ks^*(t)^3} \right)^{1/2} e^{-2s/(3s^*(t))} \quad (\text{for } s \gg s^*(t) \gg s_0) \quad (4.10)$$

where, $s^*(t) = JKt^2/6$.

Self-similar time evolution of the distribution $n(s)$

According to Eq(4.7) the distribution at all times for $s \gg s_0$ depends on time only via s^* , which is defined as the typical cargo amount beyond which distribution crosses over from a gradual power law decay into an abrupt exponential decay. The distribution shows a characteristic hump beyond s^* that is shifted to higher values of s with increasing time, Figure 4.3(A). The distributions at various times,

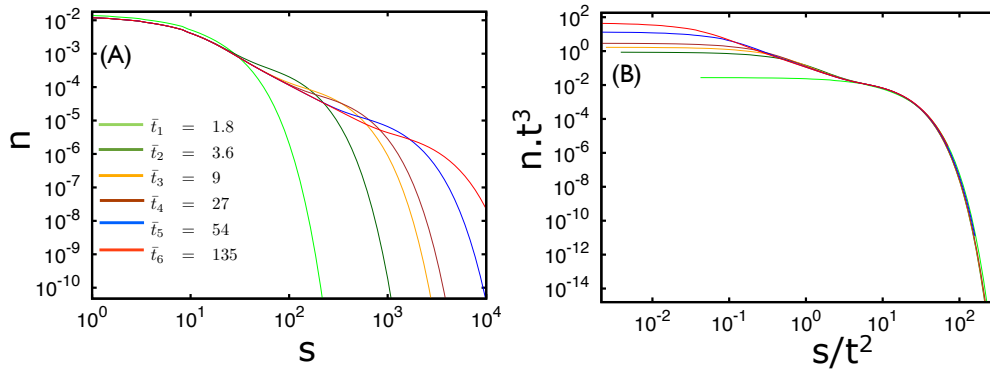


Figure 4.3: **Self preserving time evolution**

The distribution $n(s, t)$ evolves in time in a self similar manner. To demonstrate this, we plot in (A) the distributions at various times during time evolution, as $n(s)t^3$ versus s/t^2 , since $s^*(t) \simeq t^2$ as shown in (B).

shown in Fig.4.3(A), perfectly collapse on to a single curve when rescaled as $n(s)t^3$ versus s/t^2 Fig.4.3(B), where we have used the relation $s^* \sim t^2$. This shows that the distribution $n(s)$ evolves in time in a self-similar manner. Distributions that evolve in a self-similar manner have a single characteristic size in the system, here denoted by s^* as evident from Fig.4.3.

4.1.2.2 Steady state distribution $n(s)$ for $s \gg s_0$

Even though the total amount of cargo in endosomal population, Φ does not reach a steady state, theoretically the distribution $n(s, t)$ in the intermediate range of cargo intensity $s_0 \ll s \ll s^*(t)$ reaches a steady state $n(s)$. This is evident from Eq. (4.5) in which at very long times ($t \rightarrow \infty$) $h(z, t)$ becomes time-independent which implies steady state for $n(s)$. At steady state

$$h(z, t) = -\frac{\bar{k}}{K} \quad (4.11)$$

The steady state distribution $n(s)$ for $s \gg s_0$ can be obtained by taking the appropriate limit in the above equation and finally taking the inverse transform of Eq.(4.5) (see Appendix for details), and is given by,

$$n(s) = \left(\frac{J}{2\pi K}\right)^{1/2} \frac{1}{s^{3/2}} \quad (4.12)$$

The distribution obeys a power law with a $-3/2$ exponent. This is a classical result in the field of aggregation phenomena.

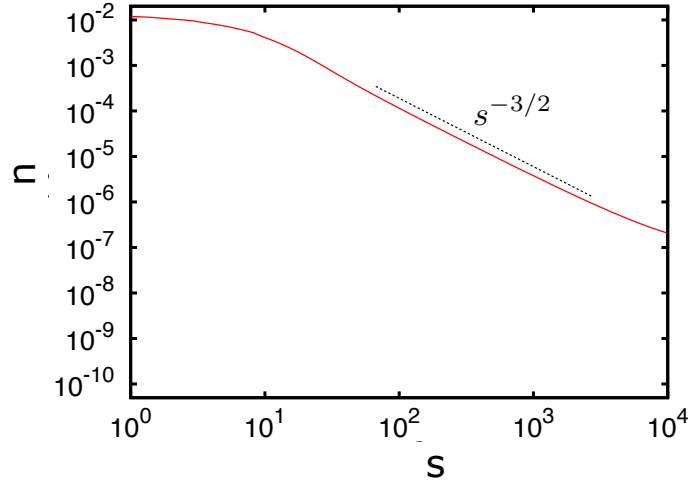


Figure 4.4: **Entry-Fusion model**

At long times the timecourse of $n(s, t)$ shown in Fig.4.2(A) reaches a steady state in the range $s < s^*$. The steady state distribution $n(s)$ displays a strict power law with slope $-3/2$ in this range for $s \gg s_0$.

Power law in steady state and self-similarity in time evolution : Fusion determines it all

The steady state profile and the time evolution of the distribution depend strongly on the choice of the fusion kernel, $\mathcal{K}(s, s')$. One of the important property that the

fusion kernel should satisfy, in order to exhibit self-similarity during time evolution and power law at steady state is that it should be a symmetric and a homogeneous function of its arguments s and s' . Homogeneity implying a scale-free nature of the kernel, i.e

$$\mathcal{K}(s, s') = \mathcal{K}(s', s) \quad (4.13)$$

$$\mathcal{K}(as, as') = a^\lambda \mathcal{K}(s, s') = a^\lambda \mathcal{K}(s', s) \quad (4.14)$$

for any positive real number a and homogeneity exponent λ . The condition given by Eq.4.14 ensures that the particles undergoing fusion, or as would be in our case, the cargo carrying early endosomes are homogeneously distributed all over the cytoplasmic space of the cell.

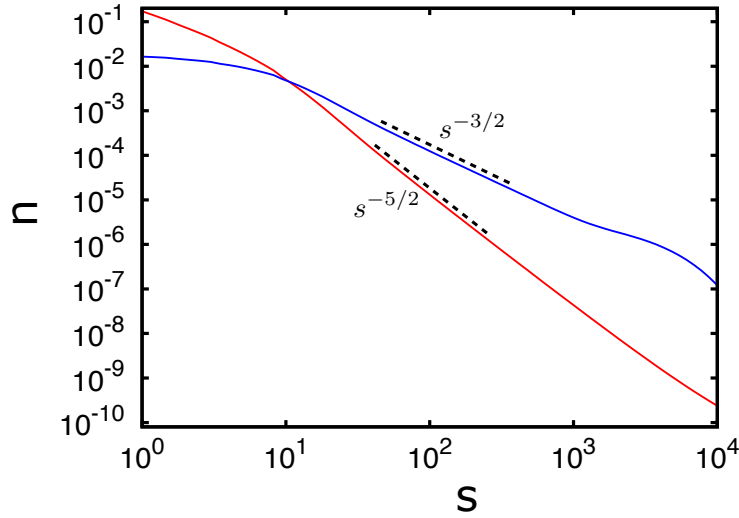


Figure 4.5: **Cargo dependent fusion rate**

In the Entry and Fusion scenario with the choice of fusion kernel given by Eq.(4.15) the distribution $n(s)$ reaches a steady state with a power law distribution exponent of which is given by Eq.(4.16). Here we used $\mu = \nu = \lambda/2$. For the red curve $\lambda = 2$ and for the blue curve $\lambda = 0$.

Physically it would mean the system has a perfect mixing of the particles with continuous distribution of sizes. Eq. 4.1 for such kernels has been already studied using dynamical scaling analysis [52, 60, 61, 64]. One can thus write down a general form of the kernel that encapsulates the above mentioned properties.

$$\mathcal{K}(s, s') = \frac{K_0}{2}(s^\mu s'^\nu + s^\nu s'^\mu) \quad (\mu + \nu = \lambda) \quad (4.15)$$

With the above mentioned choice of fusion kernel it can be shown that at the steady state,

$$n(s) \sim s^{-\theta} \quad (\theta = (3 + \lambda)/2). \quad (4.16)$$

and that the characteristic cargo amount $s^*(t) \sim t^{1/(2-\theta)}$.

In general it has been shown the steady state solution for $n(s)$ is given by Eq.4.16 for any fusion kernel that exhibits the properties of symmetry and homogeneity and which can be approximated for $s \gg s'$ as

$$\mathcal{K}(s, s') = K_0 s^\mu s'^\nu \quad (\text{for } s \gg s') \quad . \quad (4.17)$$

§ **Gelling model:** For $\lambda > 1$ the amount of cargo associated with the distribution $\int_0^\infty ds sn(s)$ remains constant. But in the absence of a cargo exit, the total amount of cargo is ever increasing. This extra cargo is accumulated in one endosome. The distribution at steady state in this case would read as,

$$n(s) \sim s^{-\theta} + n(s_\infty) \quad (n(s_\infty) \rightarrow \delta(s - s_\infty)) \quad . \quad (4.18)$$

In the literature of aggregation phenomena this is referred to as *gelation*.

§ **Non-Gelling model:** For $\lambda \leq 1$ the distribution at steady state does not result in an infinite accumulation of cargo. The distribution thus displays a pure power law distribution $n(s) \sim s^{-\theta}$ for $s_0 < s < s_c$.

4.1.3 General properties of the cargo distribution $n(s, t)$ for small s

The time-dependence of $n(s, t)$ for $s \ll s_0$ in the Entry-Fusion model can be obtained from the Eq.(4.5), which is written as follows,

$$h(z, t) = -\frac{\bar{k}(z)}{K} \tanh\left(\frac{t}{2} \bar{k}(z)\right) \quad . \quad (4.19)$$

In the limit $s \ll s_0$, Eq.(4.19) can be written as

$$h(z, t) = -\left(\frac{2J}{K}\right)^{1/2} \left(1 - \frac{1}{2(1 + zs_0)}\right) \tanh\left(\left(\frac{3s^*(t)}{s_0}\right)^{1/2}\right) \quad (4.20)$$

where $s^*(t) = JKt^2/6/$. Finally by taking inverse Laplace transformation of Eq.(4.20) we obtain,

$$n(s, t) \simeq \left(\frac{J}{sKs_0}\right)^{1/2} e^{-s/s_0} \tanh(t/\tau) \quad (\text{for } s \ll s_0) \quad . \quad (4.21)$$

From Eq.(4.21) we see that the amplitude of the distribution varies with time as

$$n_{max}(t) \simeq \tanh(t/\tau) \quad (4.22)$$

where $\tau = (JK/(2s_0))^{-1/2}$ is the characteristic time in which the amplitude of the distribution reaches the steady state. Eq.(4.21) also tells us that the shape of the distribution $n(s)$ for all times and for $s \ll s_0$ has the functional form of e^{-s/s_0} . One should be reminded here that this function is the same as the source function $A(s) = (J/s_0^2)e^{-s/s_0}$. In other words, for a constant fusion rate $\mathcal{K}(s, s') = K$, the shape of the distribution at all times preserves the profile of the source function.

4.2 Entry-Fusion-Exit : Conversion model

In the preceding sections we had studied an over simplified model which we called as Entry and Fusion scenario. In this scenario new endosomes carrying low amount of cargo denoted by s_0 enter the network and subsequently undergo fusion. Even though the Entry and Fusion scenario is an extremely simple model it exhibits rich properties which we explored in the previous sections analytically and confirmed numerically. However in the absence of a mechanism for exit of cargo from early endosomal network, which is the case in the Entry and Fusion scenario, cargo keeps on accumulating forever in the endosomal network. This does not seem to be reasonable for two reasons. First, endosomes are enclosed by membrane and their internal structure renders them with a certain amount of rigidity and thus only a limited capacity to carry cargo. Second, the number of endosomes of a specific population, for example Rab5-positive endosomal population, is finite. For these reasons, in this and the sections that will follow hereafter, we will extend the Entry and Fusion scenario by introducing two different mechanisms for exit of cargo from a population of Rab5-positive early endosomes. In the present section we will study the scenario we will call "Conversion model" or EFE-C model. In this model the cargo from the Rab5-positive endosomal population is lost by conversion of a cargo carrying Rab5-positive endosome into a non-Rab5 endosomal structure. Such a process could be the Rab5-Rab7 conversion in the case of a degradative cargo, reported in [20, 26]. The choice of parameters for the EFE-C model is given in Fig.4.6(Table).

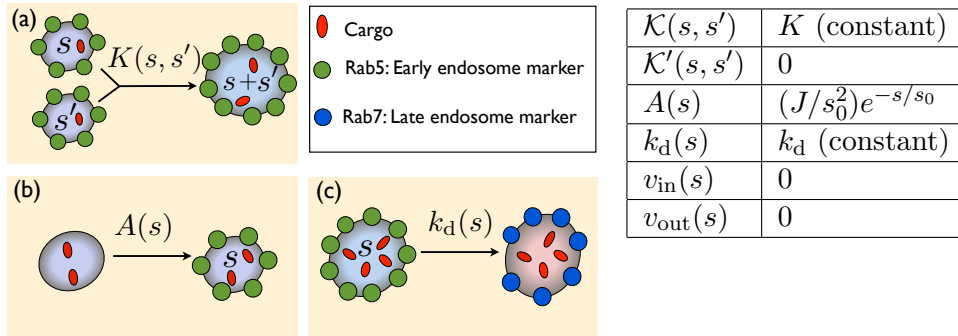


Figure 4.6: **Conversion model**

The schemes (a-c) represent the different processes in Conversion model, that govern the distribution of cargo $n(s)$ in early endosomes. (a) Homotypic fusion of two endosomes carrying the cargo amounts s and s' . (b) As cargo flows new endosomes carrying the amount s of cargo appear at the rate $A(s)$. (c) Early endosomes disappear from the system by undergoing conversion to late endosomes at the rate $k_d(s)$.

The dynamic equation for the distribution $n(s)$ with the choice of parameters

given in the table of Fig. 4.6 reads as,

$$\frac{\partial n(s, t)}{\partial t} = \frac{K}{2} \int_0^s n(s')n(s - s')ds' - K \int_0^\infty n(s)n(s')ds' + A(s) - k_d n(s) \quad . \quad (4.23)$$

The above equation can be solved by the Laplace transform technique already introduced in the previous section, see Section 4.1.1, also see [Appendix](#). Introducing the function $h(z, t)$ as defined in the Section 4.1.3, Eq.(4.23) can be transformed to

$$\frac{\partial h}{\partial t} = \frac{K}{2} h^2 - \frac{Jz}{(1 + zs_0)} - k_d h \quad . \quad (4.24)$$

The solution

$$h(z, t) = -\frac{\bar{k}(z)}{K} \tanh \left(\frac{t}{2} \bar{k}(z) + \tanh^{-1} \left(\frac{k_d}{\bar{k}(z)} \right) \right) + \frac{k_d}{K} \quad (4.25)$$

where we have introduced,

$$\bar{k}(z) = \left(\frac{2JKz}{1 + zs_0} + k_d^2 \right)^{1/2} \quad (4.26)$$

Inverse Laplace transform of Eq.(4.25) gives the full time dependent solution of $n(s)$. However, analytically it is not possible to perform the inverse Laplace of Eq.(4.25) we therefore resort to the numerics to obtain the time dependent solution of Eq.(4.23). Numerical solution of Eq.(4.23) with arbitrary parameter values is shown in Fig.4.7(A). At early times, see Fig.4.7(A), the cargo distribution $n(s)$ is narrow and peaked around s_0 . Its amplitude rapidly saturates after a characteristic time $\tau = (JK/(2s_0))^{-1/2}$ which depends on the fusion rate and rate of endosome appearance. Subsequently, fusion leads to broadening of the distribution which covers an increasingly large range of cargo amount s After a characteristic time set by k_d^{-1} , the distribution reaches the steady state profile. The profile of the distribution and its characteristic features at the steady state defined as,

$$\frac{\partial n(s, t)}{\partial t} = 0 \quad (4.27)$$

is studied in the following section.

4.2.1 Steady state distribution $n(s)$ in the conversion model

Eq.(4.25) shows that at very long times becomes independent of time, this is the steady state of the distribution $n(s)$. At steady state

$$h(z) = -\frac{\bar{k}(z)}{K} + \frac{k_d}{K} \quad . \quad (4.28)$$

We want to look at the $s \gg s_0$, which in the Laplace space would imply $xs_0 \ll 1$. We redefine $\bar{k}(z)$ given by Eq.(4.26) in the limit $xs_0 \ll 1$,

$$\bar{k}(z) = \left(2JKz + k_d^2\right)^{1/2} \quad (4.29)$$

the inverse Laplace transform of Eq.(4.28) leads to the expression

$$n(s) = \left(\frac{J}{2\pi K}\right)^{1/2} s^{-3/2} e^{-s/s^*} \quad (s \gg s_0) \quad . \quad (4.30)$$

where,

$$s_\infty^* = 2JK/k_d^2 \quad . \quad (4.31)$$

One readily observes that the profile of steady state for Conversion model, Eq.(4.30) bears much similarity to that of the Entry-Fusion model Eq.(4.12). Indeed, for times $t \ll k_d^{-1}$ the Conversion model displays all the dynamical properties of the Entry-Fusion model where $k_d(s) = 0$, discussed in Section (4.1.3).

4.2.2 Total amount of cargo and total number of endosomes: Different timescales for saturation

The total amount of cargo in early endosomal population $\Phi(t)$ obeys:

$$\frac{d\Phi}{dt} = J - k_d\Phi \quad . \quad (4.32)$$

The solution is,

$$\Phi(t) = (J/k_d)(1 - e^{-k_d t}) \quad . \quad (4.33)$$

Eq.(4.33) tells that the total amount of cargo in early endosomal network reaches the steady state after a time $t \gg k_d^{-1}$, Fig.4.7(C). The total number of cargo carrying early endosomes $N(t)$ obeys,

$$\frac{dN}{dt} = -\frac{KN^2}{2} + \frac{J}{s_0} - k_d N \quad . \quad (4.34)$$

The solution is,

$$N(t) = \left(\frac{k_d^2}{K^2} + \frac{2J}{Ks_0}\right)^{1/2} \tanh\left(t\left(\frac{k_d^2}{4} + \frac{JK}{2s_0}\right)^{1/2} + \tanh^{-1}\left(\frac{k_d}{(k_d^2 + 2JK/s_0)^{1/2}}\right)\right) - \frac{k_d}{K} \quad (4.35)$$

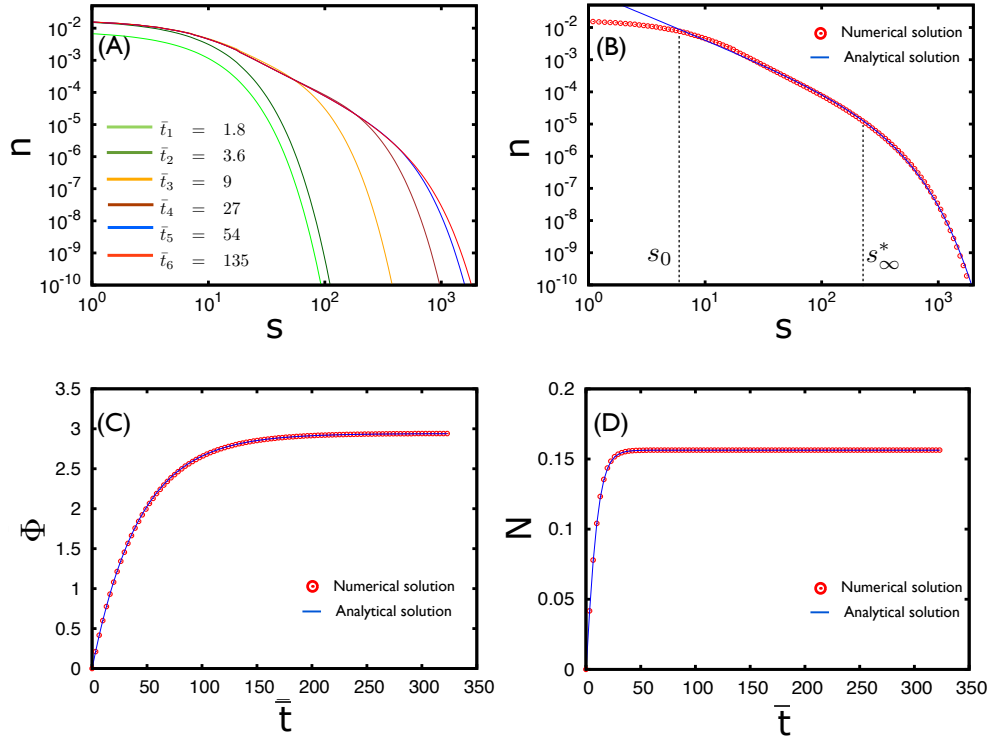


Figure 4.7: **Conversion scenario - theoretical and numerical results**

(A) Numerical solution of the kinetic equation for the EFE-C model at different times given in dimensionless units, after allowing the internalization of the labelled cargo into the endosomal network. At the initial time $t = 0$, the system does not contain cargo $n(s, t = 0) = 0$. (Here we set $J/K = 1.8 \cdot 10^6$ FI, $s_0 = 1885$ FI, $k_d/K = 2.9$).

(B) Steady state distribution $n(s)$ for the choice of parameters given in (A). The distribution obtained from the numerical solution shows very good agreement with the analytical solution given by Eq.(4.30) for $s > s_0$.

(C) Total amount of cargo Φ in the endosomal network as a function of dimensionless time.

(D) Total number of cargo-carrying Rab5-positive endosomes as a function of dimensionless time.

The blue curve in (C) and (D) is the analytical solution for Φ given by Eq.(4.33) and N given by Eq.(4.35).

If the endosome loss by fusion out-numbers endosome conversion, $\tau \ll 1/k_d$, where $\tau = (JK/(2s_0))^{-1/2}$, the solution of Eq.(4.34) is

$$N(t) = N_0 \tanh(t/\tau) \quad . \quad (4.36)$$

where, $N_0 = (2J/(Ks_0))^{1/2}$ is the steady state number of cargo-carrying early endosomes. N reaches the steady state value after the characteristic time τ . Note that conversion process has no effect on the distribution for $s \ll s_0$ therefore the distribution amplitude also saturates in the same typical time τ as N , see Section 4.1.3.

Eq.(4.33) and Eq.(4.36) tells us that the total amount of cargo Φ and the total number of endosomes N reach their respective steady states after a characteristic time which are not the same. Infact, N reaches steady state value much earlier than Φ , see Fig. 4.7(C) and (D). For a given rate of influx J , the time for N to reach steady state value depends upon the fusion rate K , whereas for Φ it depends on the conversion rate k_d . In other words $k_d \ll (JK/(2s_0))^{1/2}$.

4.2.3 Effect of cargo dependent fusion and conversion rates

The rate at which cargo carrying early endosomes can undergo fusion as well conversion can in general be cargo dependent. In the case of a cargo dependent fusion kernel $\mathcal{K}(s, s') = (K_0/2)(s^\mu s'^\nu + s^\nu s'^\mu)$ and cargo dependent conversion rate $k_d(s) = k_d s^\alpha$ a more general solution for steady state for the Conversion model can be obtained,

$$n(s) = \left(\frac{J}{2\pi K} \right)^{1/2} s^{-(3+\mu+\nu)/2} e^{-s/s_\infty^*} \quad \text{for } s > s_0 \quad (4.37)$$

where,

$$s_\infty^* = \left(\frac{2JK}{k_d^2} \right)^{1/(1+\alpha-\lambda)} \quad . \quad (4.38)$$

Scaling analysis and numerical investigations reveal that as long as $k_d(s)$ is not a decreasing function of s the features reported in the Section 4.1.3 and 4.2.1 remains unchanged [67]. Only the shape of the distribution at very large s at steady state and the dependence of s^* on the different parameters at steady state (Section 4.2.1) are modified, see Fig.(4.8). If $k_d(s)$ was an increasing function of s , the cross-over from the linear growth of $\Phi(t)$ with time to the plateau would be much sharper, as shown in Fig.(4.8).

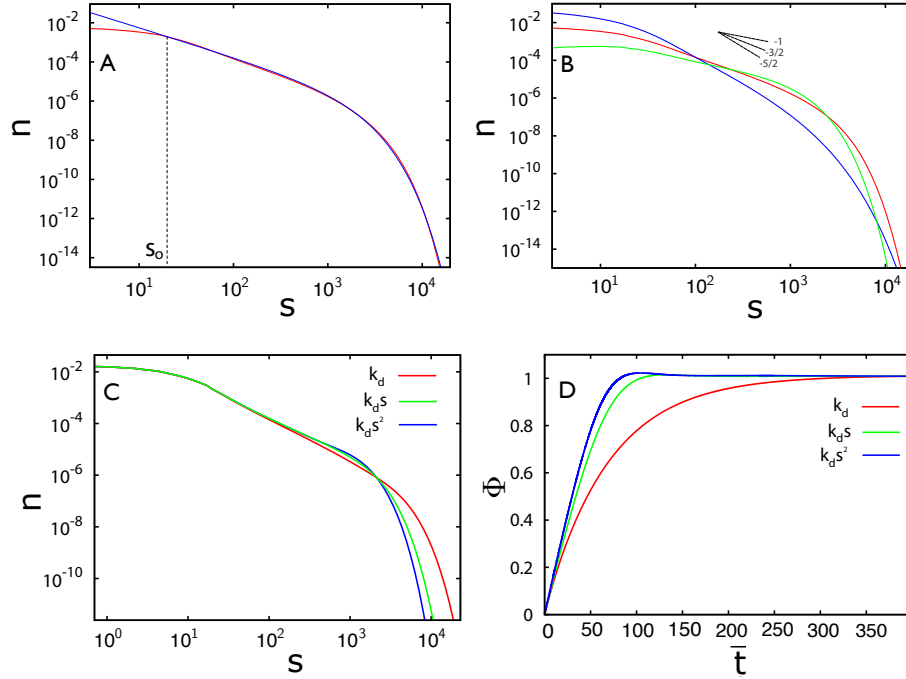


Figure 4.8: **Effect of cargo dependent conversion rate.**

(A) Steady state cargo distribution $n(s)$ obtained for the Conversion model (EFE-C) using a choice constant fusion kernel. The numerically obtained distribution shows a good agreement with the analytical solution given by Eq.(4.30). (Here we set $J/K = 1.8 \cdot 10^6$ FI, $s_0 = 1885$ FI, $k_d/K=2.9$)

(B) Steady state distribution for the Conversion model with the fusion kernel given by the function $K(s, s') = K(ss')^{\lambda/2}$, for different values of lambda. Numerical results are shown by the red curve $\lambda = 0$, green curve $\lambda = -1$ and blue curve $\lambda = 2$. Other parameters are as in (A). The analytical solution $n(s) \sim s^{-(3+\lambda)/2}$ is indicated by the short black lines and associated with the respective power law exponent.

(C) Comparison of numerical results for three different choices of conversion rate as indicated in the legend. Except for very large s , the steady state distributions $n(s)$ for the three choices of conversion rate coincide well.

(D) Total amount of cargo Φ as a function of time t for the Conversion model using different choices of conversion rate $k_d(s)$.

4.3 Entry-Fusion-Exit: Budding model

In the Conversion model the cargo exit from the early endosomes occurred via conversion of a cargo carrying Rab5-positive early endosome into a Rab7-positive late endosome. In this section we will consider an alternative possibility for the cargo exit where the cargo leaves the early endosomal network via heterotypic fission of cargo-carrying vesicles from an early endosome which subsequently fuse with a late endosome. The dynamic equation for $n(s, t)$ in this model is given as,

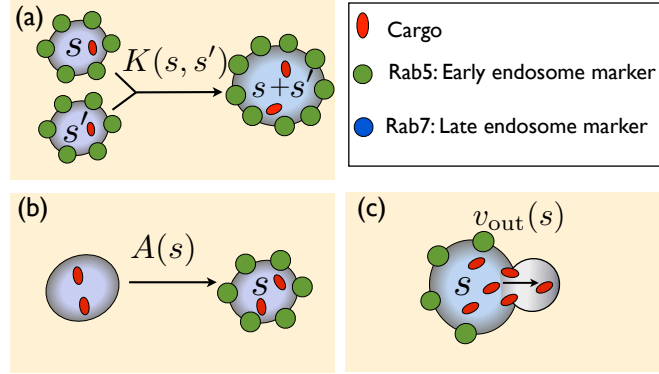


Figure 4.9: **Budding model**

The schemes (a-c) represent the different processes in Conversion scenario, that govern the distribution of cargo $n(s)$ in early endosomes. (a) Homotypic fusion of two endosomes carrying the cargo amounts s and s' . (b) As cargo flows new endosomes carrying the amount s of cargo appear at the rate $A(s)$. (c) Endosomes can lose cargo by budding off vesicular structures. The current $v_{out}(s)$ are the average cargo amount per unit of time respectively lost by an endosome carrying the cargo amount s .

$$\begin{aligned} \frac{\partial n(s, t)}{\partial t} &= \frac{1}{2} \int_0^s \mathcal{K}(s', s-s') n(s') n(s-s') ds' - \int_0^\infty \mathcal{K}(s, s') n(s) n(s') ds' \\ &+ A(s) + \frac{\partial(v_o(s)n(s))}{\partial s} \quad . \end{aligned} \quad (4.39)$$

With in the Budding model we will consider two scenarios:

§ **Constant out-flux:** In this scenario the cargo out-flux from an endosomes is independent of the amount of cargo carried by the endosome. Thus in this scenario

$$v_{out}(s) = v_o \quad . \quad (4.40)$$

This scenario displays a subtle behavior wherein one observes a phase transition by tuning either K , J or v_o .

§ **Constant budding rate:** In the other scenario that we will consider, instead of a constant out-flux the budding of the cargo carrying vesicles from an endosomes occurs at constant rate. In other words, the out-flux of cargo from an endosome is proportional to the amount of cargo it carries. In this scenario,

$$v_{out}(s) = v_o s \quad . \quad (4.41)$$

4.3.1 Constant out-flux: Phase transition scenario

The ingredients of the constant out-flux scenario are summarized in the table. The

$\mathcal{K}(s, s')$	K (constant)
$\mathcal{K}'(s, s')$	0
$A(s)$	$(J/s_0^2)e^{-s/s_0}$
$k_d(s)$	0
$v_{in}(s)$	0
$v_{out}(s)$	v_o (constant)

Table 4.2: Choice of parameters for the Budding model with constant out-flux

time evolution of the total number of cargo carrying early endosomes obeys

$$\frac{dN}{dt} = -\frac{KN^2}{2} + \frac{J}{s_0} \quad . \quad (4.42)$$

The time evolution of the total amount of cargo obeys

$$\frac{d\Phi}{dt} = J - v_o N \quad . \quad (4.43)$$

In order to derive a condition for the existence of a steady state, we write down the next higher moment of the distribution $M_2 = \int_0^\infty ds s^2 n(s)$

$$\frac{dM_2}{dt} = K\Phi^2 - 2v_o\Phi + 2Js_0 \quad . \quad (4.44)$$

At steady state we obtain

$$\Phi = \frac{v_o}{K}(1 - \sqrt{\rho}) \quad (4.45)$$

where the parameter ρ which has been introduced can be positive or negative and is defined as follows,

$$\rho = 1 - \frac{2JKs_0}{v_o^2} \quad . \quad (4.46)$$

We will re-write the above equation in terms of dimensionless parameters as

$$\rho = 1 - \frac{2\bar{K}}{\bar{v}_o^2} \quad (4.47)$$

where, $\bar{K} = Ks_0/J$ and $\bar{v}_o = v_o/J$.

$\rho > 0$: From Eq.(4.43-4.45) one can see that the quantity Φ has a steady state only for the case when $\rho \geq 0$. In this case the distribution $n(s)$ at the steady state,

i.e when $d\Phi/dt = 0$ can be solved starting from Eq.(4.39) and using the parameter choice given in table 4.3.1. The steady state distribution $n(s)$ is given as,

$$n(s) \simeq \left(\frac{Js_0^2}{6\pi K} \right)^{1/2} s^{-5/2} e^{-s/s^*} \left(\frac{s}{s^*} + \frac{3}{2} \right) \quad . \quad (4.48)$$

where s^* is given by,

$$s^* = \frac{2JKs_0^2}{3\rho v_o^2} \quad . \quad (4.49)$$

The distribution displays a power law decay $n(s) \sim s^{-5/2}$ up till a critical cargo amount denoted by s^* beyond which the distribution crosses over into a sharper exponential decay. In this regime the total amount of cargo Φ reaches a steady state in the characteristic time τ . This characteristic time τ to reach steady state is the same for total number of endosomes N and is given by $\tau = (2s_0/(JK))^{1/2}$. The limit $\rho = 0$ is a critical point where s^* diverges and the total amount of cargo attains a maximum value,

$$\Phi_{max} = \frac{v_o}{K} \quad . \quad (4.50)$$

The distribution $n(s)$ in this regime displays a pure power law given as $n(s) \sim s^{-5/2}$.

$\rho < 0$: In this regime the influx of cargo J is much greater than the out-flux v_o to be balanced by it and the total amount of cargo in the network Φ never reaches a steady state. One could, in this case, neglect the contribution of v_o . However, the total number of endosomes N , irrespective of the value of ρ always reaches steady state and always in the same characteristic time, given by $\tau = (2s_0/(JK))^{1/2}$. The distribution in the cargo range $s_0 \ll s \ll s_c$ at large times is given by

$$n(s) \simeq \left(\frac{J}{2\pi K} \right)^{1/2} s^{-3/2} \quad (\text{for } s \gg s_0). \quad (4.51)$$

Fig.4.10 shows the phase plot for the control parameter ρ which separates the two regimes discussed above.

4.3.2 Constant budding rate

In this section we will study the scenario wherein the cargo exit from Rab5-positive endosomes via budding occurs at a constant rate v_o . In the preceding section we looked at the scenario wherein budding takes place at a constant flux. The ingredients of this scenario are summarized in the table.

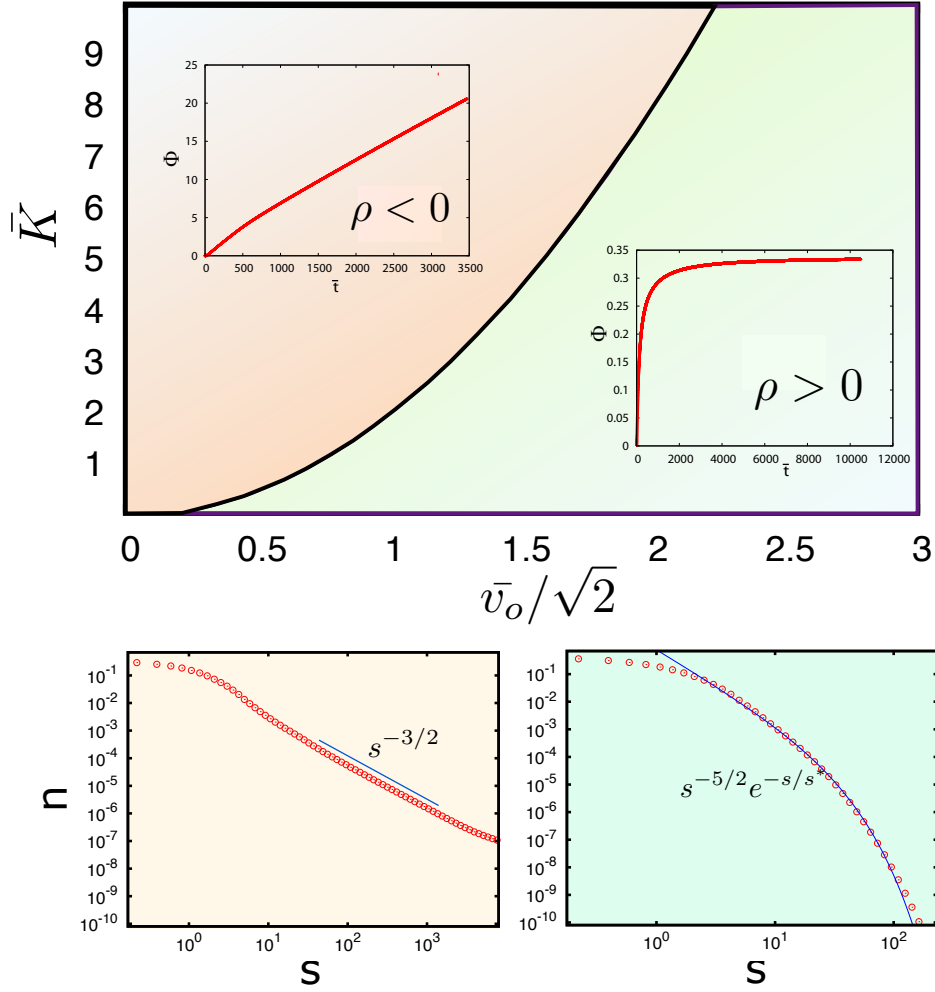


Figure 4.10: **Phase diagram for the budding model with a constant out-flux**
 Tuning the order parameter ρ given by Eq.(4.47) drives the system to one of the two states.
 If $\rho < 0$ the system never reaches a steady state and leads to infinite accumulation of the total amount of cargo. In this state the cargo distribution at long times displays a power law with exponent $-3/2$.
 If $\rho > 0$ the cargo out flux can balance the in flux eventually and thus the system reaches a steady state. In this state the distribution has a profile given by $s^{-5/2}e^{-s/s^*}$, where s^* is given by Eq.(4.49).

In the Laplace space and the limit $s \gg s_0$ the dynamic equation for $n(s)$ Eq.(4.39) with the parameter choice given in the table 4.3.2 reads as

$$\frac{\partial h(z, t)}{\partial t} = \frac{1}{2}Kh(z)^2 - Jx + v_o x \frac{\partial h(z)}{\partial z} \quad . \quad (4.52)$$

$\mathcal{K}(s, s')$	K (constant)
$\mathcal{K}'(s, s')$	0
$A(s)$	$(J/s_0^2)e^{-s/s_0}$
$k_d(s)$	0
$v_{\text{in}}(s)$	0
$v_{\text{out}}(s)$	$v_o s$

Table 4.3: Choice of parameters for the Budding model with constant rate

For the steady state defined as $\frac{\partial h(z,t)}{\partial t} = 0$, Eq.4.52 can be solved in the limiting case

$$\begin{aligned}
 n(s) &\simeq \left(\frac{J}{2\pi K}\right)^{1/2} s^{-3/2} & (s_0 \ll s \ll s_\infty^*) \\
 n(s) &\sim e^{-s/s_\infty^*} & (s \gg s_\infty^*)
 \end{aligned} \tag{4.53}$$

where $s_\infty^* = (2JK)/v_o^2$. Fig.4.11(A) shows the steady state solution for EFE model wherein cargo exit from an endosome occurs via budding at a constant rate, Eq.(4.53). The Conversion model (Section4.2) and the Budding model with constant release rate share some similarities in the properties of steady state distribution. In both the models the distribution $n(s)$ at steady state is given by,

$$\begin{aligned}
 n(s) &\simeq \left(\frac{J}{2\pi K}\right)^{1/2} s^{-3/2} & (s_0 \ll s < s_\infty^*) \\
 n(s) &\sim e^{-s/s_\infty^*} & (s \gg s_\infty^*) \quad .
 \end{aligned} \tag{4.54}$$

Even though the steady state distribution may have some characteristic properties, the distribution are qualitatively different, as shown in Fig.4.11(B).

4.3.3 Total amount of cargo and total number of endosomes

The total amount of cargo in early endosomal population $\Phi(t)$ obeys:

$$\frac{d\Phi}{dt} = J - v_o\Phi \quad . \tag{4.55}$$

The solution is,

$$\Phi(t) = (J/v_o)(1 - e^{-v_o t}) \quad . \tag{4.56}$$

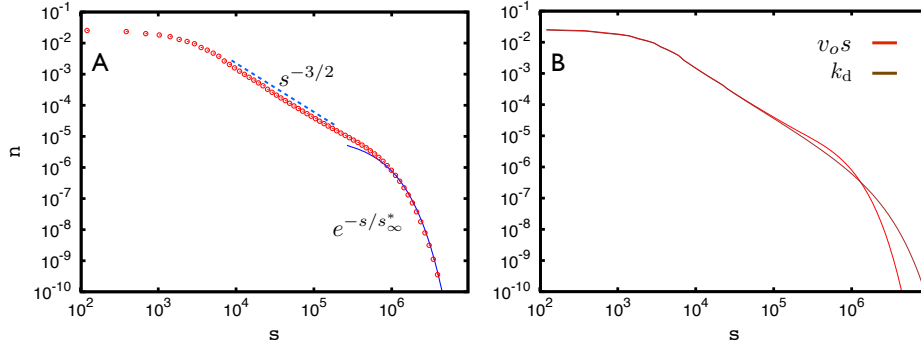


Figure 4.11: **Constant budding rate : steady state distribution**

(A) The steady state distribution for the constant budding rate model.

(B) Comparison of the steady state for the conversion scenario with a constant conversion rate (brown curve) and budding scenario with a constant budding rate (red curve). Both the distribution shown here are obtained numerically for the parameter set with the same magnitude.

The total amount of cargo in early endosomal network reaches the steady state after a time $t \gg v_o^{-1}$. The total number of cargo carrying early endosomes $N(t)$ obeys,

$$\frac{dN}{dt} = -\frac{KN^2}{2} + \frac{J}{s_0} \quad . \quad (4.57)$$

The solution is,

$$N(t) = N_0 \tanh(t/\tau) \quad . \quad (4.58)$$

where, N_0 and τ are the same as given for Eq.(4.36). Observing Eq.(4.56) and Eq.(4.33) for total amount of cargo and Eq.(4.58) and Eq.(4.35) for the total number of endosomes, one can see straightaway that the two models have striking similarities in several of their properties. In the next rather short section we will summarize these two models in terms of their similar features.

4.4 Conversion and Budding at constant rate: Similarities between the models

The Conversion (EFE-C) model and the Budding (EFE-B) model bear some striking similarities in their properties. We summarize in the table below some of the properties which the Conversion and Budding model bear in common.

	Conversion model	Budding model
Steady state, $n(s)$	$\sim s^{-3/2}e^{-s/s_\infty^*}$	$\sim s^{-3/2}$ for $s_0 \ll s \ll s_\infty^*$ $\sim e^{-s/s_\infty^*}$ for $s \gg s_\infty^*$
Typical cargo amount at steady state s_∞^*	$(2JK_0)/k_d^2$	$(2JK_0)/v_o^2$
Number of endosomes $N(t)$	$\simeq N_0 \tanh(t/\tau)$ for $k_d \ll (K_0N)/2$	$N_0 \tanh(t/\tau)$
Total amount of cargo $\Phi(t)$	$(J/k_d)(1 - e^{-k_d t})$	$(J/v_o)(1 - e^{-v_o t})$

Table 4.4: Similarities between conversion and budding model with constant exit rate.

4.5 Conclusion

In this chapter we have studied analytically and numerically a very simple theoretical model describing an out of equilibrium process, which we refer to as Entry-Fusion-Exit model. The model describes the dynamics of a closed compartment of Rab5-positive endosomes with variable cargo content s . We start from a situation where there are no cargo carrying endosome in the compartment. Endosomes carrying a low amount of cargo appear per unit time in the compartment and subsequently undergo fusion. In the absence cargo exit from endosomes, the distribution reaches a pseudo steady state, which is characterized by a broad power law. The exponent of the power is linked directly to the homogeneity exponent λ of the fusion kernel. Far from steady state, the distribution evolves in time in a self-similar manner. This means that the whole distribution at each time is characterized by only one characteristic endosome size or endosomal cargo amount that evolves in time. So, the distribution at various times when rescaled with respect to this characteristic size collapse on to one curve. We extend the Entry and Fusion model by introducing a mechanism for the exit of cargo from early endosomes. Cargo exit process influences the steady state distribution only for endosomes with large amount cargo. The distribution converges into an exponential decay beyond some critical cargo amount. Within the Entry-Fusion-Exit model we studied two different mechanisms governing cargo exit from Rab5-positive endosomes. One being the Conversion model and the other Budding. The simplest case of constant conversion rate k_d and budding at constant rate $v_o s$ show striking similarities in several of their properties which we summarized in the Table 4.4. However, the steady state distribution in the two aforementioned cases differ qualitatively. It would be of interest to compare the two scenarios to experimental distribution and to see which explains the data better. In the next chapter we will introduce cargo

uptake experiments and compare the results from experiments and theory in order to gain some understanding of the endosomal trafficking.

Chapter 5

Comparison between theory and experiment

In the previous chapters we developed a general theoretical framework to describe the dynamic properties of endosomal networks. Our theoretical description takes into account the distribution of cargo within the network as a function of time. We studied the properties of a simple model which we call “Entry-Fusion-Exit” (EFE) model. We showed that a source of new cargo carrying endosomes described by a narrow distribution can evolve in time by homotypic fusion between the endosomes, into a very broad distribution at late times. The distribution at such long times is characterized by a power law followed by an exponential decay. The exponent of the power law depends on the fusion kernel that describes how a population of individual endosomes fuse with each other.

In this chapter we will compare experiments with our theoretical results. To understand the dynamics of cargo trafficking in early endosomal population, we will first look at the data of continuous cargo uptake experiments. In these experiments the cargo used, namely Low Density Lipo-protein (LDL) predominantly undergoes degradation in lysosomes. Following endocytosis the pathway of a degradative cargo such as LDL includes transport via early endosomes followed by late endosomes and eventually culminating in lysosomes where it is degraded. The details of experiments and the image and data analysis is explained in Chapter 2. We will first compare the profile of the cargo distribution in Rab5-positive early endosomes at late times with the results of the EFE model and determine the nature of the fusion kernel by estimating the homogeneity exponent. We compare the results of EFE model with the time course data of the continuous cargo uptake experiments. We will compare of the cargo distribution at late times using two different models, where the difference lies only in the mode of cargo exit from early endosomes. These two different models we referred to and discussed in detail in Chapter 4 as “Conversion” and “Budding”. Finally, we will compare the full

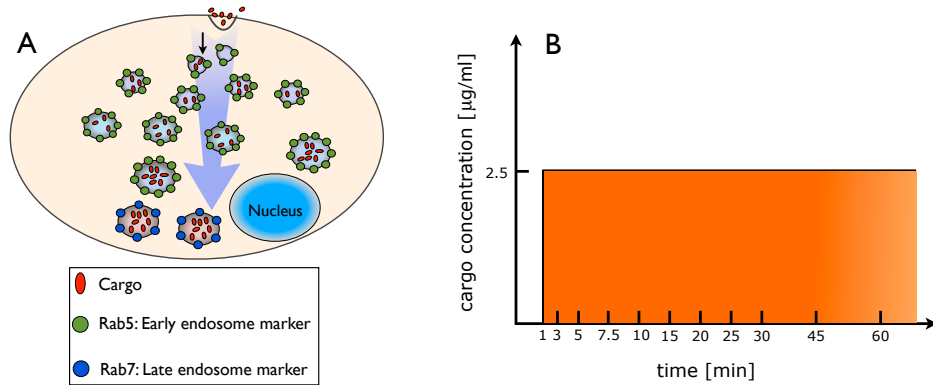


Figure 5.1: **Continuous cargo uptake experiment**

(A) In continuous uptake experiment the cells are allowed to internalize cargo for a fixed duration of time. The internalized cargo is delivered first to a population of Rab5-positive early endosomes. The cargo, which in this case is a degradative cargo, is delivered to Rab7-positive late endosomes to be eventually degraded in lysosomes.

(B) With increasing durations of cargo uptake, the cargo gradually fills up the early endosomal network.

time course of cargo distribution from experiments and numerical simulations and determine the kinetic parameters associated with various biological processes.

Having developed such a quantitative method to describe time evolution of cargo distribution in early endosomal population, we will test our theoretical predictions about the dependence of various quantities on the cargo influx. We will present experiments where the cargo influx into early endosomal population can be varied and test our theoretical predictions with results from such experiments. Finally we will present the pulse chase experiments, wherein the cargo supply to the cells is blocked after a continuous cargo uptake for 60 minutes. We will test our EFE model by comparing the distributions during the cargo chase.

5.1 Continuous cargo uptake experiment

In order to study the flux of cargo through the endosomal network, we performed continuous cargo uptake experiments in which labelled LDL was added at time $t = 0$ at a concentration that was maintained constant at later times. Using quantitative image analysis of still images of populations of cells taken at different times after LDL addition we identified about 27 ± 2 Rab-5 positive vesicular object per cell in each image. For details of image and data analysis see Chapter 2.

At each time point, the distribution of cargo in the entire network of Rab5-positive endosomes can be characterized by the number density $n(s)$ of endosomes per cell with LDL fluorescence intensity s . The total number of cargo carrying

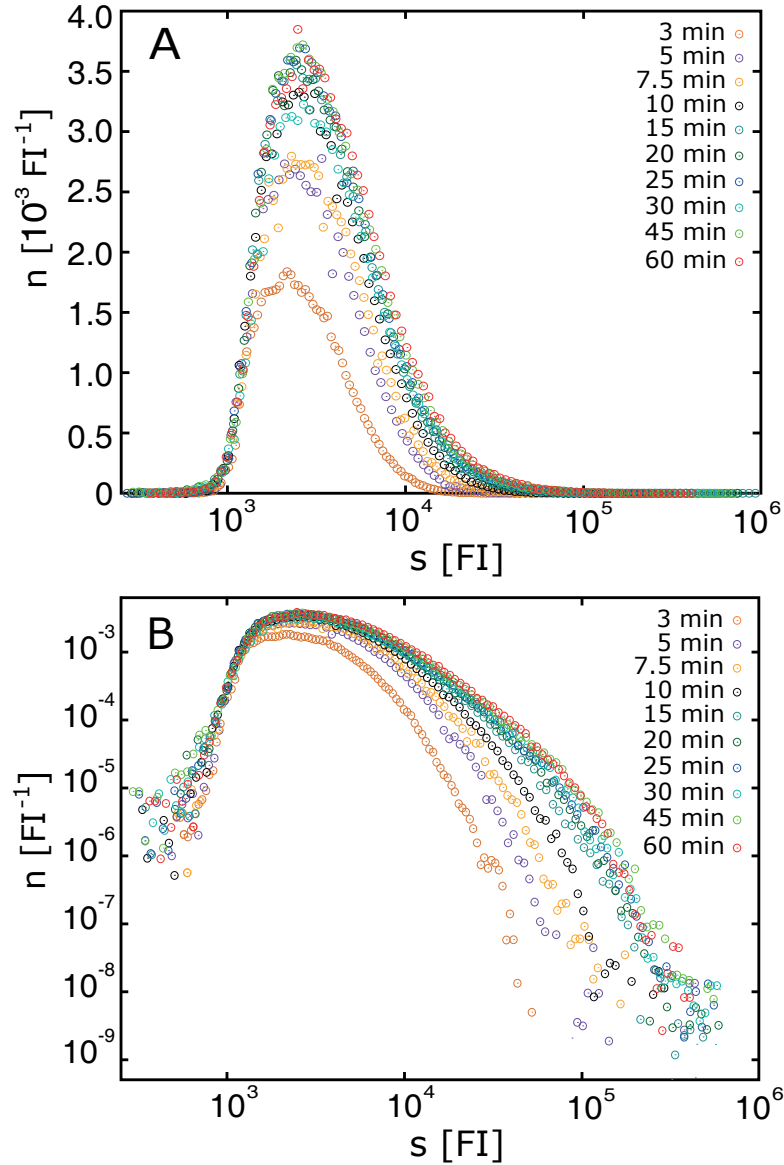


Figure 5.2: Time evolution of the number density $n(s)$, of Rab5-positive endosomes carrying an amount s of LDL.

The number of Rab5-positive endosomes with LDL amount in between s and $s + \Delta s$ is given by $n(s)\Delta s$.

(A) Cargo distribution $n(s)$, in log-linear scale, at different times after addition of LDL. The total intensity of LDL in a Rab5-endosome is denoted s .

(B) Same data plotted in log-log scale.

endosomes per cell is $N = \int_0^\infty n(s)ds$ and the total LDL fluorescence of the endosomes is $\Phi = \int_0^\infty sn(s)ds$. In the course of cargo uptake, the change over time

of $n(s)$ reflects the collective endosome dynamics and, thus, provides a means for deducing microscopic kinetic parameters of the trafficking of cargo through the population of endosomes in the network. Fig. 5.2 (A) and (B) show experimentally observed cargo distributions $n(s)$ at different times after addition of $2.5 \mu\text{g/ml}$ LDL. This data shows that LDL quickly enters many endosomes in small amounts and subsequently concentrates at higher amounts in an increasing number of endosomes. After about 30 minutes, the distribution $n(s)$ reaches a steady state. In this steady state the distribution of cargo amounts in individual endosomes has a broad tail and ranges over three decades of fluorescence intensity, Fig. 5.2 (B). Note that because of the limited microscope resolution the number of endosomes with small LDL amount is underestimated.

5.1.1 Processes shaping the steady state cargo distribution

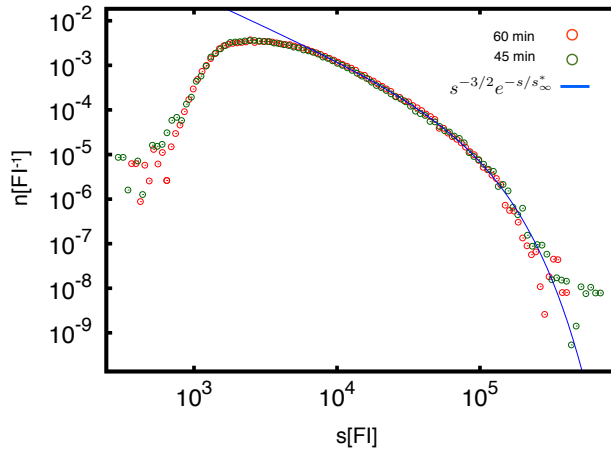


Figure 5.3: **Steady state LDL distribution** $n(s)$

Cargo distribution $n(s)$ in a population of Rab5-positive endosomes at 45 min (green curve) and 60 min (red curve). The distributions almost completely overlap indicating that the distributions have reached a steady state. The blue curve is the function given by Eq.(5.1). The fit to experimental data gives the magnitude of $\theta \simeq -1.5$.

Experimental cargo distribution $n(s)$ shown in Fig.5.2 (A) and (B) reaches a steady state after about 30 minutes. To show this clearly, Fig.5.3 shows the LDL distributions at 45 and 60 minutes respectively. The distribution show very little change and overlap very well when plotted together. The profile of the steady state LDL distribution shown here can be quantified by fitting a function having a form

$$n(s) = s^{-\theta} e^{-s/s_{\infty}^*} . \quad (5.1)$$

The function fits the data very well, see Fig.5.3 and gives the value of $\theta = 1.5 \pm 0.07$. From the general theoretical framework, Fig.3.10, the minimum set ingredients that would give rise to a steady state distribution given by Eq.(5.1) are, a) homotypic endosome fusion, b) cargo loss from Rab5-positive endosomes and c) a source of cargo-loaded endosomes with very low amount of cargo, Chapter 4 (Section 4.2). We referred to a model with such a combination of ingredients as Entry-Fusion-Exit model, Chapter 4. The value of $\theta \simeq -1.5$ suggests that a constant fusion could be a good approximation. This would be mean that all Rab5-positive endosomes fuse at the same rate or with the same probability irrespective of the amount of cargo each one of the fusing endosomes is carrying.

5.2 Entry-Fusion-Exit model to describe LDL trafficking

The general theoretical description of the endosomal network presented in Chapter 3 embraces several cargo exchange mechanisms. In the previous section we saw that the necessary ingredients to describe the steady state distribution of LDL are the ones summarized in Entry-Fusion-Exit model. In this section we will show that the main features of the experimentally observed LDL distributions, not only steady state but time dependent too, can be captured by the Entry-Fusion-Exit model with a simplified choice of a) a constant fusion K , b) a constant conversion k_d and c) a source of cargo-loaded endosomes described by a source function $A(s) = (J/s_0^2)e^{-s/s_0}$, where s_0 is a typical cargo amount in newly appearing endosomes, see Fig.4.6. Within the EFE model, the specific case in which cargo exit from the early endosomal network occurs via only conversion $k_d(s)$ is referred to as Conversion scenario (EFE-C). The alternate case would be when cargo exit occurs via only budding $v_{out}(s)$, which we refer to as Budding scenario (EFE-B). We discussed the theoretical aspect and properties of these two scenarios in the preceding chapter. Since most of the properties of the Conversion and Budding scenario are similar we will use framework of the Conversion model to begin with, for the analysis of the experimental data. Later in the chapter we will also compare the two models in the context of experimental data.

An example of the time evolution of $n(s)$ obtained by numerical solution of the kinetic equation using the parameters of the EFE-C model and ignoring endosome fission ($K' = 0$) and other cargo exchange processes ($v_{in} = 0$ and $v_{out} = 0$) is shown in Fig. 5.4(A). At early times the cargo distribution $n(s)$ is narrow and peaked around s_0 as it is dictated by the source function $A(s)$. Its amplitude rapidly saturates after a characteristic time $\tau = (JK/(2s_0))^{-1/2}$ which depends on the homotypic endosome fusion K and on the influx J . Subsequently, fusion leads

to broadening of the distribution which covers an increasingly large range of cargo amount s in which the distribution follows a power-law decay $n(s) \sim s^{-3/2}$. After a characteristic time set by k_d^{-1} , the distribution reaches the steady state profile

$$n(s) \simeq \left(\frac{J}{2\pi K} \right)^{1/2} \frac{e^{-s/s_\infty}^*}{s^{3/2}} \quad (5.2)$$

for $s > s_0$. This profile is characterized by a power-law followed by an exponential tail for $s > s_\infty^*$, where $s_\infty^* = 2JK/k_d^2$.

We tested the predictions of this model by comparison with the experimental results. The experimental data exhibit all key features predicted by our EFE model. For an LDL concentration of 2.5 $\mu\text{g/ml}$, the characteristic time for the amplitude of the distribution to reach steady state is about $\tau = 7 \pm 0.5$ min. Fig.5.4(B). The theoretical prediction that the shape of the distribution for $s > s_0$ only depends on time via s^* can be tested by plotting the experimental data as $n(s) (s^*)^{3/2}$ versus s/s^* (see Fig.5.4(C)). This figure shows that the data at different time collapse on the same functional form (black line) as predicted. The time dependence of s^* is shown in Fig.5.4(D). As predicted by the theory, it increases with time as t^2 (blue line) at early times and saturates at later times. The experiments also obey the theoretical predictions for the total number of LDL-carrying endosomes $N(t)$ and for the total LDL intensity $\Phi(t)$. The time dependence of the number of cargo-carrying endosomes $N(t)$ and of the total LDL fluorescence $\Phi(t)$ of the endosomes after initiating cargo uptake at $t = 0$ are displayed in Fig.5.4(E) and (F). Both N and Φ start from zero, initially increase linearly with time and reach a steady state value. Interestingly, the functional forms of $N(t)$ and $\Phi(t)$ are different. The endosome number N reaches a plateau value earlier than the total fluorescence intensity Φ . Our theory allows explaining such a difference. In the EFE model, the total number of cargo-carrying endosomes $N(t)$ obeys:

$$\frac{dN}{dt} = -\frac{K_0 N^2}{2} - k_d N + \frac{J}{s_0} \quad (5.3)$$

The time dependent behavior of total number of cargo-carrying endosomes $N(t)$, in the case that the endosome loss by fusion out-numbers endosome conversion i.e $k_d \ll KN/2$, is given by:

$$N(t) = N_0 \tanh(t/\tau) \quad . \quad (5.4)$$

where, $N_0 = (2J/(Ks_0))^{1/2}$ is the steady state number of cargo-carrying early endosomes and $\tau = (JK/(2s_0))^{1/2}$ is the characteristic time in which N reaches the steady state value. Note that the distribution amplitude also saturates in the same typical time. The observed time dependence of the total number of cargo

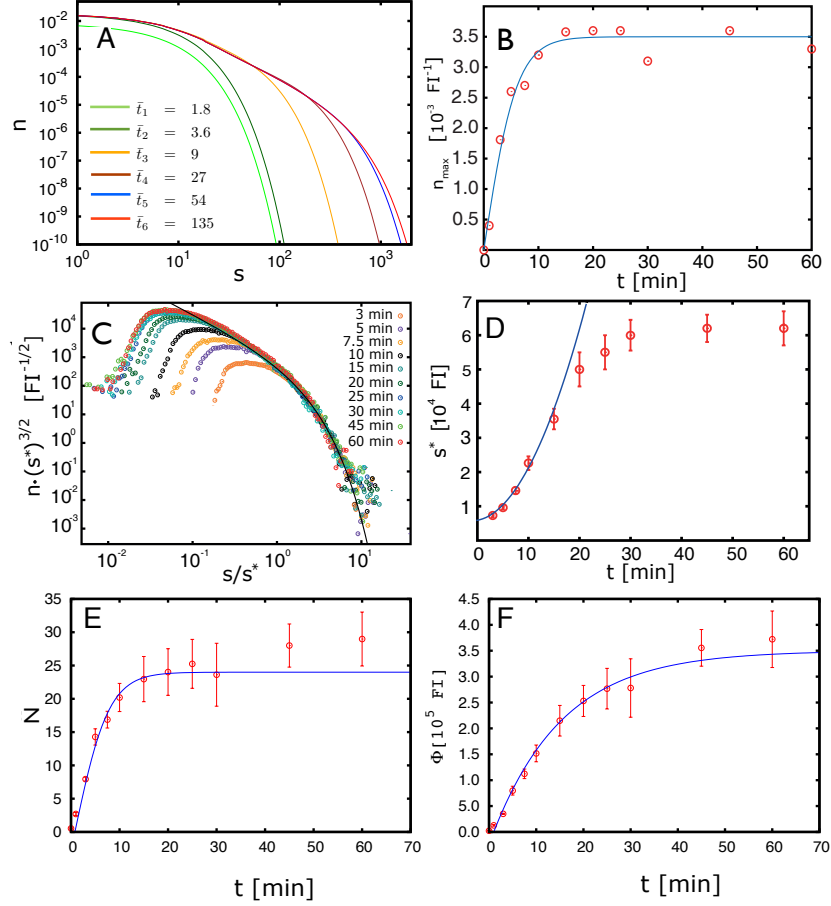


Figure 5.4: **Time dependent properties of LDL trafficking**

(A) Numerical solution of the kinetic equation for the EFE model (parameters shown in Table I) at different times 3 min – 60 min after allowing the internalization of the labelled cargo into the endosomal network. At the initial time $t = 0$, the system does not contain cargo $n(s, t = 0) = 0$. (Here we set $J/K = 1.8 \cdot 10^6 \text{ FI}$, $s_0 = 1885 \text{ FI}$, $k_d/K = 2.9$).

(B) The maximum n_{max} of the distributions $n(s)$, shown in Fig.5.2, as a function of time. The solid line represents the fit of the function $n_{max}(s, t) \simeq \tanh(t/\tau)$ to the data.

(C) Rescaled LDL distributions $n(s)$ reveals data collapse on the line $n_0(s/s^*)^{-3/2} e^{-s/s^*}$ (shown in black) where s^* is a time dependent scaling factor and $n_0 = 1.4 \cdot 10^3 \text{ FI}^{-1}$.

(D) s^* at different times (red circles). At early times, $s^*(t)$ is well fit to a t^2 function (blue curve).

(E) Total number of LDL-carrying Rab5-endosomes $N(t)$ at different times after addition of LDL.

(F) Total LDL fluorescence intensity in Rab5-endosomes $\Phi(t)$ at different time after addition of LDL. The solid blue lines in (E) and (F) represent the fit of the functions given in Eq.(5.4) and Eq.(5.5) to the data. The EFE model can explain the cause of fast saturation of N and relatively slow saturation of Φ .

carrying endosomes can indeed be well fit to the function given in Eq.(5.4), see Fig. 5.4(E). Furthermore, the time dependent behavior of $\Phi(t)$ is given by:

$$\Phi(t) = (J/k_d)(1 - e^{-k_d t}) \quad . \quad (5.5)$$

The theory predicts that total intensity Φ relaxes exponentially during a time k_d^{-1} to a steady state value J/k_d . The observed behavior of total LDL intensity shown in Fig.5.4(F) is well fit by the function given in Eq.(5.5). We have thus identified two different time scales governing the endosome network dynamics. The fast relaxation of endosome number N occurs in a characteristic time τ which depends on the kinetics of fusion processes and of endosome appearance. In addition, there is a comparatively slow saturation of total cargo amount Φ which occurs after a characteristic time k_d^{-1} which is governed by cargo exit from the network.

The simplified EFE model can account quantitatively for the full shapes of observed cargo distributions $n(s)$ as a function of time, see Fig.5.5. Here, the solid lines indicate fits of numerical solutions to the dynamic equation for $n(s)$ to the experimental data. These fits are obtained by solving the dynamic equation given in Figure 3B for the EFE model with parameters given in Table I. From this fit the values of all kinetic parameters can be obtained. For details of the fitting procedure, see the Supplemental Information. For an LDL concentration of $2.5 \mu\text{g/ml}$ we find $K = 1.4 \cdot 10^{-4} \text{ s}^{-1}$, $s_0 = 3562 \pm 220 \text{ FI}$, $k_d = 1.3 \cdot 10^{-3} \text{ s}^{-1}$ and $J = 494 \pm 25 \text{ FI s}^{-1}$. These values imply that approximately 9 new endosomes with typical cargo amount of $s_0 = 3562 \pm 220 \text{ FI}$ appear per cell per minute. At steady state, the average time between two fusion events for a cargo-carrying endosome is about $1/(KN_0) \simeq 2.8 \pm 0.2 \text{ min}$. Here, $N_0 = 32$ is the total number of Rab5-positive early endosomes containing internalized LDL per cell confocal section at steady state. Finally, the conversion rate is found to be $k_d^{-1} \simeq 13 \pm 0.7 \text{ min}$.

5.2.1 Effect of varying cargo concentration

Having developed a quantitative understanding of the cargo trafficking of LDL by Rab5-positive endosomes we wanted to understand how the endocytic system responds to the increased cargo flow. In this section we will study the effect of varying the LDL concentration in the external medium in which the cells are cultured, on the cargo uptake influx J . Continuous LDL uptake experiments were performed for four different concentrations of LDL in medium. Fig.5.6 shows the total LDL intensity in a population of Rab5-positive endosomes at various times after the start of the experiments, for four different concentrations of LDL. The observed behavior of total LDL intensity shown in Fig.5.6(A) is well fit by the function given by Eq.(5.5). We used this fit to obtain the influx J and the conversion rate k_d for the different LDL concentrations, Fig.5.6(B)-(C). Whereas

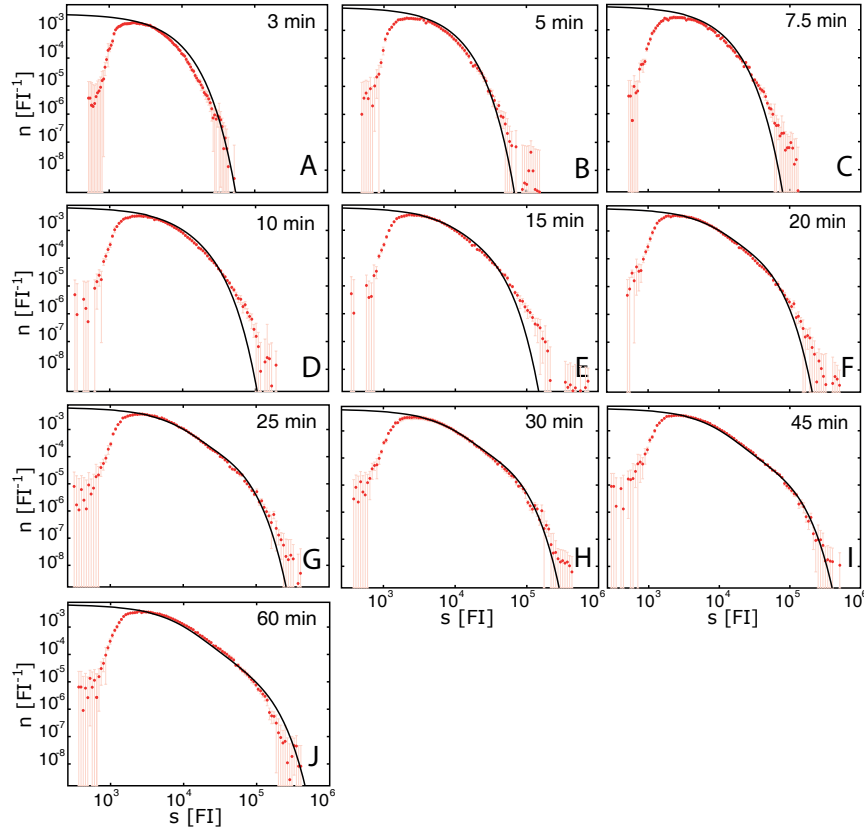


Figure 5.5: Time course of LDL distribution in Rab5 endosomes - theory compared to experiments

(A-J) Fit of the experimental distributions (red circles) at different times after addition of LDL to the Entry-Fusion-Exit model (Table I). The purple solid lines are the solutions of the kinetic equation (Figure 3B) with the parameters choice reported Table I. The parameters value obtained from the fit are $J = 494 \text{ FI s}^{-1}$, $s_0 = 3562 \text{ FI}$, $K = 1.42 \cdot 10^{-4} \text{ s}^{-1}$ and, $k_d = 1.3 \cdot 10^{-3} \text{ s}^{-1}$.

the influx J increases more or less proportionally with external concentration of LDL Fig.5.6(B), the conversion rate however does not change with varying external concentration of LDL. We will now test the accuracy of the EFE model by studying the influence of LDL influx J on the shape of the cargo distribution $n(s)$ at a given time. The LDL influx J depends on the concentration of labelled cargo, see Figure 3E. The observed distributions at 60 min differ for different cargo concentration, see Figure 4C. The steady state cargo distribution according to the EFE model

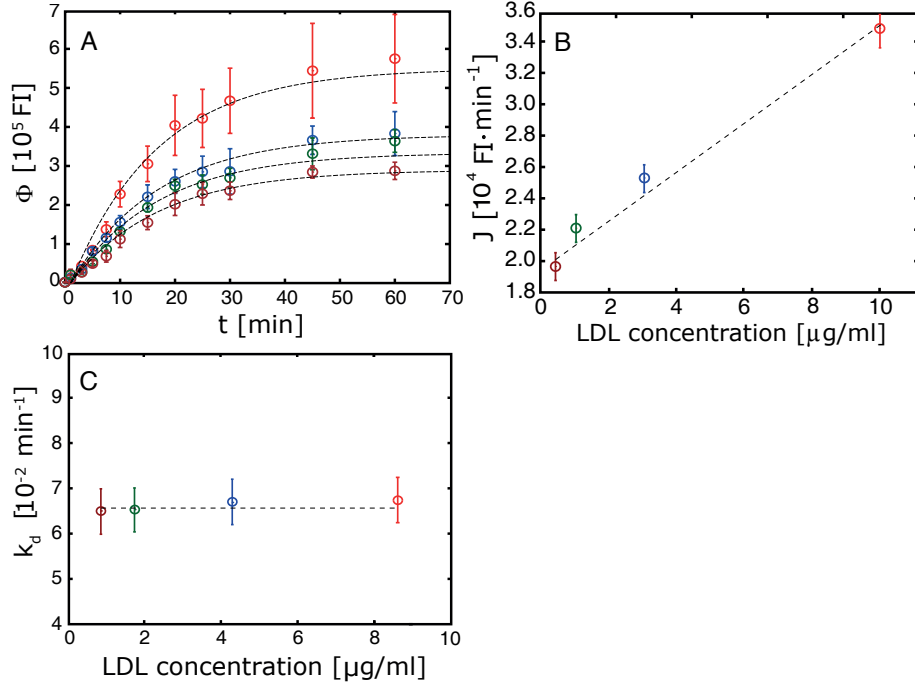


Figure 5.6: **LDL uptake increases proportionally to the external LDL concentration.** (A) Total LDL fluorescence intensity in Rab5-endosomes $\Phi(t)$ at different time after addition of LDL for different concentration of LDL. The dashed lines represent the fit of the functions given in Eq.(5.5) to the data. (B) LDL influx J in Rab5-endosomes for different LDL concentrations obtained from the fit of Eq.(5.5) to the data for $\Phi(t)$, shown in (A). (C) Rate of LDL exit from the network of Rab5-endosomes k_d , for different LDL concentration obtained from the fit of $\Phi(t)$ shown in (A).

with a constant fusion and conversion rate is given by

$$n(s) = \left(\frac{J}{2\pi K_0} \right) s^{-3/2} e^{-s/s_\infty^*} \quad (5.6)$$

where, $s_\infty^* = 2JK_0/k_d^2$. Thus the model predicts that the distribution amplitude increases proportionally to the square root of J , $n(s) \sim J^{1/2}$ and that at steady state $s^* \sim J$. However, in the case of constant fusion and conversion rates $s^* \sim J$ at any time point even before steady state, see Chapter 3. Re-writing Eq.(5.6) such that the intensity scale s is scaled by s_∞^* and substituting dependence $s_\infty^* \sim J$ we get

$$n(s) \sim J^{-1} (s/s_\infty^*)^{-3/2} e^{-s/s_\infty^*} \quad (5.7)$$

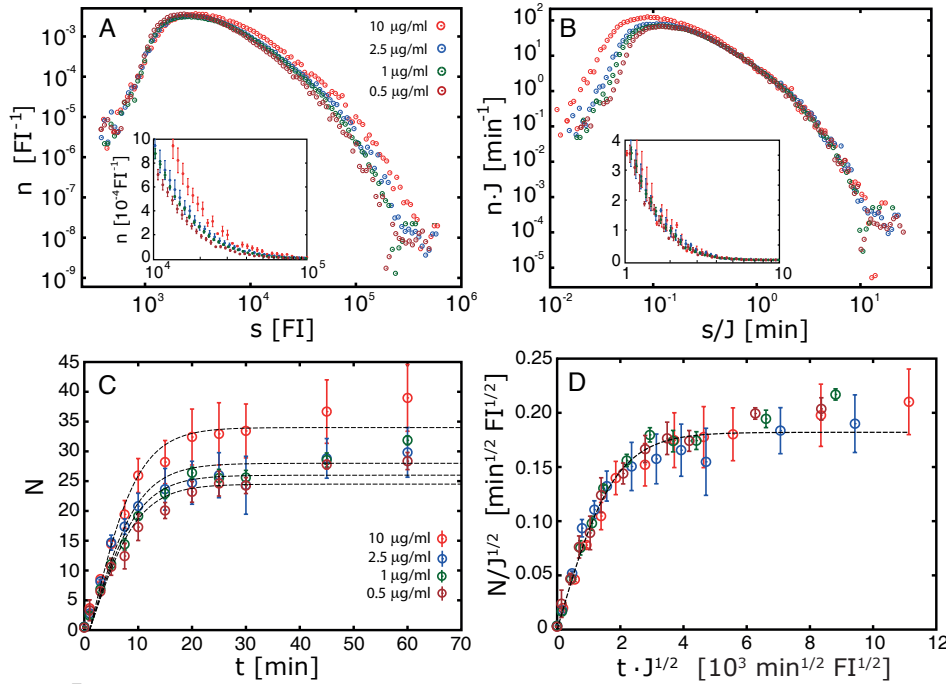


Figure 5.7: **Test of EFE model predictions for varying cargo uptake J .**

(A) LDL distribution $n(s)$ after 45 minutes internalization for four different concentrations of LDL.

(B) Same distributions rescaled by the LDL influx J reveals the data collapse as predicted by the theory. The insets in (A) and (B) show the same collapse in semi-log scale.

(C) Total number of LDL-carrying Rab5-endosomes $N(t)$ at different times after addition of LDL for four different concentrations of LDL.

(D) Plots of the number of cargo-positive Rab5-endosomes as a function of time $N(t)$ shown in (C) rescaled by $J^{1/2}$. The dashed line in (C) and (D) represents the theoretical prediction, Eq.(5.4).

The experimental data follows these predictions as can be seen in Fig.5.7(B) where the data of Fig.5.7(A) collapse on a single curve when plotted on axes that are rescaled by the LDL influx J as dictated by Eq.(5.7).

In the Entry-Fusion-Exit model, the time dependent behavior of the total number of cargo-carrying endosomes is given by Eq.(5.4), which is an approximation that is only valid when the endosome loss by fusion outnumbers endosome conversion, $k_d \ll K_0 N/2$. The observed time dependence of the total number of cargo carrying endosomes can indeed be well fit to the function given in Eq.(5.4), see Fig.5.7(C). Eq.(5.4) predicts that the observed functions $N(t)$ should collapse on the same curve provided that the total endosome number N and the time t are

appropriately rescaled by the LDL influx J . This is indeed the case, see Fig.5.7(D).

5.2.2 Entry-Fusion-Exit: Conversion model versus budding model

The Entry-Fusion-Exit model encapsulates two scenarios which are similar to a large extent as far as the mechanism governing Entry and Fusion is concerned. These two model however differ in the mode of exit of cargo from the early endosomal network. In other words, these two scenarios which we refer to as "Conversion" and "Budding", differ only in the mechanism by which cargo is transported to the late endosomal network. In the Conversion model the transfer of cargo

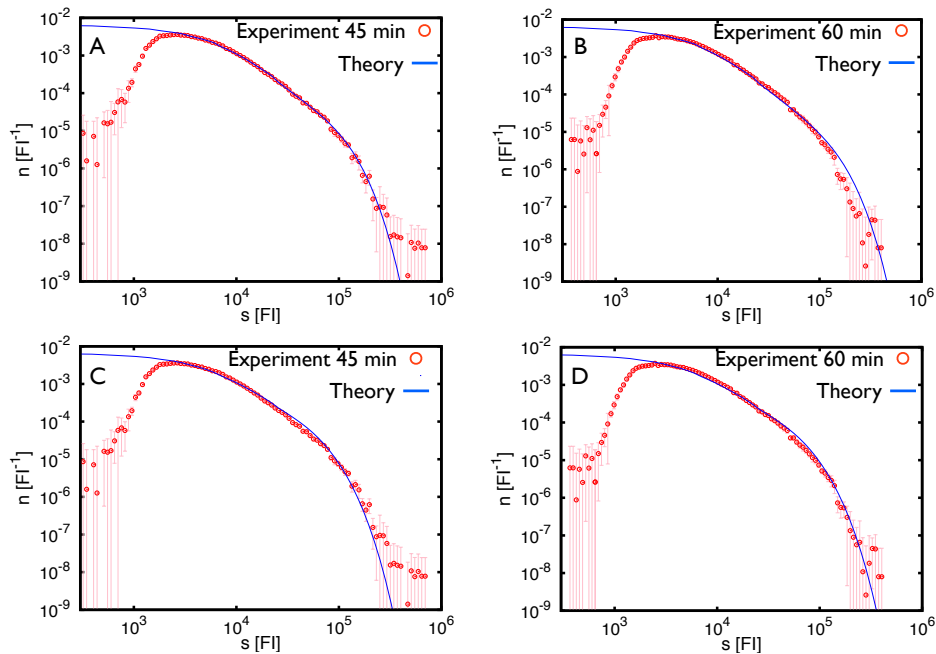


Figure 5.8: **Conversion and Budding model - Comparison of experimental distributions with the theory at late times**

(A-B) Fit of the experimental distributions (red circles) at 45 min and 60 min after addition of LDL to the Conversion model. The purple solid lines are the solutions of the kinetic equation with the parameters choice reported in Table 4.6. The parameter values are the same as reported in Fig.5.5.

(C-D) Fit to the Budding model. The purple solid lines are the solutions of the kinetic equation with the parameters choice reported in Table 4.3.2.

from early to late endosome occurs by conversion of Rab5-positive endosome into a Rab7-positive endosome. In Budding model the transfer of cargo from early to

late endosome occurs by budding of carrier vesicles from early endosomes and subsequent fusion with late endosomes. Even though Budding model differs from the Conversion model in the mode of cargo exit, most of the properties of these two models, in the case of a constant exit rate, are similar. For instance most of the scaling properties exhibited by the Conversion model which have been confirmed in the experiments (see preceding sections) are also exhibited by the Budding model. In Chapter 4 and Section 4.4 we have summarized some of the properties which the Conversion and Budding model bear in common, see Table 4.4 . Thus, within the framework of continuous cargo uptake experiments it would be difficult to find major difference between these two models. However, if we look at the steady state distribution obtained from Conversion and Budding model they show slight difference qualitatively. In Fig.(5.8) we fit the experimental distribution at 45 and 60 min to the steady state distribution obtained from Conversion and Budding model. The Conversion model yields a better quality fit as compared to the Budding model, Fig.(5.8).

5.2.3 Existence of homotypic fission

In the preceding sections we discussed the Entry-Fusion-Exit model in the context of continuous cargo uptake experiments. The experiments are well described by the rather simple EFE model that takes into account, a source of new cargo carrying Rab5-positive endosomes which subsequently undergo homotypic fusion and convert to Rab7-positive endosomes. But what about endosomal fission? In this section we will present analysis that provide some evidence for the presence of homotypic fission of endosomes. This analysis is only qualitative in nature. Fig.5.5 shows the fit of the Entry-Fusion-Exit model to the time evolution of the LDL distribution $n(s)$. Integrating over the distribution obtained from the theory (black solid lines in the figure) for each time point we obtain the total number of endosomes N as a function of time for the given concentration, i.e $2.5\mu\text{g/ml}$. Now, tuning the influx J in the same proportion as in experiments Fig.5.6(B) and keeping the other parameters i.e the fusion rate K_0 and conversion rate k_d same, we obtain N as a function of time for the corresponding four different LDL concentrations. Fig.5.9(A) shows the quantity N obtained from numerical solution of EFE model for the four different LDL concentrations. When $N(t)$ curves obtained from the numerical solution for the four different LDL concentrations are rescaled appropriately as suggested by Eq.(5.4) we see that the curves do not collapse perfectly, Fig.5.9. This means that within the range of the magnitude of parameters that best fit the experimental distribution the conversion rate cannot be considered negligible as compared to the fusion rate. Therefore the approximate solution of N is not correct which becomes evident when rescaling is done and curves fail to completely collapse. Fig.5.9(C) shows the same rescaling car-

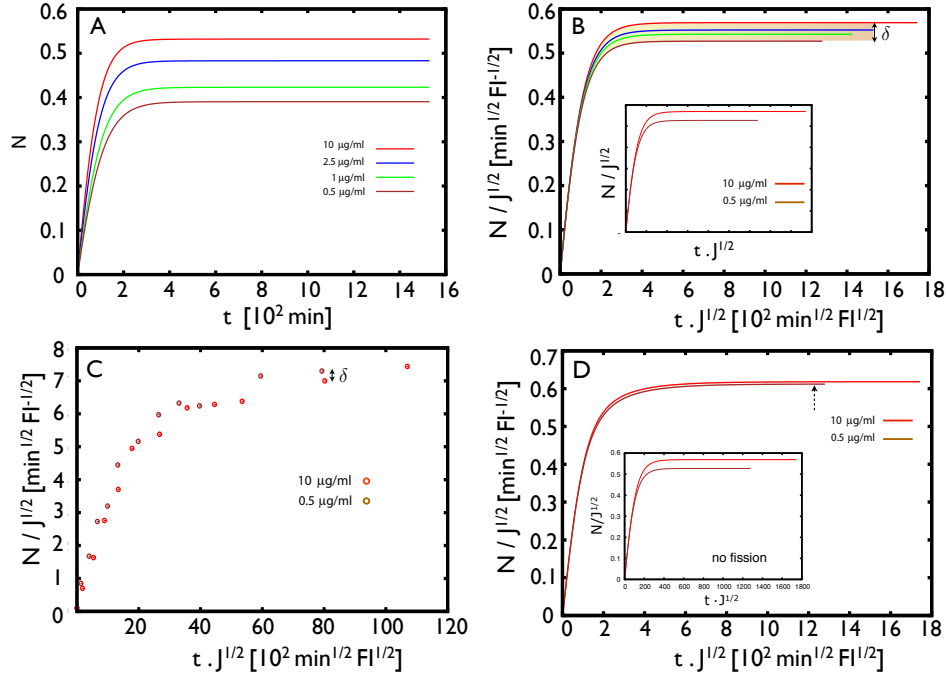


Figure 5.9: Collapse of number of LDL carrying early endosomes for different LDL concentration

(A) From the fit of EFE model to experimental time course distributions we obtain the number of LDL carrying endosomes $N(t)$ for LDL concentration $2.5\mu\text{g/ml}$. Numerically by tuning only the influx J we obtain $N(t)$ curves for four different LDL concentrations.

(B) Rescaling the N curves in (A) by LDL influx J for different LDL concentrations as suggested by Eq.(5.4), we find that the curves do not collapse perfectly.

(C) Experimental curves for N for the highest and the lowest LDL concentration collapse to a higher degree than the theoretical prediction (shown in (B)) when rescaled by J .

(D) Including asymmetric fission to the EFE model improves the degree of collapse of the curves shown in (B).

ried out for experimental data for the highest and lowest concentration. One can straightaway see that the experiments show much higher degree of collapse than the theory for the two extremes of the concentration variation. One can quantify this deviation from the perfect collapse by introducing a quantity δ_{norm} which is the difference between the steady state value of N for the highest concentration, i.e $10\mu\text{g/ml}$ and the lowest concentration $0.5\mu\text{g/ml}$ after both of the values have been normalized to maximum.

$$\delta_{\text{norm}} = N_0(10\mu\text{g/ml}) - N_0(0.5\mu\text{g/ml}) \quad (5.8)$$

We find that $\delta_{\text{norm}}^{\text{exp}} (\sim 0.04) < \delta_{\text{norm}}^{\text{theo}} (\sim 0.06)$. The question we are faced with here is this, how can the width of the envelope of collapse be decreased by a very simple extension of EFE model, at the same time fixing the parameter values of EFE model, obtained by the fit to the experimental time course distributions. The only explanation that holds in this case is that there must exist fission of cargo carrying Rab5-positive endosomes which tends to counter act the effect of conversion. Introducing a constant asymmetric fission given by,

$$K'(s, s') = K' \left(\delta(s - s_f) + \delta(s' - s_f) \right) \quad (5.9)$$

into the EFE model and solving for $N(t)$ gives,

$$N(t) = \left(\frac{\kappa^2}{K^2} + \frac{2J}{Ks_0} \right)^{1/2} \tanh \left(t \left(\frac{\kappa^2}{4} + \frac{JK}{2s_0} \right)^{1/2} + \tanh^{-1} \left(\frac{\kappa}{(\kappa^2 + 2JK/s_0)^{1/2}} \right) \right) - \frac{\kappa}{K} \quad (5.10)$$

where, $\kappa = k_d - K'/s_f$. Thus by tuning the effective fission rate K' the magnitude of conversion rate k_d can be weakened in comparison to the fusion rate K . Theoretically one can tune the magnitude of fission rate to a value such that it exactly balances out the conversion rate thus leaving no term linear in N . At such a point the equation for $N(t)$ is the same as in the case when there were no conversion or fission processes existing, even though the distribution would be qualitatively different in the two cases. In conclusion, if the conversion rate is not negligible compared to fusion rate and deviates the collapse of N for different LDL concentrations then, including a constant asymmetric fission can improve the collapse, see Fig.5.9(D). Fig.5.9(D) shows the rescaling of N for highest and lowest concentration wherein a constant asymmetric was included into the EFE model. Inset shows, for comparison, the same rescaling in the absence of fission.

5.3 Dynamics of Rab5

Up until now we had studied the trafficking dynamics of endocytosed cargo LDL in a population of Rab5-positive early endosomes. Rab5 is always present inside the cell and therefore the distribution of total Rab5 on endosome is always at steady state, as shown in Fig.2.5 (A) of Chapter 2. Since only a small population of Rab5-positive endosomes carry LDL, the basic ingredients that govern the dynamics of Rab5-positive endosomes with or without LDL should be the same. Our analysis shows that the EFE model, which describes time course distribution of LDL, can be extended in a very simple fashion to describe the steady state Rab5. For the parameters of the EFE model we used the same values used to describe LDL

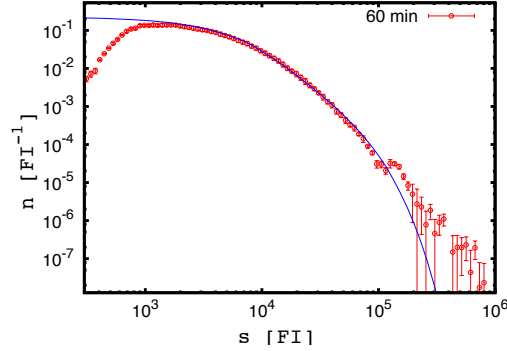


Figure 5.10: **Steady state distribution of endosomal fluorescence intensity of Rab5 and LDL.**

(A) Distribution of total Rab5 fluorescence intensity of vesicles in the whole cell after 60 minutes. The magnitude of parameters of EFE model are the same as used for LDL dynamics, see Fig.5.5. With just the inclusion of one more parameter, that accounts for out-flux $v_{\text{out}}(s) = v_o$, to the EFE model, we can describe the steady state distribution of Rab5 very well. The data fit gave $v_o = 2 \cdot 10^{-6} \text{ FI s}^{-1}$.

dynamics, Fig.5.5. The dynamic equation that describes the time evolution of Rab5 distribution $n(s, t)$ is,

$$\begin{aligned} \frac{\partial n(s, t)}{\partial t} = & \frac{K}{2} \int_0^s n(s')n(s-s')ds' - K \int_0^\infty n(s)n(s')ds' \\ & + J \frac{e^{-s/s_0}}{s_0^2} - k_d n(s) + v_o \frac{\partial n(s)}{\partial s} \end{aligned} \quad (5.11)$$

where, we have considered a constant out-flux v_o . Eq.(5.11) is just an extension of EFE-conversion model with the additional term that accounts for out-flux. We find that, by simply including the outflux denoted by $v_{\text{out}}(s)$ we can describe the steady state distribution of Rab5, Fig.5.10.

5.4 Conclusion

In this chapter we presented experimental studies of endosomal populations in which LDL distributions in Rab5-positive endosomes are quantified in continuous LDL uptake experiments. Experimental distributions evolve in time and eventually approach a steady state. Our analysis shows that the dynamics of LDL trafficking through the endosomal system can be quantitatively described by considering mainly entry, fusion and exit via conversion of endosomes, Section 5.2. We studied the effect of varying LDL concentration in the medium in which cells are incubated, Section 5.2.1. Varying external LDL concentration influences the rate of LDL influx into the cell and subsequently into the early endosomal network. This provides a direct means to test several predictions of the theory that involve cargo influx. We tested these predictions in experiments and showed that EFE model can indeed explain the data very well. Within the framework of EFE model we also studied two different models namely, Conversion (EFE-C) model and Budding (EFE-B) model. These two models differ only in the mechanism of cargo exit from early endosomes to late endosomes, Section 5.2.2. Theoretically these two models exhibit great similarity in several of their properties. Thus, within the context of only continuous cargo uptake experiments it is not possible to clearly differentiate between these two models. Further, we presented a qualitative analysis of the experimental data which indicate the need to include other processes like homotypic fission of endosomes, Section 5.2.3. The analysis also provides a limit to the contribution of fission in LDL trafficking and suggests that this processes does not play a dominant role in trafficking of LDL. Finally, we extended our analysis to study the distribution of Rab5 in the cell, which remains at steady state during the course of experiment. We use the same framework of EFE model, used to describe LDL dynamics, to describe Rab5 distribution. Our analysis shows that with only one extra parameter we can describe Rab5 distribution. This parameter $v_{\text{out}}(s)$ corresponds to exchange of Rab5 on the vesicle with the cytosol.

Chapter 6

Summary and outlook

In this study, we have developed a theoretical framework to describe how the structure and large scale properties of the endosomal network emerge from the collective behaviour of many endosomes. In our theoretical description of endosomal dynamics we have taken into account individual endosomes and interactions among them. Microscopic interactions among endosomes leads to a distributed network where cargo is sorted and transported to various destinations inside the cell.

Dynamics of endosomal trafficking - Experiments and Observations

In Chapter 2 we have introduced the experiments, their methods and how the data of number density distribution of various markers of an endosome is obtained. We particularly looked at the Continuous cargo uptake experiments. In these experiments cells which initially do not contain fluorescently labelled cargo molecules are incubated in a fixed concentration of the same. The cargo is endocytosed or internalized into the cell via endocytosis. We introduced the steps involved in image analysis that eventually provides us with the statistical information of the various fluorescent markers of an endosomes. We looked at the number density distribution of the total cargo inside the cell at different times following cargo uptake. The cargo distribution evolves, from being a narrow distribution at early times to a much broader distribution at late times, for example around 30 minutes. The total cargo is present in various different intracellular compartments. Organelles that make up these compartments are mostly non interacting across the compartments. To limit ourselves to one compartment of interacting organelles, termed endosomes, we looked at the cargo in sorting/early endosomal compartment. Early endosomal compartment is made up of Rab5-positive early endosomes. These endosomes undergo fusion and fission and thus interact with each other and share and re-distribute the cargo. To obtain the statistical data related to cargo in only Rab5-positive endosomes we introduced the colocalization scheme. We therefore limited ourselves to statistical information from only those endosomes that

harbor Rab5-GFP and fluorescent cargo molecule. The specific cargo we use in our study here is LDL. We presented the number density distribution of LDL in Rab5-positive endosomal population. The distribution also evolves in time, but interestingly approaches a steady state after 25 minutes of LDL uptake. At late times the LDL distribution shows characteristic features like a power law followed by an exponential. What gives rise to the distribution? What are processes that shape it? What gives rise to the exponent of the power law? Addressing these questions from a theoretical standpoint will give us a better understanding of the endosomal trafficking.

Physical description of endosomal dynamics In Chapter 3 we developed a general theoretical framework to describe endosomal trafficking dynamics. Our description is based on the distributions of endosomal markers. Endosomes regularly undergo fusion and fission and thus form a dynamic network for interacting endosomes. Such endosomes regularly interact with each other via fusion and fission their size and shape keeps changing with time. Although the theory presented here is very general and applies to any population of interacting endosomes, we focused on population of Rab5-positive early endosomes. We started off with the description for the time evolution of number density of endosomes with a certain amount of Rab5. At this level of our description the state of an endosome is characterized by the amount of Rab5 it carries. In this description we take into account the microscopic interactions of endosomes like fusion and fission, in addition to influx and outflux of Rab5. We then extended our framework to include the cargo endocytosed into the cell. For this purpose we extend our definition of an endosome, by including the amount of cargo an endosome carries in addition to the amount of Rab5. We refer to this as the two component description. Finally, to study the dynamics of cargo trafficking limited to a population of only Rab5-positive endosome, we integrate the two component description over the variable that identifies with amount of Rab5. We now have an effective description of cargo trafficking in a specific endosomal population. Experimentally we can obtain the distribution of cargo only in a specific population of endosomes, for example Rab5-positive early endosomes. It will be interesting to compare theory and experiments for a particular cargo, which is done in later chapters.

Entry-Fusion-Exit model We studied theoretically a simple model referred to as Entry-Fusion-Exit (EFE) model. This model is developed as a possible description of cargo trafficking in a population of Rab5-positive endosomes. New Rab5-positive endosomes carrying cargo appear following endocytosis. Subsequently these endosomes undergo fusion with each other. And finally, cargo molecules can leave the early endosomal network by either the early to late endosome conversion or via heterotypic fission of small vesicles cargo carrying from Rab5-positive endosomes. We explore the system theoretically and numerically.

An interesting property of such a system is that the interactions among the sub units of the systems, in this case the cargo carrying Rab5-positive endosomes, leads to distribution of endosomes with different sizes and cargo amount. We find the cargo number density distribution evolves in time and reaches a steady state which displays characteristic features, like a power law followed by exponential decay. The distribution of cargo in the endosomal network reaches a steady state, wherein the fluxes balance each other. Some aspects of cargo distribution at steady state and its time dependent properties are sensitive to the specific parameters choice. We find that exponent of the power law at steady state is determined by the fusion kernel, which describes how endosomes fuse with each other. The exponential decay is shaped by the conversion process. The characteristic size beyond which the distribution converges into an exponential is determined by the influx, fusion rate and conversion rate. During the time evolution the distribution evolves in self similar manner. The emergence of a power law distribution in the steady state and a self similar time evolution is strongly linked to the choice of fusion kernel. The fusion kernel should be symmetric and homogeneous function of its arguments. The degree of homogeneity of the fusion kernel determines the exponent of the power law. We studied the two modes of cargo exit, i.e conversion and budding, independently. We find that the two scenarios display strikingly similarity when it comes to several of their properties. In the next chapter we compared the results of our simple theoretical model with the experiments.

Comparison between theory and experiment We have tested the EFE model by experimental studies of endosomal populations in which LDL carrying early endosomes are analyzed using cell imaging and quantitative image analysis. Our systems analysis led to four important conclusions. First, despite the multiplicity of regulatory steps and trafficking mechanisms (Fig.3.10) reflected in the complexity of the pattern of endosomal objects (Fig.2.4), we have shown that the main features of LDL transport through the endosomal network and its trafficking dynamics can be understood with very few simple rules, where homotypic endosome fusion plays a key role. Second, the combination of theory and experiments supports the spatio-temporal funnel model of endosome progression [20, 21]. Third, our approach allows measuring kinetic transport rates which are normally difficult to determine experimentally from a series of still images. Finally, our results suggest that Rab conversion instead of vesicle budding is the principal mode of transport of LDL from early to late endosomes. Our theoretical framework predicts specific scaling properties of cargo distributions which we confirmed in experiments in which endosomal parameters such as the number of endosomes and their cargo content were measured quantitatively. Furthermore, we have shown that the whole time course of cargo distribution in the endosomal network can be quantitatively accounted for by our theory. From our analysis

we deduced that three main processes mainly govern LDL trafficking and dynamics through the endosomal network: A source of cargo-carrying early endosomes (cargo entry), homotypic fusion between early endosomes (cargo concentration) and the exit of cargo from the early endosomal network via endosome conversion (for cargo degradation). Our parameter estimates show that the fusion kernel is constant to a good approximation and that fusion does not depend on LDL levels. This implies that the endosomal system functions largely independently of the presence or absence of LDL. Evidently, the endocytic pathway operates to a certain extent autonomously, i.e. supporting membrane turnover irrespective of the influx of endocytic cargo. However, other types of cargo such as those endowed with signalling functions (e.g. EGF) are known to exert a pronounced influence on the behaviour of the endocytic network [20, 21]. By a fit of the theoretical results to the experimental data, we demonstrated that it is possible to extract values of key kinetic parameters that otherwise are difficult or impossible to measure.

Outlook Our approach differs from traditional studies which are based on biochemical measurements and typically measure average concentrations and fluxes in the cell and the associated kinetic rates. By using image data we could exploit information about the spatial organization of the network and the distribution of cargo in distinct endosomes. The discrete nature of vesicular objects in the network is thus taken into account. The analysis of endosome populations and their statistics reveals properties such as the characteristic time τ of relaxation of the number of cargo-positive endosomes. The large number of endosomes observed allows us to obtain very good statistics of the endosome population. Therefore, we can obtain statistically significant data about the properties of the tails of cargo distributions which carry interesting information about the endosomal network dynamics. This model, which is based on endosome tracking in living cells and functional genomics studies, characterizes the endosomal system as a continuously evolving population of endosomes that progressively grow in size and concentrate cargo for degradation and prepare for conversion [20, 21]. A key result of our work is that homotypic endosome fusion plays a key role in shaping the network. This probably reflects the need to progressively accumulate LDL from many small endosomes into few large endosomes for degradation [20]. The situation might be different for other cargo types, for example Transferrin, which recycles from early endosomes to the cell surface attached to its receptor on the membrane. In this case, endosome fission might play a more important role than for LDL. It has been postulated that cargo induces the assembly of the endocytic transport machinery thereby determining the kinetic properties of the endosomal network [36]. Notably, our approach allows us to determine kinetic parameters of endosome dynamics by analyzing still images taken at different times. For example, we could deduce the rates of cargo influx, homotypic endosome fusion and early-to-late endosome conversion. This shows the great potential of our theoretical framework as a general tool for the quantitative analysis of intracellular transport between compartments. It can also be applied to other endosome markers, e.g. EEA1, other types of cargo, e.g. Transferrin or to other vesicular structures in the cell. Quantitative image analysis data coupled to theory can thus be aimed at studying the collective properties of cellular organelles in general and their underlying mechanistic design principles. Previous studies have shown that transfer of cargo from early to late endosomes can occur via two, non exclusive mechanisms. Whereas viral cargo exits from early endosomes harbouring Rab5 by the budding of Rab-7 positive vesicles [28, 24], LDL-containing endosomes undergo conversion from a Rab5 to a Rab7 compartment [20]. The fact that the Entry-Fusion-Exit model can account for all key features of the experimental data in different experimental conditions suggests that endosome conversion is the predominant mechanism for the cargo and cellular model systems analysed here. In the case of LDL, endosome

fission and cargo exchange processes play a minor role for overall network shape and dynamics. An estimate of the kinetic rates of these sub-dominant processes will thus require further experimental data and data analysis. These conclusions, however, do not exclude the possibility that cargo other than LDL may exert a more active role on the dynamics of the endosomal network. For example, EGF has a more active effect on the endosomal parameters [20, 21] and its mode of transfer from early to late endosomes may not necessarily occur mainly by conversion. We have shown that the population analysis of many endosomes provides reliable and robust information about endosomal network dynamics. Because the cargo distribution can vary in response to changes of the endocytic system, our analysis provides a powerful tool for the study of genetic and chemical perturbations that may alter specific systems properties. This could allow understanding the function of specific genes that regulate for example endosome fusion and fission by analyzing alterations of the cargo distributions under gene knockout or knock-down condition. Finally our population analysis of endosomal networks could be applied to different cargo systems such as the secretory pathway and in more physiological systems such as tissues and organs where kinetic properties can normally be inferred only by technically demanding live imaging approaches.

Appendix A

Numerical analysis of continuum description

The distribution $n(s)$ has to be calculated on a wide range $]0; s_{max}[$ (at least three decades) of s values. To limit the number of computed points but still keep enough precision in the small s part of the curve, the equation is discretized on a grid in which the step-size increases exponentially. For this purpose, we follow and extend the method described in [59]. We first make the change of variable as, $s = e^z - 1$ and $\varphi(z, t) = n(s(z), t)$. The infinity in the integral upper limit is replaced by a large but finite value s_{max} to which correspond the largest z value, $z_{max} = \ln(s_{max} + 1)$. At very large s , the distribution usually fall-off rapidly beyond a typical value s^* because of the sink terms of the kinetic equation. We chose $s_{max} \simeq s^*$ so that the finiteness of integration range has a negligible effect. We usually take $s_{max} = 10000$. The kinetic equation of the EFE model (Eq.(3.41)) becomes,

$$\begin{aligned}
\frac{\partial \varphi(z, t)}{\partial t} = & \frac{1}{2} \int_0^z \mathcal{K}(e^{z'} - 1, e^z - e^{z'}) \varphi(z', t) \varphi(\ln(e^z - e^{z'} - 1), t) e^{z'} dz' \\
& - \int_0^{z_{max}} \mathcal{K}(e^z - 1, e^{z'} - 1) \varphi(z', t) \varphi(z, t) e^{z'} dz' \\
& + \int_0^{z_{max}} \mathcal{K}'(e^z - 1, e^{z'} - 1) \varphi(z + z', t) e^{z'} dz' \\
& - \frac{1}{2} \int_0^z \mathcal{K}'(e^{z'} - 1, e^z - e^{z'}) \varphi(z, t) e^{z'} dz' \\
& + A(e^{z'} - 1) - k_d(e^{z'} - 1) \varphi(z, t) \\
& - e^{-z} \partial_z \left(v_{in}(e^z - 1) \varphi(z, t) \right) + e^{-z} \partial_z \left(v_{out}(e^z - 1) \varphi(z, t) \right) \quad (\text{A.1})
\end{aligned}$$

z is discretized with a constant step size $\Delta z = z_{max}/i_{max}$ where i_{max} is the number of points of the grid (we usually use $i_{max} = 100$). The integrals over z' in Eq.(A.1)

are calculated using the trapezoidal rule. To compute the first integral in Eq.(A.1), we need to know n at the point $s - s'$ i.e., φ at the point $\ln(e^z - e^{z'} - 1)$ which does not correspond to a point of the grid. To evaluate φ at a point z in between the grid point z_i and z_{i+1} , we use the interpolation formula,

$$\ln \varphi(z) \simeq \ln \varphi(z_i) + \left(\frac{\ln \varphi(z_{i+1}) - \ln \varphi(z_i)}{z_{i+1} - z_i} \right) (z - z_i) \quad . \quad (\text{A.2})$$

The derivative in the first term (v_{in} term) on the 6th line of Eq.(A.1) is calculated by taking $\partial_z f(z) = (f_i - f_{i-1})/(\Delta z)$ and using the zero-flux boundary condition $f_{-1} = 0$. For the second term of the 6th line (v_{out} term), we calculate the derivative as $\partial_z f(z) = (f_{i+1} - f_i)/(\Delta z)$. To calculate the derivative at the upper boundary, we need the distribution value at $z_{\text{max}+1}$. For this we use the extrapolation formula,

$$\ln \varphi(z_{\text{max}+1}) \simeq \ln \varphi(z_{\text{max}}) + \left(\frac{\ln \varphi(z_{\text{max}}) - \ln \varphi(z_{\text{max}-1})}{z_{\text{max}} - z_{\text{max}-1}} \right) (z_{\text{max}+1} - z_{\text{max}}) \quad . \quad (\text{A.3})$$

To compute the time evolution, we use the first order Euler method, $\varphi(z, t_{j+1}) = \varphi(z, t_j) + \partial_t \varphi(z, t_{j+1}) \Delta t$. To ensure the stability and the accuracy of the solution obtained using this scheme, the time is discretized with a time step $\Delta t = 0.01$. Altogether, this numerical scheme allows integrating the considered kinetic equation up to $t = 60$ minutes within ~ 35 seconds on a standard desktop computer.

Appendix B

Fit of EFE model to experimental data : procedure

We estimate the parameters K, J, s_0 and k_d of the Eq.(4.23) (see Chapter 4) by fit of the theory to the experimental data. For this purpose we rewrite the kinetic equation in dimensionless form. We introduce the dimensionless quantities:

$$x = s/s_0, \quad \psi(x) = n/\tilde{n}, \quad \tilde{t} = t/\tau, \quad \tilde{k}_d = k_d\tau \quad , \quad (\text{B.1})$$

where,

$$\tilde{n} = \sqrt{J/(Ks_0^3)}, \quad \tau = 1/(K\tilde{n}s_0) \quad . \quad (\text{B.2})$$

Applying this transformation to Eq.(4.23) becomes:

$$\frac{\partial\psi(x, \tilde{t})}{\partial\tilde{t}} = \frac{1}{2} \int_0^x \psi(x-x')\psi(x')dx' - \psi(x) \int_0^\infty \psi(x)dx' + e^{-x} - \tilde{k}_d\psi \quad . \quad (\text{B.3})$$

The theory predicts a steady state for the distribution $n(s)$ as also observed in experiments. The steady state is defined as $d\Phi(t)/dt = 0$. First we fit the distribution at steady state, i.e. time points 30, 45 and 60 minutes, employing the standard least square fitting approach. We fit the distribution only in the region in s space that extends from the peak of the distribution, s_0 , up to the tail, i.e. $s > s_0$. We minimize the following χ^2 parameter.

$$\chi^2 = (1/N) \sum_{i=0}^{i=N} \left(\frac{n(s_i^{exp}) - n(s_i^{the})}{\sigma(s_i^{exp})} \right)^2 \quad (\text{B.4})$$

where N is the number of data points, $n(s_i^{exp})$ is the magnitude of the experimental distribution at the i^{th} data point, $n(s_i^{the})$ is the magnitude of the theoretical

distribution at the i^{th} data point, $\sigma(s_i^{exp})$ is the variance in the experimental data at the i^{th} point.

The steady state is fit with three parameters, $s_0, \tilde{n}, \tilde{k}_d$. Consequently, the fit of the steady state reveals ratios of the kinetic parameters. Subsequently, we look at the time evolution and tune the parameter τ such that the numerical solutions best match the experimental data at each point. This is achieved by minimizing the average χ^2 for the whole time course, which yields the parameter τ . From τ together with $s_0, \tilde{n}, \tilde{k}_d$ we can deduce the magnitude of all physical parameters.

Appendix C

Contribution of Influx via CCV fusion

In Chapter 5 we showed the comparison of the EFE model to the data of continuous LDL uptake experiment. The theory describes data very well. In our theoretical description we had discussed that the cargo influx into the early endosomal network can occur either via the appearance of new cargo carrying early endosomes or via the fusion of cargo carrying endocytic vesicles like clathrin coated vesicles (CCVs) with already existing cargo carrying early endosomes. The former process in our description is denoted by the term $A(s)$ and the latter by $v_{\text{in}}(s)$. In the EFE model that we discussed in Chapter 5, we had considered the influx only via $A(s)$. In this section we will study the effect of including the cargo influx via $v_{\text{in}}(s)$. We will limit ourselves to the case of constant influx $v_{\text{in}}(s) = v_{\text{in}}$. The qualitative analysis that we present in this section suggests that the influx via $v_{\text{in}}(s)$ cannot contribute more than 30% of the total influx. In the EFE model for continuous LDL uptake, the total amount of LDL in rab5-positive endosomes as a function of time is given by Eq.(5.5). Eq.(5.5) predicts that the observed functions $\Phi(t)$ for different LDL concentrations should collapse on to the same curve when total amount of LDL Φ is divided by the corresponding J . Numerically we confirmed this prediction as shown in Fig.C.1(B), where $\Phi(t)$ curves for four different concentrations of LDL shown in Fig.C.1(A) were appropriately rescaled by the influx J . The curves display a total collapse on to a single curves. Experimentally we tested this prediction by first obtaining the total LDL influx from the $\Phi(t)$ curves for the four different LDL concentrations. Independent of the specific mode of influx it can be shown that at early times the total amount of cargo Φ grows linearly with time,

$$\Phi = (J_v + J_s)t = J_{\text{tot}} t \quad (\text{C.1})$$

where J_v corresponds to the influx due to v_{in} and J_s to the influx via $A(s)$. We obtain the magnitude of J_{tot} from a linear fit of Φ up till only 10 minutes, Fig.C.1(C).

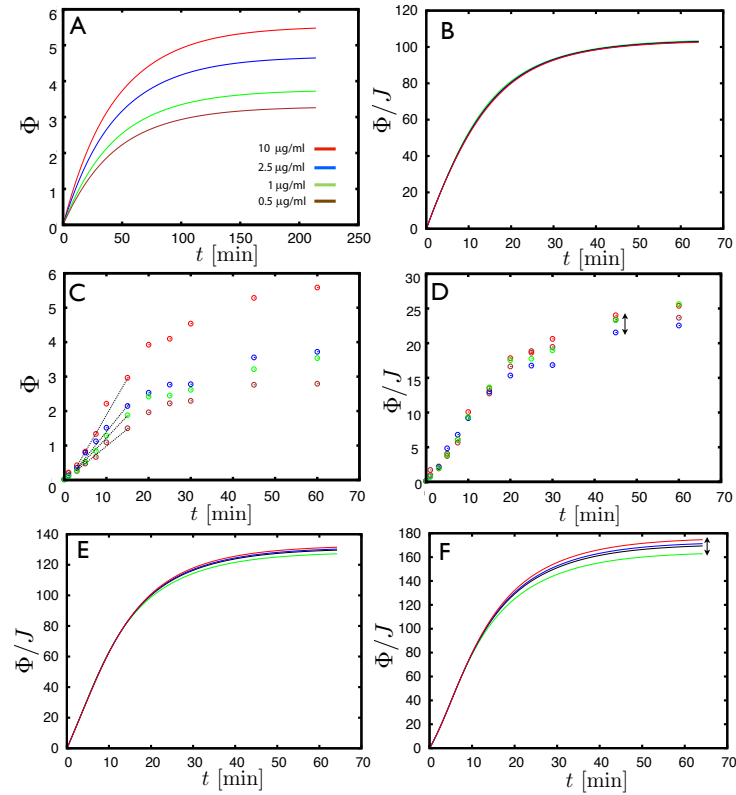


Figure C.1: **Cargo influx via fusion of early endosomes with endocytic vesicles-effects and contribution**

(A) Theoretical curves for the total amount of cargo Φ in early endosomes obtained for EFE model for four different concentrations J .

(B) The Φ curves for four concentrations collapse on to a single curve scaled appropriately by J , as dictated by Eq.(5.5).

(C-D) Experimental curves for Φ show a slight deviation when rescaled by J as suggested by EFE model Eq.(5.5).

The explanation for this deviation is the inclusion of influx via heterotypic fusion of Rab5-positive endosomes with cargo carrying endocytic vesicles, denoted by $v_{in}(s)$ to the existing EFE model.

(E-F) Theoretically we can see that including $v_{in}(s)$ and assuming it has a constant rate, rescaling the Φ with J_{tot} (given by Eq.(C.1)) deviates the curves from a total collapse. This suggests that influx via heterotypic fusion of vesicles with endosomes might exist to extent.

We rescale the Φ curves for different concentrations appropriately by J_{tot} as suggested by Eq.(5.5), Fig.C.1(D). The rescaled data deviates slightly from total collapse which is evident at late times. The EFE model however predicts a total collapse as shown in Fig.C.1(B). The simplest explanation for any slight deviation from the total collapse of Φ is the presence of influx via v_{in} besides $A(s)$. In order to study this effect we extend our EFE model by including a constant influx v_{in} .

Rescaling in the presence of a constant influx v_{in} indeed deviates the curves from a total collapse as shown in Fig.C.1(E), where we fixed the influx due to v_{in} to 20% of the total influx. Increasing the contribution of influx due to v_{in} deviates the curves further from a total collapse as in Fig.C.1(E), where the influx due to v_{in} contributes to 50% of the total influx. Looking at the collapse of experimental data Fig.C.1(D) we suggest that the influx due to v_{in} can contribute around $\sim 40\%$ of the total influx.

Bibliography

- [1] Mellman, I. (1996). Endocytosis and molecular sorting. *Annu. Rev. Cell. Biol.* *12* 575-625.
- [2] Mellman, I. (1986) Acidification of the endocytic and exocytic pathways. *Ann. Rev. Biochem.* *55* 663-700.
- [3] Conner, S.D. and Schimd, S. L. (2003). Regulated portals of entry into the cell. *Nature* *422* 37-44.
- [4] Miaczynska, M., and Stenmark, H. (2008). Mechanisms and functions of endocytosis. *J. Cell Biol.* *180*, 7-11.
- [5] Zerial, M., and McBride, H. (2001). Rab proteins as membrane organizers. *Nature Rev. Mol. Cell Biol.* *10*, 287-292.
- [6] Grosshans, B.L., Ortiz, D., and Novick, P. (2006). Rabs and their effectors: Achieving specificity in membrane traffic. *Proc. Natl. Acad. Sci. USA* *103*, 11821-11827.
- [7] Pfeffer, S. and Aivazian, D. (2004). Targeting Rab GTPase to distinct membrane compartments. *Nat. Rev. Mol. Cell Biol.* *5* 886-896.
- [8] Stenmark, H. (2009) Rab GTPases as coordinators of vesicle traffic. *Nat. Rev. Mol. Cell Biol.* *10* 513-525
- [9] Maxfield, F.R., and McGraw, T.E. (2004). Endocytic recycling. *Nature Rev. Mol. Cell Biol.* *5*, 121-132.
- [10] González-Gaitán, M., and Stenmark, H. (2003). Endocytosis and Signaling: A relationship under Development. *Cell* *115*, 513-521.
- [11] Gould, G.W., Lippincott-Schwartz, J. (2009). New roles for endosomes: from vesicular carriers to multi-purpose platforms. *Nature Rev. Mol. Cell Biol.* *2*, 107-117.

- [12] González-Gaitán, M. (2003). Endocytic trafficking during drosophila development. *Mechanisms of Development* 11, 1265-1282.
- [13] van der Goot, F.G. and Gruenberg, J. (2006). Intra-endosomal membrane traffic. *Trends Cell Biol.* 16, 514-521.
- [14] Miyauchi, K., Kim, Y., Latinovic, O., Morozov, V. and Melikyan, G.B. (2003). HIV enters cells via endocytosis and dynamin-dependent fusion with endosomes. *Cell* 137, 433-444.
- [15] Olkkonen VM, Stenmark H. (1997) Role of Rab GTPases in membrane traffic. *International Review of Cytology* 176, 1-85.
- [16] Mayor, S., Presley, J, F., Maxfield, F, R. (1993). Sorting of Membrane Components from Endosomes and Subsequent Recycling to the Cell Surface Occurs by a Bulk Flow Process. *J. Cell Biol.* 121, 1257-1269.
- [17] Ullrich, O., Reinsch, S., Urb, S., Zerial, M., Parton, RG. (1996). Rab11 regulates recycling through the pericentriolar recycling endosome. *J. Cell Biol.* 135 (4) 913-924.
- [18] Russell, M. R., Nickerson, D. P., Odorizzi, G. (2006). Molecular mechanisms of late endosome morphology, identity and sorting. *Curr. Opin. Cell Biol.* 8 (4) 422-428.
- [19] Gruenberg, J. (2001). The endocytic pathway: a mosaic of domains. *Nature.* 2, 721-730.
- [20] Rink, J.C., Ghigi, E., Kalaidzidis, Y., Zerial, M. (2005). Rab conversion as a mechanism of progression from early to late endosomes. *Cell* 122, 735-749.
- [21] Collinet, C., Stöter, M., Bradshaw, C.R., Samusik, N., Rink, J.C., Kenski, D., Habermann, B., Buchholz, F., Henschel, R., Mueller, M.S., Nagel, W.E., Fava, E., Kalaidzidis, Y., and Zerial, M. (2010). Systems survey of endocytosis by multiparametric image analysis. *Nature* 464, 243-249.
- [22] Poser, I., Sarov, M., Hutchins, J.R., Heriche, J.K., Toyoda, Y., Pozniakovsky, A., Weigl, D., Nitzsche, A., Hegemann, B., Bird, A.W. (2008) BAC TransgeneOmics: a high-throughput method for exploration of protein function in mammals.
- [23] Jekely, G. (2003) Small GTPases and the evolution of the eukaryotic cell. *BioEssays* 25

- [24] Murphy, R.F. (2008). Maturation models for endosome and lysosome biogenesis. *Trends Cell Biol.* *1*, 77-82.
- [25] Misaki, R., Nakagawa, T., Fukuda, M., Taniguchi, T., Taguchi, T. Spatial segregation of degradation- and recycling-trafficking pathways in COS-1 cells. *Biochemical and Biophysical Research Communications.* *360*, 580-585.
- [26] Poteryaev, D., Datta, S., Ackema, K., Zerial, M., Spang, A. (2010) Identification of the switch in early-to-late endosome transition. *Cell*, *141*, no. 3, 497-508, (2010)
- [27] Dunn, K. W. and Maxfield, F. R. (1992) Delivery of ligands from sorting endosomes to late endosomes occurs by maturation of sorting endosomes. *J. Cell Biol.* *117* 301-310.
- [28] Vonderheit, A., and Helenius, A. (2005). Rab7 associates with early endosomes to mediate sorting and transport of semliki forest virus to late endosomes. *PLOS Biology* *3*, 1225-1238
- [29] Sönnichsen, B., De Renzis, S., Nielsen, E., Rietdorf, J., and Zerial, M. (2000). Distinct membrane domains on endosomes in the recycling pathway visualized by multicolor imaging of Rab4, Rab5, and Rab11. *J. Cell Biol.* *149*, 901-913.
- [30] Roberts, R.L., Barbieri, M.A., Chua, M., Morisaki, M.H., Stahl, P.D. (1999). Endosomes fusion in living cells overexpressing GFP-Rab5. *Journal of Cell Science* *112*, 3667-36675.
- [31] Griffiths, G., Back, R., Marsh, M. (1989). A quantitative analysis of the endocytic pathway in baby hamsters kidney cells. *J. Cell Biol.* *109*, 2703-2720
- [32] Schmid, S.L., Fuchs, R., Male, P., Mellman, I. (1988). Two distinct subpopulation of endosomes involved in membrane recycling and transport to lysosomes. *Cell* *52*, 73-83.
- [33] Becker, V., Schilling, M., Bachmann, J., Baumann, U., Raue, A., Maiwald, T., Timmer, J., Klingmüller, U. (2010). Covering a broad dynamic range: information processing at the erythropoietin receptor. *Science* *328* 1404-1408.
- [34] Tzafiriria, A.R., Wua, D., and Edelmana, E.R. (2004). Analysis of compartmental models of ligand-induced endocytosis. *Journal of Theoretical Biology* *229*, 127138.
- [35] Del Conte-Zerial, P., Bruschi, L., Rink, J.C., Collinet, C., Kalaidzidis, Y., Zerial, M., Deutsch, A. (2008). Membrane identity and GTPase cascades regulated by toggle and cut-out switches. *Molecular Systems Biology* *4*, 206.

- [36] Lakadamyali, M., Rust, M.J. and Zhuang, X. (2006). Ligands for clathrin-mediated endocytosis are differentially sorted into distinct populations of early endosomes. *Cell* *124*, 997-1009.
- [37] Sheff, D.R., Daro, E.A., Hull, M., and Mellman, I. (1999). The receptor recycling pathway contains two distinct populations of early endosomes with different sorting functions. *J. Cell Biol.* *145*, 123-39.
- [38] Klausner, R., van Renswoude, J., Harford, J., Wofsy, C. and Goldstein, B. (1985). Mathematical modeling of receptor-mediated endocytosis in endocytosis, Pastan, I., and Willingham, M.C., ed.(New York: Plenum Press), 259-277.
- [39] Lauffenburger, D.A. and Lindermann, J.J. (1993). Receptors: models for binding, trafficking and signaling (New York: Oxford University Press).
- [40] Kalaidzidis, Y. (2007). Intracellular objects tracking. *European Journal of Cell Biology* *86*, 569-578.
- [41] von Smoluchowski, M. (1917). Drei vorträge über diffusion Brownsche molekulare bewegung und koagulation von kolloidteilchen. *Physik. Z.* *17*, 557-571.
- [42] Hogg, R., Healy, T.W. and Fuerstenau, D.W. (1966). Mutual coagulation of colloidal dispersions. *Trans. Faraday Soc.* *62*, 1638-1651.
- [43] Ziff, R.M. (1980). Kinetics of polymerization. *J. Stat. Phys.* *23*, 241-263.
- [44] Turner, M.S., Sens, P., and Succi, N.D. (2005). Nonequilibrium raftlike membrane domains under continuous recycling. *Phys. Rev. Lett.* *95*, 168301.
- [45] Cates, M.E., and Candau, S.J. (1990). Statics and dynamics of worm-like surfactant micelles. *J. Phys.: Condens. Matter* *2*, 6869.
- [46] Turner, M.S., and Cates, M.E. (1990). The relaxation spectrum of polymer length distributions. *J. Phys. (Paris)* *51*, 307-316.
- [47] Meakin, P. (1992). Droplet deposition growth and coalescence. *Rep. Prog. Phys.* *55*, 157.
- [48] Brangwynne, C.P., Eckmann, C.R., Courson, D.S., and Rybarska, A., Hoegge, C., Gharakhani, J., Jülicher, F., Hyman, A.A. (2009). Germline P granules are liquid droplets that localize by controlled dissolution/condensation. *Science* *324*, 1729-1732.
- [49] Brangwynne, C.P., Mitchison, T. J. and Hyman, A.A. (2011). Active liquid-like behavior of nucleoli determines their size and shape in *Xenopus laevis* oocytes. *Proc. Natl. Acad. Sci. U.S.A* *108* 43344339.

-
- [50] Gradstein, I.S., and Ryzhik, I.M (1994). Tables of integrals, series and products.
- [51] Deaconu, M., and Etienne, T. (2002). Smoluchowski's coagulation equation : probabilistic interpretation of solutions for constant, additive and multiplicative kernels. *Scoula Normale Superiore*.
- [52] van Dongen, P.G.J., and Ernst, M.H. (1985). Dynamic scaling in kinetics of clustering. *Phys. Rev. Lett.* *54*, 1396-1399.
- [53] van Dongen, P.G.J., and Ernst, M.H. (1988). Scaling solution of smoluchowski's coagulation equation. *J. Stat. Phys.* *50*, 295-329.
- [54] Rácz, Z. (1985). Agregation in the presence of sources and sinks: A scaling theory. *Phys. Rev. A* *32*, 1129-1133.
- [55] Wattis, J.A.D. (2006). An introduction to mathematical models of coagulation-fragmentation processes: A discrete deterministic mean-field approach. *Physica D* *222*, 1-20.
- [56] Krapivsky, P.L., and Redner, S. (1996). Transitional aggregation kinetics in dry and damp environments. *Phys. Rev. E* *54*, 3553-3561.
- [57] Takayasu, H. (1989). Steady-State Distribution of generalized aggregation system with injection. *Phys. Rev. Lett.* *23*, 2563-2566.
- [58] Vigil, D.R., Ziff, R.M., and Lu, B. (1988). New universality class for gelation in a system with particle breakup. *Phys. Rev. B* *38*, 942-945.
- [59] Krivitsky, D.S. (1995). Numerical solution of the Smoluchowski equation and asymptotics of the distribution function. *J. Phys. A: Math. Gen.* *28*, 2025-2039.
- [60] Hayakawa, H. (1987). Irreversible kinetic coagulations in presence of a source. *J. Phys. A: Math. Gen.* *20*, L801-L805.
- [61] Cueille, S., and Sire, C. (1998). Droplet nucleation and Smoluchowski's equation with growth and injection of particles. *Phys. Rev. E* *57*, 881-900.
- [62] Cueille, S., and Sire, C. (1997). Nontrivial polydispersity exponents in aggregation models. *Phys. Rev. E* *55*, 5465-5478.
- [63] Pushkin, D.O., and Aref, H. (2002). Self-similarity theory of stationary coagulation. *Phys. Fluids* *14*, 694-703.

- [64] Leyvraz, F. (2003). Scaling theory and exactly solved models in the kinetics of irreversible aggregation. *Physics Reports*. *383*, 95-212.
- [65] Cheng, F., Redner, S. and Leyvraz, F. (1989). Coagulation with a steady point monomer source. *Phys. Rev. Lett.* *62*, 2321-2324.
- [66] Lushnikov, A.A., and Kulmala, M. (2002). Singular self-preserving regimes of coagulation processes. *Phys. Rev. E.* *65*, 041604.
- [67] Crump, J.G. and Seinfeld, J.H. (1982). On existence of steady-state solutions to the coagulation equations. *Journal of Colloid and Interface Science* *90*, 470-476.
- [68] Albert, R., Barabási, A-L. (2002). Statistical mechanics of complex networks. *Rev. Mod. Phys.* *74*, 47-97.
- [69] Newman, M.E.J. (2005). Power-laws, Pareto distributions and Zipf's law. *Comptemporary Physics* *46*, 323-351.
- [70] Newman, M.E.J. (2010). *Networks: an introduction* (New York: Oxford University Press).
- [71] Chan, C.C., Epstein, D., Hiesinger, P.,R., (2011). Intracellular trafficking in Drosophila visual system development: A basis for pattern formation through simple mechanisms. *Dev. Neurobiol.* *not yet printed (available online)*
- [72] Newman, M.E.J. (2010). *Trafficking Inside Cells: Pathways, Mechanisms and Regulation (Texas: Landes Bioscience)*.
- [73] Shilo, B., and Schejter, E, D. (2011) Regulation of developmental intercellular signalling by intracellular trafficking. *The EMBO Journal.* *30*, 3516-3526 .
- [74] Dunn, K.W., McGraw, T.E. and Maxfield, F.R. (1989) Iterative fractionation of recycling receptors from lysosomally destined ligands in an early sorting endosome. *J. Cell Biol.* *109* 3303-3314.
- [75] Steer, C.J. and Hanover, J.A. (1991) *Intracellular trafficking of proteins.* (Cambridge University Press)
- [76] Pastan, I. and Willingham, M.C. (1985). *Endocytosis* (New York: Plenum Press).
- [77] Seto, E.S., Bellen, H.J., and Lloyd, T.E. (2002) When cell biology meets development: endocytic regulation of signaling pathways. *Genes Dev.* June 1, 2002 *16*: 1314-1336

-
- [78] Brangwynne, C.P., Koenderink, G. H., MacKintosh, F.C., Weitz, D.A. (2009) Intracellular transport by active diffusion. *Trends in Cell Biol.* *19 (9)* 423-427.
- [79] Kasza, K. E., Rowat, A. C., Liu, J., Angelini, T.E., Brangwynne, C.P., Koenderink, G.H., Weitz, D. A. (2006) The cell as a material. *Curr. Opin. Cell Biol.* *19(1)* 101-107.
- [80] Bonifacino, J. S. and Lippincott-Schwartz, J. (2003) Coat proteins: shaping membrane transport. *Nat. Rev. Mol. Cell Biol.* *4(5)* 409-414.
- [81] Misteli, T. (2001) The concept of self-organization in cellular architecture. *The Journal of Cell Biology* *155(2)* 181-185.
- [82] Mayor, S. and Pagano, R.E. (2007) Pathways of clathrin-independent endocytosis. *Nat. Rev. Mol. Cell Biol.* *8* 603-612.
- [83] Chavrier, P., Parton, R.G., HAuri, H.P., Simons, K. and Zerial, M. (1990) Localization of low molecular weight GTP binding proteins to exocytic and endocytic compartments. *Cell* *62(2)* 317-329.
- [84] Citri, A. and Yarden, Y. (2006) EGF-ERBB signalling: towards the system level. *Nat. Rev. Mol. Cell Biol.* *7* 505-516.
- [85] Downward J. (2001) The ins and outs of signalling. *Nature* *411* 759-762.
- [86] Steinberg, G. (2007) On the move: endosomes in fungal growth and pathogenicity. *Nat. Rev. Microbiol.* *5* 309-316.
- [87] Welte, M. A. (2010) Bidirectional transport: Mating for motors. *Curr. Biol.* *20 (9)* R410-R413.
- [88] Nielsen, E., Severin, F., Backer, J.M., Hyman, A.A. and Zerial, M. (1999) Rab5 regulates motility of early endosomes on microtubules. *Nat. Cell Biol.* *1* 376-382.
- [89] Driskell, O.J., Mironov, A., Allan, V.J., Woodman, P.G. (2007). Dynein is required for receptor sorting and the morphogenesis of early endosomes. *Nat. Cell Biol.* *9* 113-120.
- [90] Parton, R. G., Schrotz, P., Bucci, C. and Gruenberg, J. (1992) Plasticity of endosomes. *J. Cell Science* *103* 335-348.
- [91] Chen, Y. A. and Scheller, R. H. (2001) Snare-mediated membrane fusion. *Nat. Mol. Cell Biol.* *2* 98-107.

- [92] Ohya, T., Miaczynska, M., Coskun, U., Lommer, B., Runge, A., Drechsel, D., Kalaidzidis, Y., Zerial, M. (2010). Reconstitution of Rab- and SNARE-dependent membrane fusion by synthetic endosomes. *Nature* *459* 1091-1097.
- [93] Brandhorst, D., Zwilling, D., Rizzoli, S. O., Lippert, U., Lang, T., Jahn, R. (2006). Homotypic fusion of early endosomes: SNAREs do not determine fusion specificity. *Proc. Natl. Acad. Sci. USA* *103* 2701-2706.
- [94] Bucci, C., Parton, R. G., Mather, I. H., Stunnenberg, H., Simons, K., Hoflack, B., and Zerial, M. (1992). The small GTPase rab5 functions as a regulatory factor in the early endocytic pathway. *Cell* *70* 715-728.
- [95] Woodman, P.G. and Warren, G. (1988) Fusion between vesicles from the pathway of receptor-mediated endocytosis. *Eur. J. Biochem* *173* 101-108.
- [96] Simons, K. and Zerial, M. (1993) Rab proteins and the road maps for intracellular transport. *Neuron* *11(5)* 789-799.
- [97] Dikic, Ivan (2006) Endosomes. (Landes Bioscience)
- [98] Rodman, J. S. and Wandinger-Ness, A. (2000) Rab GTPase coordinate endocytosis. *J. Cell Sci.* *113* 183-192.
- [99] Cullen, J. P. (2008) Endosomal sorting and signalling: an emerging role for sorting nexins. *Nat. Rev. Mol. Biol.* *9* 574-582.
- [100] Geuze, H. J., Slot, J. W., Strous, G. J., Lodish, H. F. and Schwartz, A. L. (1983) Intracellular site of asialoglycoprotein receptor-ligand coupling: double-label immunoelectron microscopy during receptor-mediated endocytosis. *Cell* *32(1)* 277-287.
- [101] Murk, J. L. A. N., Posthuma, G., Koster, A. J., Geuze, H. J., Verkleij, A. J., Kleijmeer, M. J. and Humbel, B. M. (2003). Influence of aldehyde fixation on the morphology of endosomes and lysosomes: quantitative analysis and electron tomography. *J. Microscopy* *212 (1)* 81-90.
- [102] Mukherjee, S., Maxfield, F. R. (2000) Role of membrane organization and membrane domains in endocytic lipid trafficking. *Traffic* *1* 203-211.
- [103] Pangarkar, C., Dinh, A. T. and Mitragotri, S. (2005) Dynamics and spatial organization of endosomes in mammalian cells. *Phys. Rev. Lett.* *95* 158101-158104.
- [104] Smith, D. A. and Simmons, R. M. (2001) Models of motor-assisted transport of intracellular particles. *Biophys. J.* *80 (1)* 45-68.

-
- [105] Leduc, C., Pavin, N., Jülicher, F. and Diez, S. (2010) Collective Behavior of Antagonistically Acting Kinesin-1 Motors. *Phys. Rev. Lett.* *105*, 128103-128107.
- [106] Klein, G. A., Kruse, K., Cuniberti, G. and Jülicher, F. (2005) Filament Depolymerization by Motor Molecules. *Phys. Rev. Lett.* *94* 108102-108106.
- [107] Howard, J. (2001) *Mechanics of motor proteins and the cytoskeleton*. (Sinauer, Sunderland, Massachusetts).
- [108] Jülicher, F. and Prost, J. (1995) Cooperative molecular motors. *Phys. Rev. Lett.* *75* 2618-2621.
- [109] Runge-Roosen, F., Hennig, M., Zhang, F., Jacobs, R.M.J., Sztucki, M., Schober, H., Seydel, T. and Schreiber, F. (2011) Protein self-diffusion in crowded solutions. *Proc. Natl. Acad. Sci. USA* *108* (29), 11815-11820.
- [110] Roux, A., Cuvelier, D., Nassoy, P., Prost, J., Bassereau, P., Goud, B. (2005) Role of curvature and phase transition in lipid sorting and fission of membrane tubules. *EMBO J advance online publication*, doi: 10.1038/sj.emboj.7600631
- [111] Kwon, S., Yoon, S. and Kim, Y. (2008) Condensation phenomena of conserved-mass aggregation model on weighted complex networks. *Phys. Rev. E* *77* (6) 066105-066112.
- [112] Majumdar, S. N., Krishnamurthy, S. and Barma, M. (1998) Nonequilibrium Phase Transitions in Models of Aggregation, Adsorption, and Dissociation. *Phys. Rev. Lett.* *81*, 3691.
- [113] Nagel, K. and Schreckenberg, M. (1992) A cellular automaton model for freeway traffic. *Journal de Physique I. France*, 2:2221, 1992.
- [114] Bem-Naim, E., Krapivsky, P.L. and Redner, S. (1994) Kinetics of clustering in traffic flow. *Phys. Rev. E* *50* 822-829.
- [115] Biham, O., Middleton, A.A., and Levine, D. (1992) Self-organization and a dynamical transition in traffic-flow models. *Phys. Rev. A* *46* (10) R6124-R6127
- [116] Chowdhury, D., Schadschneider, A. and Nishinari, K. (2005) Physics of transport and traffic phenomena in biology: from molecular motors and cells to organisms. *Phys. Life Rev.* *2* (4) 318-352.
- [117] Prigogine, I. and Herman, R. (1971) *Kinematic Theory of Vehicular Traffic*. Elseviers, New York.

-
- [118] Mahnke, R. and Kaupuzs, J. (2001) Probabilistic description of traffic flow. *Networks and Spatial Economics* 1 103-136.
- [119] Kerner, B. S. and Konhauser, R. (1993) *Phys. Rev. E* 48 2335.
- [120] Helbing, D. (2001) Traffic and related self-driven many-particle systems. *Rev. Mod. Phys.* 73 1067-1141.
- [121] Truskey, G.A., Yuan, F. and Katz, D. F. (2010) *Transport Phenomena in Biological Systems*. Pearson Education Inc., Prentice Hall, New Jersey.
- [122] Bormuth, Volker; Varga, Vladimir; Howard, Jonathon; Schffer, Erik (2009) Protein friction limits diffusive and directed movements of kinesin motors on microtubules. *Science*, 325 (5942), 870-873.
- [123] Friedlander, S. K. (2000) *Smoke, Dust, and Haze*. Oxford University Press, New York.
- [124] Camazine, S., Deneubourg, J., Franks, N., Sneyd, J., Theraulaz, G., and Bonabeau, E. (2001) *Self-Organization in Biological systems*. Princeton University Press.
- [125] Prigogine, I., and Nicolis, G. (1977) *Self-Organization in Non-Equilibrium Systems*. J. Wiley and Sons, New York.

Versicherung

Hiermit versichere ich, dass ich die vorliegende Arbeit ohne unzulässige Hilfe Dritter und ohne Benutzung anderer als der angegebenen Hilfsmittel angefertigt habe; die aus fremden Quellen direkt oder indirekt übernommenen Gedanken sind als solche kenntlich gemacht. Die Arbeit wurde bisher weder im Inland noch im Ausland in gleicher oder ähnlicher Form einer anderen Prüfungsbehörde vorgelegt. Die vorliegende Arbeit wurde am Max-Planck-Institut für Physik komplexer Systeme angefertigt und von Prof. Dr. Frank Jülicher betreut.

Dresden, den 3.3.2012, Jonathan Edward Dawson

